

UNIVERSITÀ  
DEGLI STUDI  
DI PADOVA

## TESI

1 Sede Amministrativa: Università degli Studi di Padova

Dipartimento di

\_\_\_\_\_Biologia\_\_\_\_\_

CORSO DI DOTTORATO DI RICERCA IN: Bioscienze e biotecnologie

CURRICULUM: Biologia Cellulare

CICLO XXIX

**A FRET-based genome wide high content screen identifies a novel role for the Parkinson's disease gene LRRK2 as modulator of endoplasmic reticulum-mitochondria tethering**

**Coordinatore:** Ch.mo Prof. Paolo Bernardi

**Supervisore:** Ch.mo Prof. Paolo Bernardi

**Co-Supervisore:** Ch.mo Prof. Luca Scorrano

**Dottorando :** Annalisa Serafini

## Table of contents

1	Riassunto dell'attività svolta .....	3
2	Summary.....	5
3	Introduction .....	7
3.1	Inter-Organelles Connections.....	7
3.1.1	How to Measure Organelles Connections by Microscopy? .....	8
3.1.2	Mitochondria: Dynamics and Connections .....	13
3.1.3	Endoplasmic Reticulum (ER): Dynamics and Connections.....	20
3.2	MAMs (Mitochondrial associated membranes) and MERCs (Mitochondria-ER contact sites).....	26
3.2.1	Functions of MERCs .....	29
3.2.2	Tethering Mitochondria and ER.....	34
3.3	High Content Screening in Cell Biology.....	37
3.3.1	Genome Wide Screening with targeted shRNA libraries .....	40
3.4	MAMs and Neurodegeneration.....	43
3.4.1	Parkinson Disease and MAMs .....	48
3.4.2	LRRK2: Genetic and Structure .....	58
3.4.3	LRRK2 Interactome: Partners and Cellular Functions.....	62
4	Results .....	68
5	Conclusions and future perspectives .....	113

6	References .....	114
---	------------------	-----

## 2 Riassunto dell'attività svolta

La comunicazione tra organelli cellulari è una caratteristica fondamentale delle cellule eucariotiche ed esercita un ruolo fondamentale in molti processi cellulari. Uno dei processi di comunicazione tra organelli cellulari tra i più caratterizzati è quello dovuto ai siti di contatto tra le membrane di mitocondri e reticolo endoplasmatico (ER). Anche noti come “Mitochondria-associated ER membranes” (MAMs) o “Mitochondria-ER contact sites” (MERCs), la loro esistenza è stata scoperta 50 anni fa tramite studi di microscopia elettronica, ma il loro significato funzionale è iniziato ad emergere solo alla fine degli anni 90 quando è stato dimostrato il ruolo dei MERCs nello scambio di calcio dall'ER. Nonostante l'importanza di questi siti di contatto tra organelli sia in fisiologia sia in patologia, solo poche proteine coinvolte nel mantenimento strutturale della distanza tra i due organelli sono state finora identificate nei mammiferi. Mitofusina2 (MFN2) è stato il primo “tether” strutturale ad essere identificato. È stato rilevato che MFN2 è localizzata sia nella membrana mitocondriale esterna (OMM) sia sulla superficie citosolica dell'ER ed è in grado di formare intrazioni omo- ed eterotipiche con MFN1, mantenendo quindi la distanza tra i due organelli. Poiché una residua giustapposizione tra i due organelli è stata osservata in cellule MFN2<sup>-/-</sup>, ulteriori proteine che esercitano questo ruolo devono esistere. Per identificarle, abbiamo stabilito un protocollo ed eseguito due repliche di uno screening genomico su larga scala in fibroblasti embrionali di topo (MEF). Per eseguire questo screening, abbiamo sfruttato un biosensore basato sulla FRET, dove la proteina fluorescente CFP fusa con il dominio funzionale FRB e la proteina fluorescente YFP fusa con il dominio funzionale FKBP vengono fatte localizzare rispettivamente all'ER (grazie alla sequenza di segnale Sac1) ed ai mitocondri (grazie alla sequenza di segnale Akap1) (Csordas G. et al., 2010). Abbiamo modificato questo costrutto inserendo tra i cDNA delle due proteine il peptide autocatalitico Tav2A per ottenere un singolo mRNA e quindi l'espressione equimolare delle due proteine. I domini funzionali FKBP e FRB sono in grado di eterodimerizzare con l'aggiunta di Rapamicina, permettendo così la misurazione non solo dei livelli di giustapposizione basale tra i due organelli, ma anche del massimo livello di contatti che possono avvenire in una cellula. Abbiamo chiamato questo nuovo costrutto FRET ER-mitochondria probe (FEMP). Le caratteristiche uniche del FEMP ci consentono di discriminare tra le proteine il cui ruolo è quello di mantenere i due organelli vicini,

chiamate “tethers”, e proteine che invece tengono i due organelli più distanti, definiti “spacers”.

Le immagini ottenute dallo screening sono state analizzate e sono stati calcolati due indici, chiamati “basal MERC index” e “maximum MERC index”, che rappresentano rispettivamente il livello di contatti osservabili in qualsiasi momento in una cellula e il massimo livello di contatti possibile. A seguito di un’analisi delle immagini automatizzata e di un’analisi statistica effettuata su ~10,000 geni, dopo un processo di selezione abbiamo identificato 205 geni come “tethers” (geni che una volta eliminati aumentano la distanza tra i due organelli) tra mitocondri e ER e 59 geni come “spacers” (geni che una volta eliminati diminuiscono la distanza tra i due organelli) che influenzano sia il basal sia il maximum MERC index in entrambe le repliche. Inoltre, sono stati identificati 625 tethers e 696 spacers che influenzano solo il basal MERC index; e 519 tethers e 67 spacers che modificano solo il maximum MERC index. Analisi delle classi di proteine presenti in questi tre gruppi tramite Panther ha rivelato sia classi di proteine il cui ruolo in questo processo era noto, sia nuove classi di proteine il cui ruolo nella comunicazione tra ER e mitocondri deve ancora essere esplorato. Analisi della localizzazione cellulare per identificare proteine localizzate sia nell’ER sia nei mitocondri delle liste di geni esposte in precedenza, ha rivelato l’esistenza di 13 proteine tra i tethers e gli spacers comuni, 30 proteine che influenzano solo il basal MERC index e 16 proteine che influenzano solo il maximum MERC index localizzate in entrambi gli organelli. Una delle proteine presente nell’ultimo gruppo è “Leucine Rich Repeat Kinase 2” (LRRK2) che abbiamo ulteriormente caratterizzato come tether tra ER e mitocondri. Esperimenti di frazionamento cellulare dimostrano che LRRK2 è localizzata principalmente nelle MAMs. Come previsto per un tether, il livello di prossimità tra ER e mitocondri, misurato tramite FEMP, sono diminuiti in MEF LRRK2<sup>-/-</sup>. La prossimità tra i due organelli è pienamente recuperata dalla reintroduzione in MEF LRRK2<sup>-/-</sup> della proteina WT, ma non dei mutanti associati alle forme di Parkinson familiare.

In conclusione, abbiamo sviluppato un nuovo metodo per determinare la prossimità tra ER e mitocondri e abbiamo utilizzato questa tecnologia per eseguire due repliche di uno screening genomico su larga scala identificando nuovi componenti strutturali dei contatti tra mitocondri e ER.

### 3 Summary

Inter-organelle communication is a key feature of eukaryotic cells and has been found to be fundamental in many different cellular processes. One of the best characterized interorganelle cross talk due to membrane contact sites is that between Endoplasmic Reticulum (ER) and mitochondria. Also referred to as mitochondria associated ER-membranes (MAMs) or Mitochondria-ER contact sites (MERCs), their existence was discovered 50 years ago through electron microscopic studies, but their functional significance started to emerge only in late 90s when the role of MERCs in calcium exchange from ER to mitochondria was demonstrated. Despite the importance of these contacts sites in physiology and pathology, only few proteins have so far been identified involved in the structural maintenance of the distance between the two organelles in mammals. Mitofusin 2 (MFN2) was the first structural tether to be identified. MFN2 has been found on both OMM and ER cytosolic face and is able to form homo and heterotypic interactions with MFN1, thus tethering the two organelles. As residual juxtaposition between the two organelles is still observed in *Mfn2*<sup>-/-</sup> cells, additional tethering proteins have to exist. To identify them, we set out to perform two replicates of a genome wide screening in mouse embryonic fibroblasts (MEFs). In order to perform the genome wide screening, we capitalized on the FRET based biosensor, where CFP fused with FRB domain and YFP fused with FKBP domain were targeted to ER (by a Sac 1 signaling sequence) and mitochondria (by an Akap signaling sequence) respectively (Csordas et al., 2010). We modified this probe by introducing between the cDNAs of the two fluorescent proteins a self-cleaving Tav2A peptide in order to have a single mRNA construct that allows the expression of equimolar level of the proteins. FKBP and FRB binding domain are able to heterodimerize upon addition of rapamycin, thus allowing the measurement not only of the basal level of juxtaposition between the two organelles, but also of the maximum level of contacts that can occur in a cell. We called this new construct FRET ER-mitochondria probe (FEMP). FEMP unique features allow us to discriminate between proteins whose role is keeping the two organelles closer, termed as “tethers”, and proteins that keep the two organelles apart, defined as “spacers”.

We analyzed raw images from the screen and calculated two indexes, namely basal and maximum MERC index, mirroring the level of contacts observed at any given timepoint and the maximum possible level of contacts respectively. Following automated image analysis and statistical analysis performed on ~10,000 genes, after candidate selection we identified 205 genes as ER-mitochondria tethers (i.e., genes that once ablated increase the distance between the two organelles) and 59 genes as spacers (i.e., genes that once ablated decrease the distance between the two organelles) affecting both basal and maximum MERC index in both replicates. Moreover, we identified 625 tethers and 696 spacers affecting only the basal MERC index; 519 tethers and 67 spacers affecting only the maximum MERC indexes. Protein classes analysis of these three groups of genes by Panther predicted both already known and new protein classes that are yet to be explored in terms of ER-mitochondria communication. Subcellular localization analysis to identify predicted proteins to be present in both ER and outer mitochondrial membrane (OMM) of the gene lists detailed before, revealed 13 proteins among the common tethers and spacers, 30 proteins affecting only the basal MERC index and 16 proteins affecting only the maximum MERC index localized on both organelles. One of the proteins present in the last group is Leucine Rich Repeat Kinase 2 (LRRK2) and we have further characterized it as ER-mitochondria tether. Subcellular fractionation experiments showed that LRRK2 localized mostly in MAMs. As expected for a tether, levels of ER-mitochondria juxtaposition, measured with FEMP, were decreased in LRRK2<sup>-/-</sup> MEF. ER-mitochondria proximity was fully restored by reintroduction in MEF LRRK2<sup>-/-</sup> of wt protein but not of the familial PD associated mutants.

In conclusion, we have developed a new method to assess the proximity between ER and mitochondria and we have utilized this technology to perform two replicates of a high content screen identifying novel structural components of the ER-mitochondria contact sites.

## **4 Introduction**

### **4.1 Inter-Organelles Connections**

The main characteristic of eukaryotic cells is the evolution of membrane-bound organelles, enabling them to compartmentalize specialized biochemical reactions in specific locations. Individual organelles such as mitochondria, lysosomes, peroxisomes, Golgi apparatus or the endoplasmic reticulum (ER) were regarded for long time as isolated biochemical entities associated with distinct cellular tasks (Becker M. et al., 2008). However, in the last years a combination of various techniques in ultrastructural imaging, molecular biology, biochemistry, and proteomic dramatically modified this concept evidenced that cellular organelles form a highly dynamic and complex network (Schrader M. et al., 2015).

Importantly, the connections between cellular organelles must be dynamic to allow coordination of signalling activities, membrane fission and degradation by autophagy to adapt to the different physiological conditions of the cell (Klecker T. et al., 2014). The exchange of metabolites or signalling molecules through vesicular transport, diffusion, or direct physical contacts, establish a functional relationship between cellular organelles. These tasks are mediated by specialized membrane contact sites. Organelles interactions are also regulated by organelle biogenesis, membrane dynamics and degradation processes, that control in last instance the total number of organelles. Notably, membrane contact sites are involved also in the regulation of these processes (Schrader M. et al., 2015). Membrane contacts can influence also the positioning and motility of organelles, together with cytoskeleton and molecular motors (Daniele T. et al., 2014). Membrane contact sites consist in the tethering of two not fused membranes in close proximity. These sites are characterized by a particular proteins and/or lipids composition affecting both organelles (Prinz W.A. et al., 2014). Despite membrane contacts sites have been long observed in cellular organelles studies, their fundamental role in intracellular signalling, metabolism and organelle dynamics is just beginning to emerge (Helle S.C.J. et al., 2013). Moreover, an increasing number of proteins involved in the maintenance of this tethering are being discovered in yeast and mammals (Elbaz Y. et al., 2011).

In this thesis, our aim was to clarify the molecular composition of the most studied inter-organelles connections: the ones between mitochondria and the ER, by means of a high throughput screening.

#### **4.1.1 How to Measure Organelles Connections by Microscopy?**

Organelles are never really “in contact” at membrane contact sites, but the perpendicular distance separating them ranges typically from 10 to 50nm (Giacomello M. et al., 2016). The most characterized inter-organelles contact is the one occurring between mitochondria and the ER that will be discussed in Section 3.2.

One of the most commonly used technique to quantify inter-organelle contacts is confocal optical microscopy. The membranes of the two organelles of interest are labelled with one fluorophore respectively, and image stacks are acquired in few seconds using a spinning disk confocal microscope in order to reduce the movement artefacts, since both the organelles are dynamic. Image analysis typically involves overlap of the two fluorophores and measurement of the co-localisation coefficient in a 3D space (de Brito O.M. et al., 2008). Amongst the several methods available for co-localisation quantification, Manders’ coefficient is most commonly used to analyse co-localisation between ER and mitochondria (Manders E.M.M. et al., 1993). One of the main advantages of this technique is the elimination of the artefacts in organelles morphology caused by fixation of the samples, that can alter the distance between the organelles (Frigault M.M. et al., 2009). Along this line, another advantage given by this technique is the gain of additional knowledge about the morphology of the individual organelle. A major weakness of the technique is that confocal microscopy doesn’t allow precise quantification of distances of 10–30nm: indeed, its lateral resolution is approximately 250nm (Lidke, D.S. et al., 2012), about an order of magnitude less than what required. To solve this issue, other methods with improved resolutions, to better visualize and quantify 10–30nm distances, have been developed.

Electron microscopy is one of the first developed techniques that allowed the visualization of a cellular compartments at a resolution of few nanometers. In particular, for the analysis of ER-mitochondria contacts it is important to quantify also the surface area that is in contact and not simply the number of contacts (Csordas G. et al., 2006). The use of fixed samples,

which may alter the distance and the morphology of the organelles of interest is the main limitation of this technique. Moreover, the produced two-dimensional (2D) images are projections from the inherent three-dimensional (3D) structure of the sample. To overcome this limitation, the mathematical concepts of electron tomography to reconstruct a 3D volume from a set of 2D projections was applied to electron microscopy (Ercius P. et al., 2015). Electron tomography has also been successfully used in reconstruction of ER-mitochondria contacts (De Brito O.M. et al., 2008). However, fixation of the samples cannot be avoided even in this methodology.

ER-mitochondria contacts visualized with confocal microscopy, electron microscopy and electron tomography are shown in Figure 1.

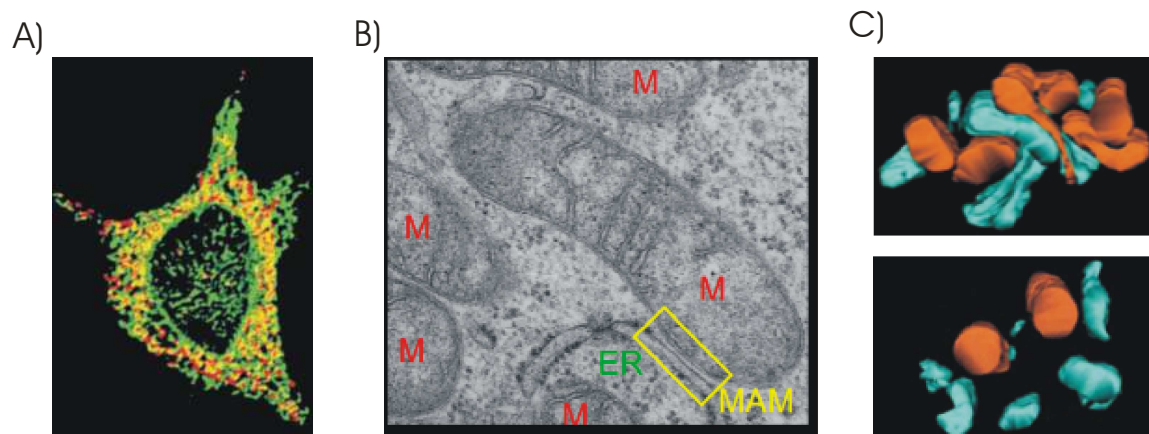


**Figure 1: Visualization of ER- mitochondria contacts by confocal microscopy, electron microscopy and electron tomography.**

**A)** Volume rendered stacks of ER (green) and mitochondria (red) by confocal microscope (from De Brito O.M. et al., 2008). **B)** Electron microscopy image shows the juxtapposition between ER and mitochondria labelled as MAM (from De Vos K. <https://www.sheffield.ac.uk/neuroscience/staff/devos>). **C)** Electron tomography images of wild type (WT) in the top and Mitofusin2 KO mouse embryonic fibroblasts (MEFs) in the bottom (from De Brito O.M. et al., 2008).

Super-resolution light microscopy methods, such as Structured Illumination Microscopy (SIM), Photo-Activation Localisation Microscopy (PALM), and Stochastic Optical Reconstruction Microscopy (STORM), provide other alternatives routes to electron microscopy for quantifying inter-organelle contacts. SIM doubles the spatial resolution in 3D by illuminating the sample with a patterned excitation light. and it can be used for multicolour imaging in living cells. It ensures lateral resolution of approximately 50nm,

with up to approximately 100Hz frequency. It requires a relatively low illumination power compared with other methods of super-resolution microscopy; in contrast the resolution enhancement is less when compared to other super-resolution techniques (Hirano Y. et al., 2015). STORM and PALM rely on localizing the position of single fluorophores by intensity profiles: this is achieved by turning on and off a subgroup of sparsely distributed fluorescent molecules in subsequent imaging cycles. These techniques provide resolutions of approximately 20nm laterally and 50nm axially (Fornasiero, E.F. et al., 2015). STORM has already been successfully utilized in live cells for the analysis of ER and mitochondria contacts (Shim S.H. et al., 2012), as shown in Figure 2. The main disadvantages of super-resolution techniques are the low temporal resolution and often photobleaching, due to the necessity of acquiring many image frames to reconstruct one super-resolution image (Hirano Y. et al., 2015).

Optical microscopes can monitor, for instance, average variations in fluorescence intensities at specific wavelengths or the lifetimes of fluorophores following an excitation pulse (De Los Santos C. et al., 2015). With this purpose, FRAP, FLIM and FRET techniques have been developed.

Fluorescence Photobleaching Recovery (FRAP) is commonly used for studying the dynamics of fluorescent molecules in living cells both on cell surfaces and within the cytoplasm (Carisey A. et al., 2011). FRAP takes advantage of the rapid and irreversible photobleaching of fluorophores within a region of interest using a laser tuned to an appropriate wavelength for short durations of time, typically less than 20ms. Following the light pulse, the fluorescence intensity is monitored over time in an area around, and including, the region of interest. Two quantitative parameters are used in FRAP quantification: the “percent recovery” measures the fraction of molecules in the photobleached area that are moving; while the “recovery-rate constant” is a measure of the speed at which molecules move in and out of the bleached area. The “recovery-rate constant” also provides indication on binding interactions within the region of interest (De Los Santos C. et al., 2015). Limitations of FRAP are the possibility of photoswitching, a form of reversible photobleaching (Dayel M.J. et al., 1999), and of localized heating caused by the laser (Axelrod D. et al., 1977). Moreover, due to the complexity of cell structure, FRAP can be used only in a qualitative way in experiments with live samples (Brown E.B. et al., 1999).

Fluorescence Life Time Microscopy (FLIM) produces spatially resolved images of fluorescence lifetime of a fluorophore, providing the additional temporal dimension of information and can be used with multiple fluorophores. Fluorescence lifetime refers to the average time electrons spend in the excited state after the fluorophore's absorption, and it is specific for each fluorophore. Video-rate or low-light imaging required to monitor organelle dynamics or to reduce potential perturbations in living cells can reduce the precision of these technique, making it not suitable for this condition. The opposite can also be true: low-light and fast measurements will maintain cell viability, but may not produce images with high signal-to-noise ratio, so both parameters have to be optimized (Chen L.C. et al., 2013).

Förster Resonance Energy Transfer (FRET) is commonly used for measuring the spatial distance between two, or multiple, fluorophores. Since the distance necessary to allow FRET is in the nanometers range (comparable to protein size, thickness of biological membranes and distances of protein-protein interaction), FRET can be considered an *in vivo* "nanoscale ruler" (Cardullo R.A. et al., 2013). FRET occurs when the emission spectrum of a FRET donor (D) overlaps with the excitation spectrum of the FRET acceptor (A). After donor excitation, non-radiative energy transfer occurs to the acceptor only when the couple is in close proximity, and it can be detected by measuring the emission of the acceptor molecule. FRET is a dipole-dipole interaction and the FRET efficiency E is inversely proportional to the 6<sup>th</sup> grade of power of the distance between the two fluorophores, as reported in the Förster equation:

$$E = \frac{R_0^6}{R_0^6 + R_{A-D}^6}$$

where  $R_0$  is the Förster distance at which the FRET efficiency is 50%, and  $R_{A-D}$  is the acceptor-donor distance. From the above equation, it can be clearly seen that the dependence of E on  $R_{A-D}$  is highly non-linear and strongest when the donor-acceptor distance is near  $R_0$  (Förster T., 1948). Genetically encoded fluorophores, most likely fluorescent proteins, are commonly used for FRET imaging in live cells and have to be chosen based on the optimal overlap of their donor emission and acceptor excitation spectra: currently the most broadly used FRET pairs are Cyan Fluorescent Protein (CFP)- Yellow Fluorescent Protein (YFP)

variants and Green Fluorescent Protein (GFP)- Red Fluorescent Protein (RFP) variants (Day R.N. et al., 2012).

Alternative microscopy methods include utilization of “in situ proximity ligation assays” (PLA). Here, conventionally fixed cells and tissues are probed with two primary antibodies for membrane proteins residing on the cytoplasmic sides of the respective organelles of interest. The primary antibodies must be raised in different species, so that specie-specific secondary antibodies, coupled to specific oligonucleotides, called PLA probes, are then added and link to the respective primary antibody. If the two PLA probes are in close proximity, meaning that the proteins to which they are linked are likely to interact, a subsequent addition of two other DNA oligonucleotides will form a circular DNA molecule, which can then be amplified by rolling-circle amplification (RCA) primed by one of the proximity probe, thus creating a concatenated amplification product. The RCA product can subsequently be detected by hybridization of fluorescent labelled complementary oligonucleotides. *In situ* PLA enables study of endogenous proteins in their natural environment and thus can be used for clinical specimens. The distances detected by PLA are approximately 30nm (Soderberg O. et al., 2006). PLA has already been used to quantify ER–mitochondria associations (Tubbs E. et al., 2014), as depicted in Figure 2. The reaction is so efficient that care must be taken when using PLA in a quantitative manner due to the possibility of non-linear saturation of the signal, and this can be considered a disadvantage if a quantitative analysis is needed (Mocanu M.M. et al., 2011).

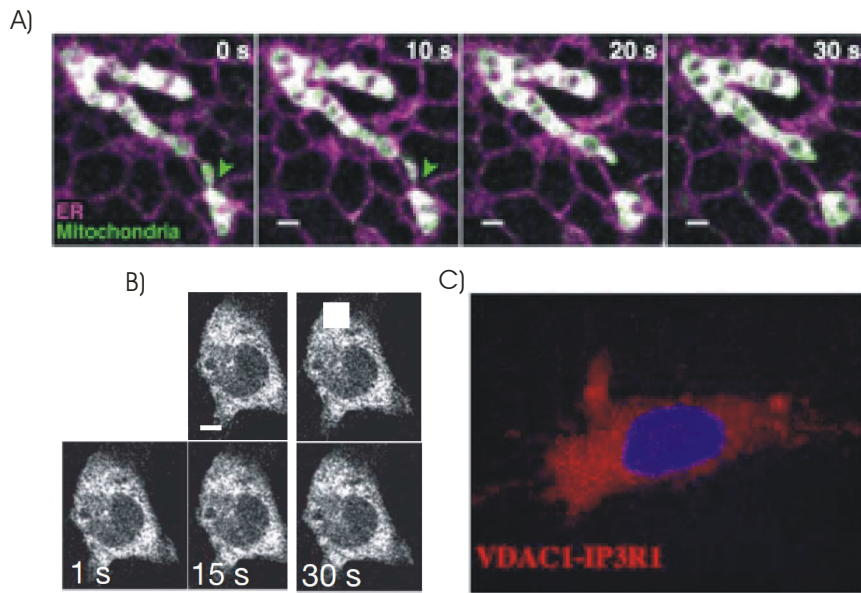


**Figure 2: Visualization of ER-mitochondria contacts by STORM, FRAP microscopy and PLA.**

**A)** Two-color STORM images of mitochondria (green) and the ER (magenta) in a live BS-C-1 cell. The snapshots are 10s long. The ER tubules at the mitochondrial fission site are indicated by green arrowheads. Scale bars, 500nm (from Shim S.H. et al., 2012). **B)** Frames from a real-time sequence of ER-YFP FRAP in MEFs. Boxes show photobleached areas. Times (seconds) after photobleaching are indicated. Scale bars, 4 $\mu$ m (from De Brito O.M. et al., 2008). **C)** Representative PLA images ( $\times 63$  and scale bar = 20 $\mu$ m) of VDAC1/IP3R1 interactions in HuH7 cells (from Tubbs E. et al., 2014).

Other methods to analyse inter-organelle contacts include genetically encoded dimerization-dependent fluorophores (ddFP). ddFP technology involves the reversible binding of two dark fluorophore monomers, each one targeted to one of the organelles of interest. The fluorescent emission associated with the heterodimeric interaction between the fluorophores is an indicator of an increase in the proximity of the monomers, proportional to organelle vicinity. This method has been used for ER-mitochondria contacts analysis (Alford S.C. et al., 2012).

#### 4.1.2 Mitochondria: Dynamics and Connections

Mitochondria are semi-autonomous organelles present in most eukaryotic cells with a large variety of functions in cellular metabolism. Mitochondria have been described as “the powerhouse of the cell” because they synthesize most of the cell supply of adenosine triphosphate (ATP), used as a source of chemical energy. In addition, mitochondria are involved in signalling, cellular differentiation, cell death, as well as in cell cycle and cell

growth (Mc Bride H.M. et al., 2006). Not surprisingly, mitochondria have been implicated in several human diseases besides primary mitochondrial disorders, such as cardiac dysfunction and neurodegenerative disorders. Mitochondrial biogenesis is temporally coordinated with these cellular processes (Valero T. et al., 2014). The number of mitochondria per cell may vary widely by organism, tissue and cell type from a large single mitochondrion to thousands in some oocytes. In most cells the relative mitochondrial volume is in the range of 15-22% of total cellular volume (Karp G. et al., 2008).

One distinctive feature of mitochondria is the presence of two membranes: one outer mitochondrial membrane (OMM) and an inner mitochondrial membrane (IMM), separated by the intermembrane space. The IMM is a tight diffusion barrier to all ions and molecules and it is composed by three specialized zones: the inner boundary membrane (IBM), the cristae junctions and the cristae (Vogel F. et al., 2006). The IMM is closely associated with the OMM at several stretches along the mitochondrial perimeter creating functionally and structurally distinct regions, called IBM. IBM constitute an important portal for the assembly and transport of proteins, since they contain translocase and assembly machineries (Reichert A.S. et al., 2002). In certain regions, the IMM is invaginated in structures known as cristae (Perkins G. et al., 1997). The bases of cristae are approximately 20–50nm in diameter, and these particular portions of the IMM are called cristae junctions. The formation of these junctions is mediated by the “mitochondrial contact site and cristae organizing system” (MICOS) complex: upon loss of one of the MICOS subunits, cristae junctions disappear (Harner M. et al., 2011). The vast majority of the respiratory chain complex are located in the cristae and, because of this, cristae are defined as the site of oxidative phosphorylation (OXPHOS) (Gilkerson et al., 2003). Cristae morphology varies among different tissues and different cellular conditions, for example during apoptosis cristae undergo complete remodelling, leading to the opening of cristae junctions to release pro-apoptotic factors, such as cytochrome c (Scorrano L. et al., 2002).

Given its particular lipid bilayer composition, the OMM is morphologically flexible and completely permeable to metabolite and cations, allowing the exchange between the cytosol and inner membrane space. The OMM can simultaneously interact with several cellular compartments and these organelle interactions influence OMM shape (Pernas L. et al., 2016). The mitochondrial structure is shown in Figure 3.

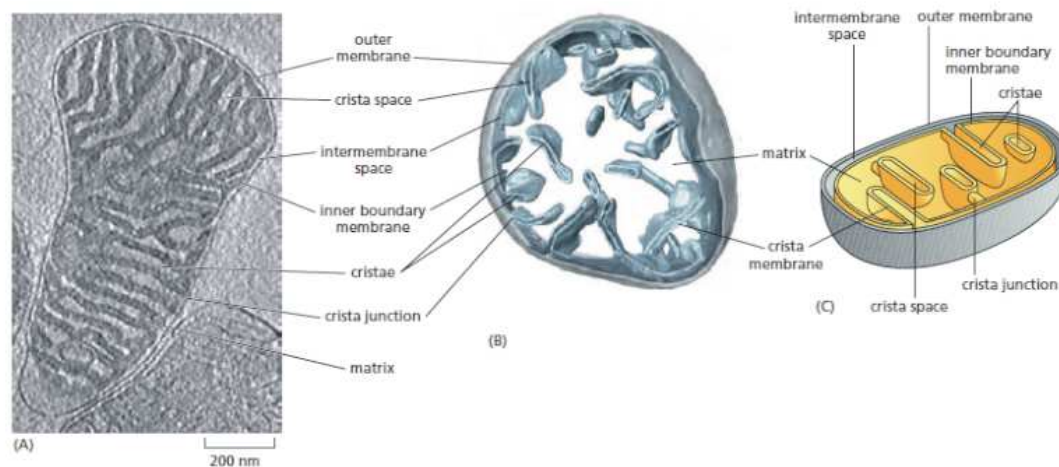


**Figure 3: Structure of a mitochondrion.** From left to right: Tomographic volume of mouse heart mitochondrion. Three-dimensional volume of a mouse heart mitochondrion determined by cryo-electron tomography. Schematic drawing of a mitochondrion: the outer membrane (grey), and the inner membrane (yellow). Note that the inner membrane is compartmentalized into the inner boundary membrane (IBM) and the cristae membrane. There are three distinct spaces: the intermembrane space between OMM and IMM, the crista space, and the matrix (from Kühlbrandt W., 2015).

It has been known for many years that mitochondria can modify their shape by elongation, shortening, branching, buckling, swelling, or division (Bereiter-Hahn J. et al., 1994). In fact, the term “mitochondrion” derives from two Greek words: “mitos” for “thread” and “chondrion” for “grain”, and was given to the organelle owing to the heterogeneity in its shape, as visualised under the light microscope.

The broad term of mitochondrial dynamics encompasses: (1) fusion: the joining of two organelles into one; (2) fission: the division of a single organelle into two; (3) transport: the directed movement of the organelle along a cytoskeletal element; and (4) mitophagy: the targeted destruction of mitochondria via the autophagic machinery. We will now discuss the processes of mitochondrial fusion and fission.

Through fusion and fission events, two or more mitochondria can distribute membranes, solutes, metabolites, and proteins. Mitochondrial fusion requires the coordination of two distinct steps: fusion of the OMM followed by fusion of the IMM. Fusion of the OMM is mediated by mitofusins (Mfn) 1 and 2. Mitofusins are nuclear-encoded proteins members of

the dynamin superfamily of large GTPases, which have homologs from yeast to humans, and were first identified in *Drosophila melanogaster* as being important for spermatogenesis (Hales K.G. et al., 1997). Mfn1 and Mfn2 share approximately 80% sequence similarity (Santel A. et al., 2003) and the same relevant structural motifs (Figure 4). Their essential amino-terminal GTPase domain contains five structural motifs, each of them playing a crucial function in binding and hydrolysing GTP (Bourne H.R. et al., 1991). They also possess two coiled-coil domains (also called heptad-repeat domains, HR1 and HR2). Both the HR2 and GTPase domain are exposed to the cytosol. HR2 mediates homotypic or heterotypic (Mfn1-Mfn2) interactions by forming a trans, anti-parallel, dimeric coiled coil that tethers two adjacent mitochondria (Koshiba T. et al., 2004). Finally, Mfns contain a bipartite carboxy-terminal transmembrane domain responsible for its anchoring into the OMM. Of note, a proline-rich region (PR), involved in protein-protein interactions, is found only in Mfn2. Mfn1 and Mfn2 mRNA or protein expression levels are only partially superimposable: Mfn1&2 are both expressed in heart and adrenal glands; Mfn1 is highly expressed also in liver, pancreas, and testis; whereas Mfn2 in skeletal muscle, brain, and brown adipose tissue (Eura Y. et al., 2003). Genetic ablation of Mfns causes the complete loss of mitochondrial fusion and leads to mitochondrial defects in both cell culture and tissues. These defects include loss of cristae, loss of mitochondrial membrane potential, depletion of mitochondrial DNA (mtDNA), as well as an increased mutational load in the mitochondrial genome in tissues (Chen H. et al., 2010), implicating a role for mitochondrial fusion in mtDNA maintenance and transmission. Moreover, Mfn1 as well as Mfn2 deletion is embryonically lethal in mice (Chen H. et al., 2003). Mfn1 mediates mitochondrial docking and fusion more efficiently than Mfn2, probably due to its higher GTPase activity (Ishihara N. et al., 2004). Mfn1, but not Mfn2, is required to mediate mitochondrial fusion of IMM (Cipolat S. et al., 2004). Nonetheless, when overexpressed, each protein is able to rescue the loss of the other and promote mitochondrial fusion (Chen et al., 2003).

Fusion of the IMM is mediated by the intermembrane space protein Optic Atrophy 1 (Opa1), another member of the dynamin superfamily. In humans, mutations of *OPA1* cause autosomal dominant optic atrophy (ADOA), a severe disease characterized by progressive degeneration of retinal ganglion cells and optic nerve and blindness (Alexander C. et al., 2000). The human *OPA1* gene encodes eight mRNA splicing variants (Satoh M. et al.,

2003). An amino-terminal mitochondrial targeting sequence, a trans-membrane domain, two coiled coil domains involved in protein-protein interactions, and a GTPase domain and a middle domain involved in higher order assembly to form Opa1 supercomplexes are common to all the variants. The GTPase effector domain, crucial for protein activity and protein-protein interactions, and the second coiled coil domain are localized at the C-terminus. While the mitochondrial targeting sequence is constitutively cleaved upon import into the organelle, the amino-terminal transmembrane domain remains and anchors the protein to the IMM: this structure is referred to as the “long-form” of Opa1 (Ishihara N. et al., 2006). Several proteases, such as Oma1 and Yme1L, can cleave Opa1 from its N-terminal transmembrane domain, producing a “short” form of Opa1 (Ishihara N. et al., 2006). These proteases are highly regulated, responding to various aspects of mitochondrial biology (Mishra P. et al., 2014). The structure of Opa1 with the main cleavage sites is depicted in Figure 5. It appears that a balance of long and short forms of Opa1, regulated by its proteolysis, is required for fusion activity (Song Z. et al., 2007), although recent studies have challenged this hypothesis and implicated only the long form of Opa1 as the primary fusion mediator (Anand R. et al., 2014). Opa1 has been shown to interact with both Mfn1 and Mfn2, probably via its GTPase effector domain (Zorzano A. et al., 2010). Besides its role in fusion, Opa1 has also been implicated in several other mitochondrial functions including apoptosis, cristae ultrastructure maintenance, and stability of respiratory supercomplexes (Cogliati S. et al., 2013). In mammals, the coordination of the steps of OMM fusion with IMM fusion has still not yet clarified. Although it is possible to decouple OMM fusion and IMM fusion with pharmacological treatment in cell culture, the relevance of this process *in vivo* remains unknown (Pernas L. et al., 2016).

The main mediator of mitochondrial fission is the dynamin-related protein (Drp1). Drp1 is another large GTPase protein; unlike the fusion proteins which are constitutively targeted to mitochondrial membranes, Drp1 lacks a lipid binding pleckstrin homology (PH) domain, so it is predominantly cytosolic and can be recruited to the mitochondrial surface to mediate fission under specific conditions. A number of adaptor proteins involved in its recruitment have been identified including fission factor 1 (Fis1), mitochondrial fission factor (Mff), Mid49 and Mid51, all of which are localized to the OMM (Loson O.C. et al., 2013). The most accepted model postulates that Drp1 translocates to and oligomerizes on the OMM,

forming a ring which constricts the organelle and eventually brings to fission after GTP hydrolysis. While the importance of Drp1 in mitochondrial fission is not questioned, recent data has suggested the involvement of other auxiliary factors and organelles, as the ER (Pernas L. et al., 2016). The structure of Drp1 and Fis1 and the model for mitochondrial fission are shown in Figure 4. The role of the ER in mitochondrial fission will be examined in depth in Section 3.2.

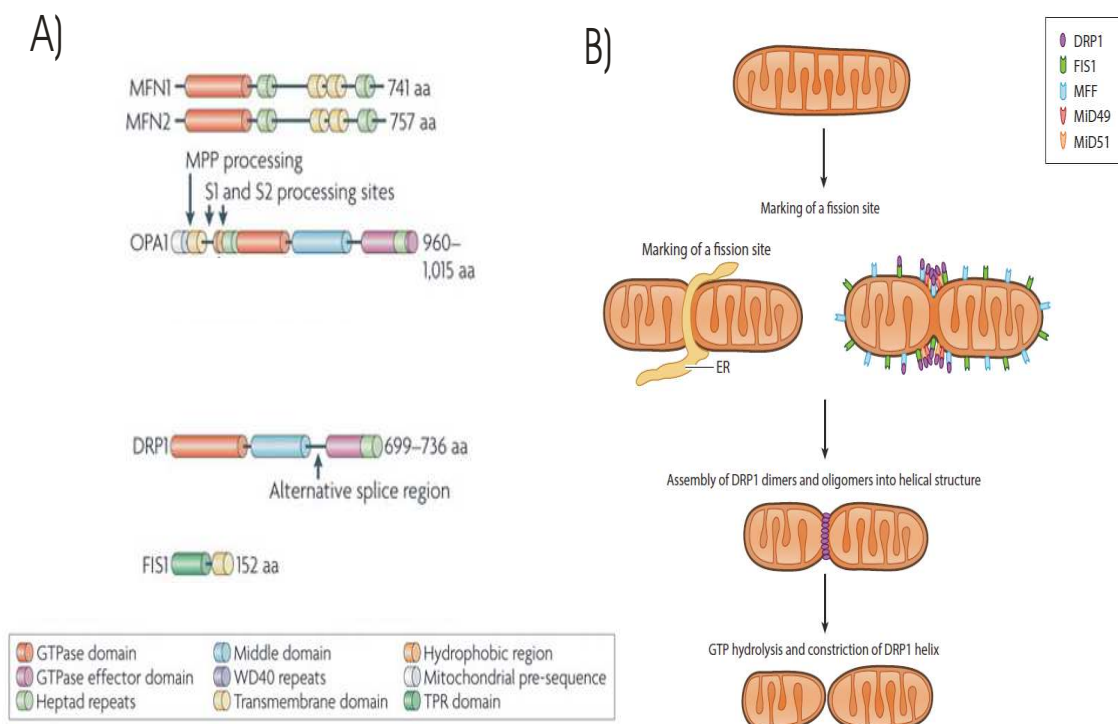


**Figure 4: Protein machinery for mitochondrial fusion and fission.**

**A)** Domain structure of proteins involved in OMM fusion (Mfn1 and Mfn2), IMM fusion (Opa1) and mitochondrial fission (Drp1 and Fis1) in mammals. Mitofusins are characterized, starting from the N-terminus, a GTPase domain and two transmembrane domains in between of heptades repeats (HR1 and HR2). Opa1 is composed of a mitochondrial targeting sequence, a transmembrane domain, a hydrophobic region with a heptad repeat and a GTPase domain. In the C-terminus there are a GTPase effector domain and a second heptad repeat. The cleavage sites in Opa1 that give rise to long (MPP processing) and short form (S1 and S2 processing sites)

are depicted. Drp1 also possesses a GTPase domain, a middle domain and a GTPase effector domain with a heptad repeat at the C-terminus. Fis1 is a short protein composed of a tetratricopeptide repeat (TPR) domain and a transmembrane domain anchored to OMM (adapted from Westermann B. et al., 2010). **B)** Schematic representation the mitochondrial fission process. First, Drp1 is recruited to the OMM by various adaptor proteins such as Fis1, Mff, Mid49, Mid51. In this phase is likely that also the ER have a role in the formation of the fission site. Subsequently, Drp1 oligomerizes, forming a ring which constricts the organelle and eventually leads to fission after GTP hydrolysis (adapted from Pernas L. et al., 2016).

In metazoans, mitochondrial transport both extracellular, such as in axons, and intracellular is regulated by mitochondrial Rho (Miro) protein (Tang B.L. et al., 2016). Miro is a small GTPase member of Ras superfamily and possess three unique features. It possesses two GTPase domains instead of the one found in other small GTPases, and it also possess two EF-hand calcium-binding domains, which allow the fine tuning of its function by calcium. Importantly, it specifically associates with mitochondria via a hydrophobic transmembrane domain. In humans there are two paralogs: MIRO1 and MIRO2 (Fransson A. et al., 2003). A yeast two-hybrid-based screen indicated that the *Drosophila* orthologue dMiro interacts with the protein Milton, a kinesin adaptor (Giot L. et al., 2003). Subsequently, this interaction was verified also between Miro and the mammalian Milton homologues OIP106/TRAK1 and GRIF-1/TRAK2 (MacAskill A.F. et al., 2009). The MIRO/TRAK complex seems to interact also with a variety of other factors, such as the mitochondrial fusion factors Mfn1 and Mfn2 (Misko A. et al., 2010) and other proteins involved in neurodegenerative disorders (discussed in Section 3.4). Its role in neurodegenerative disease is explained also by the fact that MIRO is involved in the axonal and dendritic transport of mitochondria. Axonal mitochondrial transport, both anterograde and retrograde, relies on the microtubule-based motors, namely the kinesin family proteins and dynein (Sheng Z.H. et al., 2014), and MIRO is associated with both of these classes of motor proteins.

Mitochondrial dynamics regulate mitochondrial recruitment to critical subcellular compartments and allow content exchange between them. Here, the contacts between mitochondria and other cellular organelles will be discussed.

Mitochondria are localised close to the plasma membrane in various mammalian cell types. Interestingly, most mitochondria move far from the plasma membrane after Drp1 or Fis1 overexpression, indicating that mitochondria are connected to the plasma membrane only at few points (Frieden M. et al., 2006). Connexin 32 (Cx32), a structural subunit of gap

junctions, has emerged as an interactor of different mitochondrial proteins in a proteomic study performed in murine hepatocytes, perhaps explaining how mitochondria are transiently tethered to plasma membrane in microdomains enriched in Cx32 (Fowler S.L. et al., 2013). However, most of the molecular components and physiological functions of mitochondria-plasma membrane contacts sites in metazoan remain unclear. Recently, the first molecular and functional characterization of a mitochondrion-plasma membrane contact site was reported in yeast, but metazoan homologues of the identified proteins are unknown (Klecker T. et al., 2014).

Despite their different evolutionary origins, mitochondria and peroxisomes share a close interrelationship. The two organelles are involved in common metabolic pathways, such as  $\beta$ -oxidation of fatty acids and scavenging of peroxides. Peroxisomes and mitochondria can be observed in close proximity in ultrastructural studies in mammalian cells and can also be biochemically co-purified. Drp1 and its receptors Fis1 and Mff in mammals are key components of the division machinery of both mitochondria and peroxisomes (Schrader M. et al., 2016; Koch A. et al., 2003). Human Pex11 $\beta$ , a peroxisome-specific integral membrane protein involved in peroxisome division, is able to deform peroxisomal membrane interacting with Fis1 and Mff (Kobayashi S. et al., 2007). Another shared protein between them is ganglioside-induced differentiation-associated protein 1 (GDAP1), a putative glutathione-S-transferase, which has been linked to Charcot-Marie-Tooth neuropathy (Huber N. et al., 2013), discussed in Section 3.4.

The contacts between mitochondria and ER will be discussed in Section 3.2.

Growing evidences also revealed that contacts with the plasma membrane and peroxisomes may have a role in mitochondrial dynamics and inheritance, suggesting that mitochondrial function is determined by interactions with multiple cellular organelles. It is worth to consider likely that additional, but poorly characterized, contacts with other organelles exist and have a role in these processes.

#### **4.1.3 Endoplasmic Reticulum (ER): Dynamics and Connections**

The ER is the largest membrane-bound organelle in the eukaryotic cell, but was one of the last to be discovered. Although the ER was originally described in 1902 by Emilio Veratti

(Veratti E., 1961), only 50 years later George Palade by electron microscopy “rediscover” it and make its discovery accepted by the scientific community (Palade G.E., 1955). The ER is composed of a single continuous membrane that forms a network presenting multiple domains with different structures and functions. The two major domains of the ER are the nuclear envelope (NE) and the peripheral ER (Figure 5). The NE is a distinct domain of the ER comprised of two large, flat membrane bilayers, the inner and outer nuclear membranes (INM and ONM). The INM and ONM are separated by the perinuclear space (PNS), but are connected to each other at nuclear pores (Hetzer, M.W. et al., 2005). The peripheral ER branches out of the ONM as an extensive network of sheets (or cisternae) and tubules that extends into the cytoplasm all the way to the plasma membrane.

An ER sheet is composed of two flat opposing membrane bilayers stacked over each other with a luminal space between them of 30nm in yeast and 50nm in mammals with regions of membrane curvature only at their edges (West M. et al., 2011). This consent to ER sheets to be packed with maximum efficiency (Terasaki M. et al., 2013). ER tubules are highly dynamic structures that interconnects all the domains of the ER. ER tubules have a luminal diameter of ~30nm in yeast and 50nm in animal cells, as ER sheets, but are characterized by a higher membrane curvature at their cross-section (Shibata Y. et al., 2010). Early electron microscopy studies found that sheets were covered with ribosomes, so are the so called “rough” ER, whereas tubules were largely devoid of ribosomes and therefore represent the “smooth” ER, suggesting that this structural difference was mirroring also a difference in their functions. It is now known that ER sheets, the rough ER, are the primary location for the translation, translocation, post-translational modification and folding of proteins (Voeltz G.K. et al., 2002; Shibata Y. et al., 2006).

The functions of ER tubules, the smooth ER, are less well understood, but they may be the primary regions where lipid synthesis and signalling between the ER and other organelles occur. The ratio of ER sheets to ER tubules varies in different cell types, based on cells’ metabolic roles. For instance, in cells with a high capacity to secrete proteins, such as pancreatic cells, ER sheets are abundant; whereas cell types that secrete few proteins, such as neurons, muscle cells, and epithelial cells, present a more abundant tubular network (Baumann O. et al., 2001).

Several integral membrane proteins have been implicated in the generation and maintenance of the various structural domains within the ER. Multiple regions of high membrane curvature in the ER are stabilized by the reticulon and DP1/Yop1 proteins: these regions include ER tubules and the edges of the sheets (West M. et al., 2011).

The reticulons belong to a family of conserved integral membrane proteins. In mammals, the four reticulon genes (RTN1, RTN2, RTN3, and RTN4/Nogo) encode several protein isoforms by alternative splicing (Oertle T. et al., 2003). All reticulons have a core reticulon homology domain (RHD) located at their C-terminus. The RHD consists of two hairpins transmembrane domains separated by a hydrophilic loop (Yang Y.S. et al., 2007). The N- and C-terminal domains, along with the hydrophilic loop within the RHD, all face the cytosol. The transmembrane hairpins are particularly short and are characterized by the particular feature of protruding more from the outer leaflet of the ER membrane than in the inner leaflet, this leads to membrane twist and so to the creation of regions of high curvature (Voeltz G.K. et al., 2006). The reticulon positioning in the ER membrane is depicted in Figure 5. The reticulon proteins also form immobile oligomers on the ER membrane (Shibata Y. et al., 2008). The structure of these oligomers probably determines the diameter of the tubules. The N-terminus region is very different between reticulon paralogs and their isoforms (Yang Y.S. et al., 2007), suggesting that different reticulons may have specialized functions.

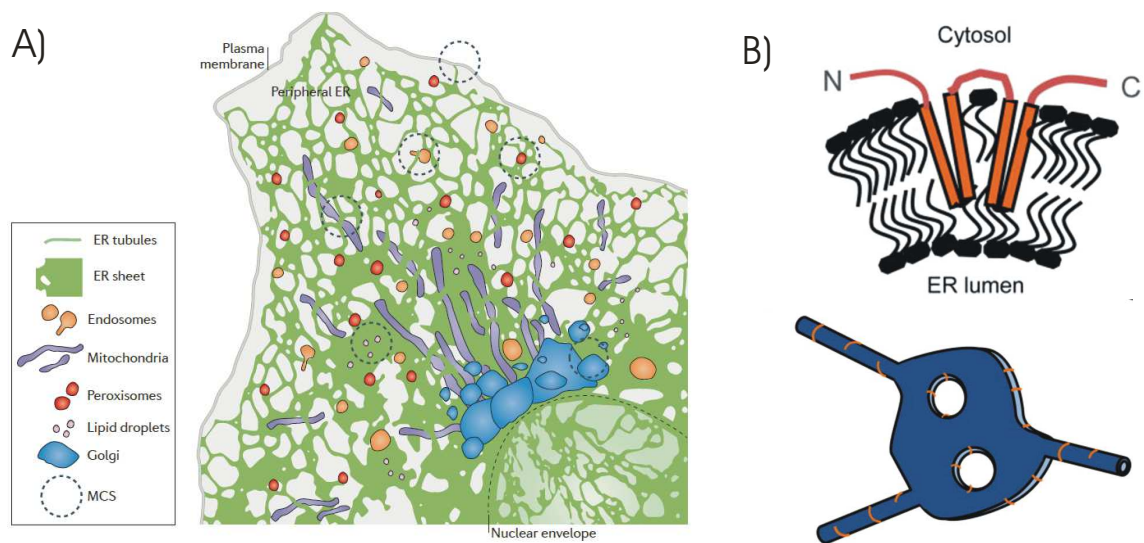


**Figure 5: ER structure, contacts and shape maintenance.**

**A)** The ER consists of a nuclear envelope (outlined with a sharp line) and the peripheral ER which is spread into the cytosol and is divided in sheets (or cisternae) and tubules. The peripheral ER forms membrane contact sites (MCS) with the plasma membrane, mitochondria, endosomes, peroxisomes, lipid droplets and Golgi (from Phillips M.J. et al., 2016). **B)** Top: Schematic of reticulon topology in the outer leaflet of the ER. Long transmembrane domains increase outer leaflet area relative to inner leaflet area, generating membrane curvature. Bottom: Schematic of ER cisternae and tubules (blue) indicating regions where reticulons (orange) have been observed to localize and shown to regulate membrane curvature, including ER tubules and the edges of cisternae and fenestra (from Friedman R. et al., 2011).

Defective in polyosis 1 (DP1), also known as REEP5, is part of the REEP family proteins (REEP1–6) and it is a ubiquitous membrane protein that has been described as regulator of ER tubules. Yeast DP1 (Yop1) is an abundant ER protein that, together with Rtn1, maintains ER structure. Like reticulons, DP1/Yop1 has been found in peripheral ER tubules and is absent in NE and peripheral sheets. It possesses two short hairpin transmembrane domains, similar to reticulons. It is able to form quasi-stationary homo-oligomers that surround the ER membrane, increasing its curvature (Hu J. et al., 2008). In contrast, very little is understood about ER sheets. In addition, other peripheral ER subdomains can be defined in the ER by their unique functions and locations, such as the ones in contact with other organelles.

The ER is the only cellular organelle that remains continuous also during cellular division (Friedman J.R. et al., 2011). To keep this feature, new ER tubules have to perform constitutive and efficient fusion when they come in contact with other ER membranes. Several recent studies have evidenced the presence of ER-localized GTPases able to mediate the fusion of ER tubules. Among these, atlastins are a family of conserved dynamin-related GTPases found in many eukariotes (Hu J. et al., 2009). Three atlastin paralogs (ATL1, ATL2, and ATL3) encoded in mammals are differentially expressed in various tissues. A unique feature of atlastin compared to other dynamins, is the presence in the C-terminus of two putative transmembrane domains, which are thought to form a hairpin, and the presence of a hydrophilic domain, that allow the exposition of most of the protein in the cytosol (Zhu P.P. et al., 2003). In this way, the structure of the atlastins resembles that of another family of large GTPases, the mitofusins (Chan P.P. et al., 2006). However, the catalytic mechanism is different compared to mitofusins, because atlastins expose a catalytic arginine finger (R77)

in the GDP-bound state to stimulate GTP hydrolysis (Byrnes L.J. et al., 2013). Similar to reticulons and DP1/Yop1, atlastins are localized in peripheral ER tubules and are not found in NE and peripheral sheets (Orso G. et al., 2009). The organization of the ER is required not only to maintain ER function, but also of the health of the whole cell. Recently, mutations in proteins affecting ER morphology, described above, have been related to several human diseases, including neurological disorders (discussed in Section 3.4).

The ER has been shown to form contact sites with almost all the other membrane-bound organelles present in the cell, including the plasma membrane, mitochondria, lipid droplets, Golgi, endosomes, and peroxisomes, as represented in Figure 5 (Friedman J.R. et al., 2011). For Golgi, peroxisomes and lipid droplets there is an additional complexity due to the fact that their biogenesis starts on the ER membrane itself (Phillips M.J. et al., 2011).

Initially believed to be a feature observed only in muscle cells, specialized apposed membrane stretches between the ER and the plasma membrane are increasingly recognized as being ubiquitously distributed in all eukaryotic cells (Stefan C.J. et al., 2013). A direct contact between ER and plasma membrane is constituted by the “plasma membrane-associated membrane of the ER” (PAM). Previous studies have identified the PAM as sites of phosphatidylinositol metabolism, non-vesicular transfer of sterols, and  $\text{Ca}^{2+}$  level regulation (Baumann N.A. et al., 2005). During ER  $\text{Ca}^{2+}$  depletion,  $\text{Ca}^{2+}$  is transported from the plasma membrane, by the process of store-operated  $\text{Ca}^{2+}$  entry (SOCE). At ER-plasma membrane junctions, STIM1 and STIM2 proteins act as resident  $\text{Ca}^{2+}$  sensors and interact with the calcium channel protein Orai1 to form a  $\text{Ca}^{2+}$ -released-activated- $\text{Ca}^{2+}$  influx (CRAC) channel to facilitate the entry of  $\text{Ca}^{2+}$  into the ER (Liou J. et al., 2005; Feske S. et al., 2006). The interaction between STIM and Orai1 at plasma membrane-ER contact sites is depicted in Figure 6.

The intricate relationship between the ER and peroxisomes includes cooperation in various metabolic pathways, such as the biosynthesis of ether-phospholipids as myelin, which starts in peroxisomes and is completed in the ER, the formation of glycosylphosphatidylinositol (GPI)-anchored proteins in the ER, and the production of polyunsaturated fatty acids (Schrader M. et al., 2013). It is well known that the ER is involved in the generation of peroxisomes as well as in the regulation of their function. However, a physical interaction between the ER and peroxisomes has been reported only in few studies.

The Golgi forms membrane contact sites with the ER to regulate the transfer of secreted proteins and lipids (Glick B.S. et al., 2009). The relationship between the ER and Golgi is mediated by anterograde, retrograde, and direct non vesicular transport between the membranes of the two organelles (Ladinsky M.S. et al. 1999). Lipid-binding proteins involved in lipid exchange between the two organelles include the ceramide- transfer protein (CERT), the glycosylceramide-transfer protein Golgi-associated four-phosphate adaptor protein 2 (FAPP2; also known as PLEKHA8) (D'Angelo G. et al., 2007), the phosphatidylinositol-transfer protein NIR2 (PYK2 N-terminal domain interacting receptor 2) (Litvak V. et al., 2005), and the cholesterol- and phosphatidylinositol-4-phosphate (PtdIns(4)P) -transfer protein oxysterol-binding protein (OSBP) (Mesmin B. et al., 2013). All the four proteins are characterized by two domains: a PH domain that is able to bind to PtdIns(4)P on the Golgi, and an FFAT motif that is interacting with the ER-localized proteins VAPs (Loewen C.J.R. et al., 2003). PtdIns(4)P is the recruiting factor of all these proteins to the Golgi, so it become of crucial importance to understand how Golgi PtdIns(4)P levels are regulated. A recent elegant study has displayed that OSBP can control both PtdIns(4)P and sterol transfer at ER–Golgi contact sites, because of its ability to bind both sterols and PtdIns(4)P thanks to its oxysterol-binding-related (ORD) domain. OSBP can regulate the transfer of sterols from the ER to the Golgi and viceversa the transfer PtdIns(4)P from the Golgi to the ER. This process is controlled by a feedback mechanism: OSBP dissociates from the Golgi when PtdIns(4)P levels at Golgi are low, and this also eliminate direct transfer of sterols from the Golgi to the ER (Mesmin B. et al., 2013). This process is represented in Figure 6.

The contacts between the ER and mitochondria will be discussed in the next session 3.2.

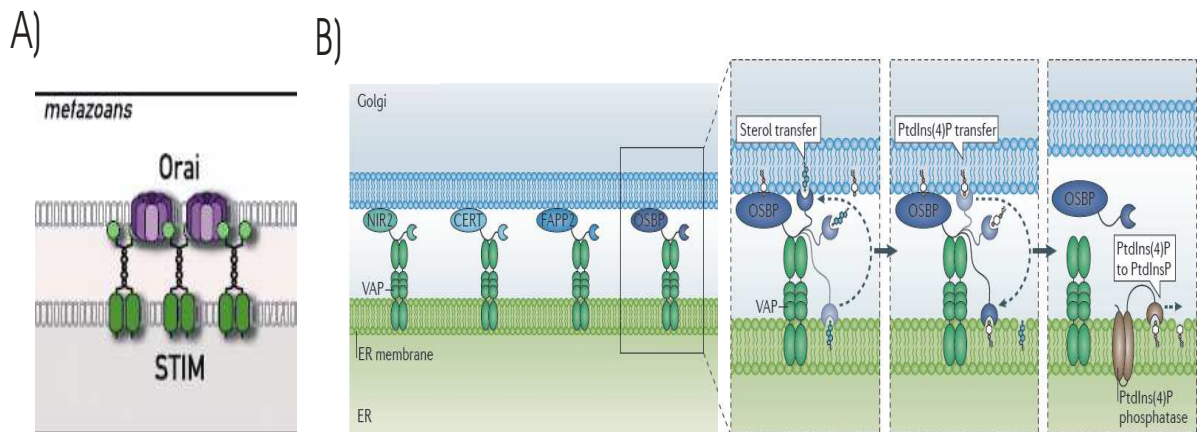


**Figure 6: ER interactions with plasma membrane and Golgi.**

A) Potential tethers between the ER and the plasma membrane in metazoan. At ER-plasma membrane junctions, STIM1 and STIM2 act as resident  $\text{Ca}^{2+}$  sensors and interact with the calcium channel protein Orai1 to form a  $\text{Ca}^{2+}$ -released-activated- $\text{Ca}^{2+}$  influx (CRAC) channel to facilitate the entry of  $\text{Ca}^{2+}$  into the ER (adapted from Helle S.C.J. et al., 2013). B) Multiple potential lipid-transfer proteins localize to the Golgi membrane and interact with ER proteins VAPs. These include the phosphatidylinositol-transfer protein NIR2 (PYK2 N-terminal domain-interacting receptor 2), the ceramide-transfer protein (CERT), the glycosylceramide-transfer protein Golgi-associated four-phosphate adaptor protein (FAPP2) and the cholesterol and phosphatidylinositol-4-phosphate (PtdIns(4)P)-transfer protein oxysterol-binding protein (OSBP). Studies specifically on OSBP (right panels) show that it associates with the Golgi membrane through PtdIns(4)P binding. The OSBP oxysterol-binding-related domain (ORD domain) can bind and transfer sterol from the ER to the Golgi and PtdIns(4)P from the Golgi to the ER. When PtdIns(4)P levels are depleted at the Golgi, OSBP dissociates from the Golgi membranes. PtdIns(4)P at the ER is then converted back to PtdInsP by ER-associated PtdIns(4)P phosphatase (from Phillips M.J. et al., 2016).

## 4.2 MAMs (Mitochondrial associated membranes) and MERCs (Mitochondria-ER contact sites)

One of the best characterized inter-organelle connection sites is that between ER and mitochondria. The first observation of sites of physical interaction between the membranes of the two organelles was obtained 50 years ago by electron microscopy (Copeland D.E. et al., 1959). The biochemical isolation of mitochondria-ER contact sites was achieved about 30 years ago by Jean Vance, who purified a fraction ("fraction X") with structural affinity to microsomes, but which showed cosedimentation with mitochondria upon Percoll

separation, leading to the hypothesis that a subfraction of the ER could be physically associated with mitochondria and was called MAMs, standing for “Mitochondria-associated ER membranes” (Vance J.E., 1990).

In broader terms, a mitochondria-ER contact site (MERC) appears in electron microscopy as the close apposition of the cytosolic face of OMM with the smooth or the rough ER membrane (Giacomello M. et al., 2016). In both situations, the length of the contacts between the two membranes is approximately 100 nanometers (Sood A. et al., 2014), with the two membranes being ~10 to ~80nm separated. These contacts sites are represented in Figure 7. “MERCs” and “MAMs” are often thought to represent the same entity, but they are different. The term “MERC” is related more to the structural and physical architecture and organization of contact sites between the two organelles and to the specific cellular functions that can take place on this particular structural compartment. The term “MAM”, instead, defines the molecular composition of proteins and lipids that form the MERCs, obtained by biochemical isolation. It has been recently proposed to use the term MAMs when referring to results obtained from the biophysical purification and biochemical characterization of mitochondria–ER contacts; and the term MERC when structurally describing this compartment, also by imaging (Giacomello M. et al., 2016).

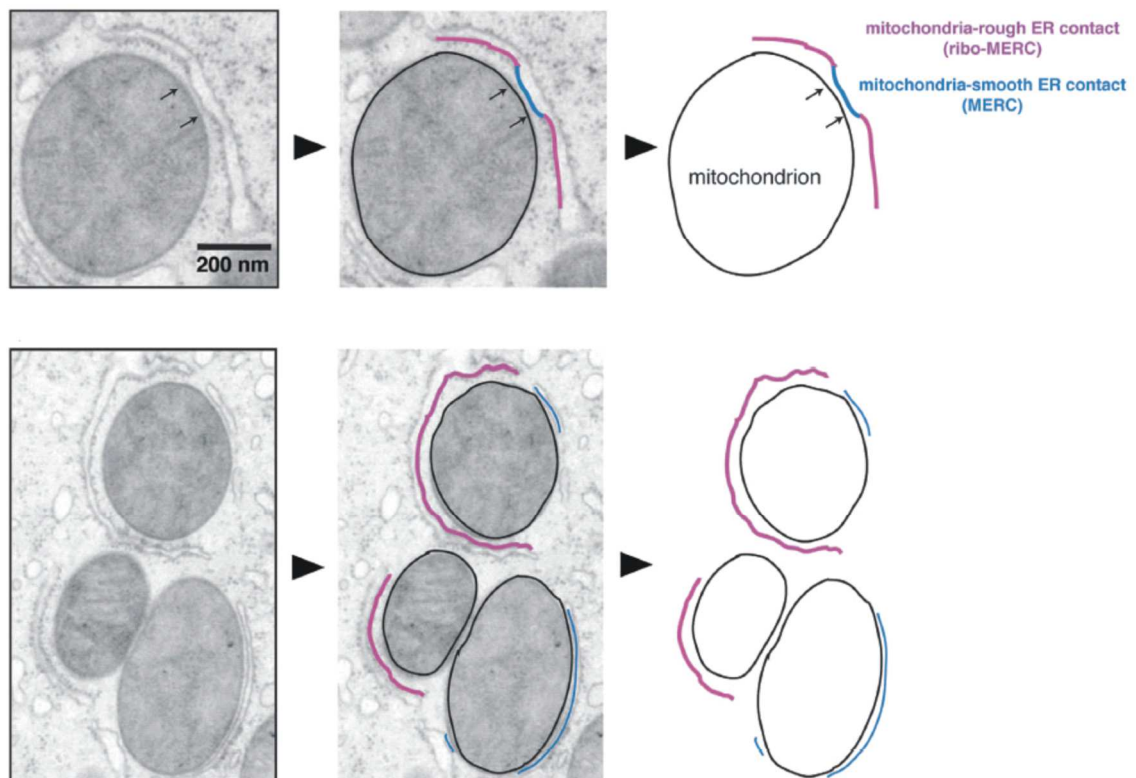


**Figure 7: Mitochondria form contact sites with the ER (MERCs).** MERCs are formed both with the smooth ER and with the ribosome-containing rough ER. These two types of structures can exist as part of a single unit (top) or as separate entities (bottom) (from Giacomello M. et al., 2016).

MERCs are defined by their number, length, and thickness. These parameters are tightly regulated in the cell and their slight variation can impact on the function of this cellular compartment and the whole cell. To date the thickness of the MERC, the only structural parameter, has been poorly analysed and whether this is a rigid or is varying according to the cellular needs has not been studied extensively, even though recent findings suggest this possibility. In the early phases of ER stress close ER–mitochondria contacts increase 2.5-fold (Bravo R. et al., 2011). During apoptosis the distance between mitochondria and ER, measured by electron microscopy, is reduced from 28.2nm to  $\cong$ 20nm (Csordas G. et al., 2006). In mouse liver both MERCs thickness and length are regulated by the metabolic state of the cells: upon nutrient deprivation, the average MERCs thickness increases from 14 to 20nm, and the average contacts length increases from 145 to 270nm. Interestingly, the number of MERCs is not altered in this condition, pointing out that the fulfilment of the

physiological processes is more influenced by the proportion of mitochondrial surface that is in contact with the smooth ER, which increases from 4 to 11%, and not by MERCs density (Sood A. et al., 2014). It is still not possible to conclude that different MERCs structural parameters are associated with distinct cell types. However, the observations that in mouse hepatocytes at least 25% of mitochondria is forming MERCs and that in HeLa cells from only 5 to 20% of the mitochondrial network surface is in contact with the ER, supports a scenario in which MERCs dynamics ultrastructure reflects key aspects of cell biology and metabolism (Giacomello M. et al., 2016).

After the discovery of the MAMs, the efforts in understanding their functional role have pointed out that this unique subcellular compartment carries out a multitude of functions, that will be discussed in the next session.

#### **4.2.1 Functions of MERCs**

Unravelling the mechanisms regulating communication between ER and mitochondria is critical given its impact on a wide variety of cellular processes, from pro-survival responses to apoptosis, mitochondrial dynamics,  $\text{Ca}^{2+}$  transfer, cell signalling, autophagy and cancer.

The first direct evidence that the distance between ER and mitochondria is sufficiently narrow to allow a synapse-like interaction in living cells was achieved by a GFP-based approach (Rizzuto R. et al., 1998). This finding was then confirmed in *Saccharomyces cerevisiae* with electron microscopy and tomography that allowed the 3D reconstruction of the structure of ER–mitochondria contacts, unveiling that these ER–mitochondria contacts might be involved in the formation of mitochondrial constriction sites (Friedman J.R. et al., 2011). The mitochondrial fission protein Drp1 concentrates at the sites where ER tubules surround the mitochondrial membrane, pointing to a crucial role for the ER–mitochondria association in the initiation of mitochondrial fission. The ER–mitochondria interactions are independent from the mitochondrial fission machinery: in fact, the ER remains able to form mitochondria constriction sites even when Drp1 or Mff are down-regulated. A potential mechanism for ER association induced by mitochondrial fission, involving actin polymerization and the ER protein Inverted Formin 2 (INF2) has been proposed (Korobova F. et al., 2013). At the mitochondria–ER contact sites, INF2 is activated and causes actin

polymerization, which in turn leads to the initial mitochondrial constriction. INF2 can contribute to actin polymerization by interaction with the actin-nucleating protein Spire1c, localized to mitochondria (Manor U. et al., 2015).

ER-mitochondria contact sites might also influence mitochondrial fusion. Mfn2 is crucial for tethering ER to mitochondria. Mfn2 in fact localizes not only to the OMM, but also to the cytosolic side of ER and is able to form both homo and heterotypic interactions with the other mitofusin Mfn1 (De Brito O.M. et al., 2008). Mfn2 activity in this compartment is controlled by a mitochondrial ubiquitin ligase called MITOL (Sugiura A. et al., 2013). MITOL binds mitochondrial, but not ER localized Mfn2, and catalyzes the addition of lysine 63-linked polyubiquitin chains, without triggering Mfn2 proteasomal degradation. Surprisingly, this polyubiquitination causes the formation of Mfn2 oligomers, a fundamental step in the tethering between ER and mitochondria due to Mfn2. Thus, MITOL is able to increase Mfn2 activity and so to regulate MERCs formation. The discovery of this double role for Mfn2 in mitochondrial fusion and ER-mitochondria contact formation indicates that ER-mitochondria contacts might be important for Mfn2 regulated mitochondrial fusion. Overall, these observations emphasize that the modulation of ER-mitochondria contacts can act as a main regulator of mitochondrial dynamics (Marchi S. et al., 2014).

Calcium transfer from ER to mitochondria through the MERCs is essential in both pro-survival responses and cell death by apoptosis. Indeed, variations in the proximity between ER and mitochondria have as consequence a modification of  $\text{Ca}^{2+}$  transfer efficiency between the two organelles. Constitutive, basal level of calcium transfer is essential for keeping cellular bioenergetics, and when this basal transfer is abolished, cells activate autophagy to guarantee an acceptable energy supply (Càrdenas C. et al., 2010). Also a limited increase in ER-mitochondria contacts can help cells to better face stress conditions that require increased metabolic response (Kopeck K.O. et al., 2010). On the other hand, mitochondrial  $\text{Ca}^{2+}$  overload make cells more prone mitochondria to apoptotic stimuli (Decuypere J.P. et al., 2011). High matrix  $\text{Ca}^{2+}$  levels lead to the opening the activation of the permeability transition pore (PTP). PTP opening results in the reduction of the mitochondrial potential, swelling of the organelle and consequent release of pro-apoptotic factors, such as cytochrome c, in the cytosol (Bernardi P., 1999). Thus, if ER-mitochondria contacts are too extensive and prolonged overtime time, the output for the cell can be the

induction of apoptosis. The ultimate reason for the existence of a specialized compartment involved in calcium transfer from ER to mitochondria is due to the fact that the channel responsible for the calcium entry in mitochondria, the mitochondrial calcium uniporter (MCU), displays a very low affinity for  $\text{Ca}^{2+}$  ( $K_D$  of 20-50 $\mu\text{M}$ ) (Clapham D.E. et al., 2007) : to overcome this problem, a concentration  $>10\mu\text{M}$  can transiently develop in the restricted area created by microdomains of close proximity between the membranes of ER and mitochondria, enriched in  $\text{Ca}^{2+}$  channel resident proteins (Giacomello M. et al., 2007). The proteins involved in calcium transfer between the two organelles will be analysed in the next section.

Mitochondrial membrane biogenesis and modifications require the continuous import of membrane phospholipids. The ER is the main site of phospholipid biosynthesis. Because mitochondria are not connected to classical vesicular trafficking mechanisms, they require direct lipid transfer from the ER and the biosynthesis of some phospholipids lies on this communication (Vance J.E. et al., 2014). Phosphatidylserine (PS), synthesized at ER by the enzymes phosphatidyl-serine synthase (PSS1 and PSS2), is transported to mitochondria, where it is converted to phosphatidylethanolamine (PE) by the mitochondrial enzyme PS decarboxylase. Then, PE comes back to the ER and is converted by phosphatidylethanolamine methyltransferase 2 (PEMT2) to phosphatidylcholine (PC), which is finally come back to mitochondria to be part of mitochondrial membranes (Rowland A.A. et al., 2012). All these enzymes are residing in MERCs. Also enzymes related to triacylglycerol synthesis pathway, like fatty acid CoA ligase 4 (FACL4), which catalyzes the binding of fatty acids chains to coenzyme A (CoA), are located at MERCs. Cholesterol metabolites, like acyl-coenzyme A, and enzymes involved in cholesterol metabolism, such as cholesterol acyltransferase-1 (ACAT1/SOAT1) that drives the formation of cholesterol esters, and diacylglycerol acyltransferase are all localised in MERCs. The cholesterol binding protein Caveolin1 (Cav1), besides play a fundamental role in the formation and composition of invaginations of plasma membranes known as caveolae, is highly enriched in MAMs and it has been shown by electron microscopy measurements that absence of Cav1 causes a dramatic decrease both in the number and length of MERCs (Echarri A. et al., 2015). This result may indicate that Cav1 is a fundamental player in MERCs ultrastructure shaping, likely acting by the recruitment of cholesterol that confer to the membranes in this

specific region a peculiar arrangement and rigidity (Sala-Vila A. et al., 2016). Furthermore, a sphingomyelinase located at MERC is fundamental for the production of ceramide, that can then be transported to mitochondria where it is converted in sphingosine-1 phosphate and hexadecenal (Naon D. et al., 2014).

A growing body of evidence also supports a relationship between the MERCs and autophagy. Macroautophagy is a self-eating process, present in all eukaryotes, by which cells is able to surround cytoplasmic contents and organelles within double-membrane vesicles, termed autophagosomes, which then fuse with lysosomes for degradation of their content. This process is essential for cellular quality control because degrade damaged or useless cellular components, and is also an adaptive response to nutrient deprivation (He C. et al., 2009). The origin of the isolation membrane for the formation of autophagosomes has been debated for many years and recently it has been associated to MERCs. It has been shown that, during aminoacid starvation, a phosphatidylinositol 3-phosphate (PtdIns3P)-enriched compartment is formed in cells. This compartment is in relationship with the ER and is required for autophagosome formation (Axe E.L. et al., 2008). Moreover, electron microscopy provided physical evidence of a direct connection between the ER and autophagosomes. Finally, several ER marker proteins localize to autophagosome membranes (Yla-Anttila P. et al., 2009). Increasing evidence supports also a link between autophagosomes and mitochondria: several autophagy-related proteins can localize to this organelle; the autophagic process is regulated by several mitochondrial proteins; the OMM is a main actor in autophagosome biogenesis under starvation conditions (Hailey D.W. et al., 2010). Furthermore, mitochondria–ER connections are critical for autophagosome formation, implying that the ER–mitochondria interface may regulate this process. A further evidence supporting this hypothesis is that when autophagy is induced by starvation, the pre-autophagosome marker ATG14 is localizing to MERCs (Hamasaki M. et al., 2013). Additionally, also ATG5, which is fundamental for autophagosome formation, is observed at MERCs during the synthesis of the phagophore and then retranslocate to the cytosol at the end of the process, hence forming a stable association with the ER and a temporary interaction with the mitochondria (Hamasaki M. et al., 2013). Additionally, disruption of MERCs by KD of Mfn2 can reduce autophagosomes formation, indicating the importance of MERCs integrity for this process (Hamasaki M. et al., 2013). The dual function of Rab32

in the control of MERCs structure and autophagy (Bui M. et al., 2010; Hirota Y. et al., 2009) might also be an indication of an indirect role of ER–mitochondria membranes in autophagosomes formation. Rab32 is a fundamental gene for cellular growth, particularly in connection to mTORC2, a structural protein of the mTOR (mammalian target of Rapamycin) complex crucial for autophagy induction by nutrient deprivation (Colombi M. et al., 2011). mTORC2 localization at MERCs is growth factor-dependent and important in the regulation of MERCs integrity, since mTORC2 deficiency causes MERCs disruption (Betz C. et al., 2013). Furthermore, the interaction between mTORC2 and ribosomes takes place at ER–mitochondria contact sites and this interaction increase in response to growth factor stimulation, and is related also to autophagy induction (Betz C. et al., 2013).

ER–mitochondria contact sites also act as scaffolding hubs for cell signaling. One of the best examples is the insulin signaling pathway, where MERCs integrity seems to be fundamental for effective signal transduction (Tubbs E. et al., 2014). Several components of insulin signaling, and other growth factor pathways, are enriched at MERCs. The protein kinase Akt, for example, localizes at the ER–mitochondria contact sites (Betz C. et al., 2013) where it reduces  $\text{Ca}^{2+}$  release, thus preventing apoptosis (Marchi S. et al., 2008).

MERCs also regulate apoptotic cell death. Mitochondrial Fis1 was reported to interact with ER Bap31 in order to recruit procaspase-8 to MERC, facilitating its activation into caspase-8 (Iwasawa et al., 2011). Several proteins are known to exert their tumorigenic or tumor suppressive functions between the ER and mitochondria. One classical example is the tumor suppressor promyelocytic leukemia protein (PML) that forms there a complex with Akt, reducing  $\text{Ca}^{2+}$  transfer from ER to mitochondria (Giorgi C. et al., 2010). Moreover, the most important tumor suppressor p53 can modulate tumor formation via a  $\text{Ca}^{2+}$ -dependent pathway. p53 has been observed at MERCs, regulating the ER-mitochondria communications and the  $\text{Ca}^{2+}$  transfer from the ER to the mitochondria, leading to  $\text{Ca}^{2+}$  accumulation in mitochondria and to subsequent apoptosis induction (Giorgi C. et al., 2015). Similarly, also the oncogene H-RAS is localized at MERCs and regulates the same pathway of calcium transfer to induce apoptosis.

Recent studies indicate a role for MERCs also in neurodegenerative disorders, as we will discuss in Section 3.4.

#### 4.2.2 Tethering Mitochondria and ER

Electron microscopy indicated that the cleft of a MERC is usually an electron-dense area is composed primarily by proteins. Despite several MAMs proteomic analysis in different tissues which identified about 1000 proteins each (Poston C.N. et al., 2013; Horner S.M. et al., 2015), the overall identity of the MAMs protein composition remains still not completely clarified. Published MAMs proteomes displayed partially overlapping results, indicating that the common proteins found are *bona fide* MERCs resident proteins. The non-overlapping proteins could represent contaminants or may indicate that MAMs are not characterized by a unique protein composition, suggesting that MERCs organization can be cell type specific, to adapt to physiological and metabolic needs of a specific tissue. The majority of the MERCs proteins identified so far are ubiquitous, but the different protein composition of MERCs can be the reason why some cells can be more susceptible to MERCs dysfunctions than others (De Mario A. et al., 2016).

It is essential to stress the difference between a MERC tethering and a MERC resident protein. The first participate in the structural maintenance of MERCs, and are possibly able to dynamically modulate the MERC thickness. The latter is a protein that localizes in MERC membranes and is involved the biochemical activities and the functional regulation of MERCs (Giacomello M. et al., 2016). From this definition, proteins participating in calcium transfer from ER to mitochondria can be considered as MERC resident proteins. In mammals, this process is performed by the cytosolic chaperone glucose-regulated-protein 75 (GRP75), which interacts with the ER transmembrane  $\text{Ca}^{2+}$  release channel, the inositol 1,4,5-trisphosphate receptor (IP3R), and the mitochondrial porin voltage-dependent anion channel (VDAC) in the OMM (Szabadkai G. et al., 2006). This indirect interaction between IP3R and VDAC provides the physical structure necessary for efficient ER-to-mitochondria  $\text{Ca}^{2+}$  transfer. By means of a drug inducible fluorescent inter-organelle linkers, it was elegantly demonstrated that an increase in ER–OMM distance to ~15nm was related to and increased efficiency in  $\text{Ca}^{2+}$  transfer from the ER to the mitochondria, while reducing the thickness between ER-mitochondria membranes to 5nm conversely diminished the calcium transfer efficiency. This seemingly counterintuitive effect is explained by the fact that reducing the distance between the membranes of ER and mitochondria obstructs the

arrangement of IP3R, which has been estimated to project 10nm from the ER membrane toward the cytosol, determining so the optimal spacing required for calcium transfer (Csordas G. et al., 2010).  $\text{Ca}^{2+}$  ions can also be released from mitochondria via the  $\text{Na}^+/\text{Ca}^{2+}$  exchanger NCLX (Palty et al., 2010) and reacquired by the ER  $\text{Ca}^{2+}$  transport ATPase (SERCA) family, residing at MERCs (Lynes et al., 2012). The ER protein sigma-1 receptor (Sig-1R) also localizes to the ER–mitochondria contact sites. Sig-1R forms in the ER lumen a  $\text{Ca}^{2+}$ -sensitive chaperone by binding to Glycoprotein 78 (grp78, also named BiP): upon  $\text{Ca}^{2+}$  reduction, Sig1R dissociates from BiP and stabilizes IP3R at MAMs, prolonging  $\text{Ca}^{2+}$  transfer duration (Hayashi T. et al., 2007). The  $\text{Ca}^{2+}$ -binding and ER quality control chaperon calnexin is another MERC resident protein and its localization is mediated by palmitoylation of its cysteines close to the organelle membrane and exposed to the cytosol. When calnexin is less palmitoylated, its MERC distribution is minimized. This enables also a shift in its function: in fact, at MERCs palmitoylated calnexin binds to SERCA2b to modulate  $\text{Ca}^{2+}$  signalling; non-palmitoylated calnexin mainly is conversely involved in protein folding and quality control in rough ER (Lynes E.M. et al., 2013). All these results indicate that chaperone complexes at both organelle membranes could coordinate the modulation of  $\text{Ca}^{2+}$  transfer between ER and mitochondria (Marchi S. et al., 2014).

Electron microscopy images evidenced that 80% of mitochondria have surfaces in close contiguity to the rough ER (Montisano D.F. et al., 1982). Here the distance between the OMM and the rough ER ranges between ~50 and ~80nm. Recent findings suggest that mitochondria are tethered to the smooth ER by distinct mechanisms compared to the rough ER, with grp78/BiP, an ubiquitin ligase (E3) localized at ER membrane, being involved in the connection with rough ER (Wang P.T. et al., 2015).

Results obtained in multiple laboratories demonstrated that Mfn2 functions as a tether (De Brito O.M. et al., 2008; Sugiura A. et al., 2013); studies claiming the opposite have recently been published (Cosson P. et al., 2012; Filadi R. et al., 2016), but this opposite finding could be conciliated by hypothesizing that the loss of MERC contacts induces compensatory mechanisms that can rescue the phenotype associated to the Mfn2 deficiency. In mouse hepatocytes the observed average thickness of MERC is ~10nm (Giacomello M. et al., 2016); immortalized Mfn2 KO cells could have more contacts characterized by this thickness, some of which might be involved in  $\text{Ca}^{2+}$  transfer by increasing 1.5–2 folds the

distance between the two membranes. Deeply analyzing the influence of cell confluence and metabolism on the distance between MERCs in Mfn2 KO MEFs will provide insights in the role of MERCs plasticity in cell physiology. Another MERC tether is the ER phosphofurin acidic cluster sorting protein (PACS2), whose KD disrupts ER-mitochondria contacts inducing mitochondria fragmentation due to BAP31 that leads to apoptosis (Simmen T. et al., 2005) and reduces autophagosomes formation, as observed for Mfn2 (Hamasaki M. et al., 2013). Moreover, PACS2 has been shown to interact with calnexin, partially controlling its localization (Myhill N. et al., 2013). Another couple of tethering resident proteins is formed by vesicle-associated membrane protein B (VAPB), an ER resident protein, that by its binding to the OMM protein tyrosine phosphatase-interacting protein-51 (PTPIP51) can modulate the thickness of MERCs (Stoica R. et al., 2014).

In Figure 8, a selection of the resident and tethering proteins at MERCs is represented.

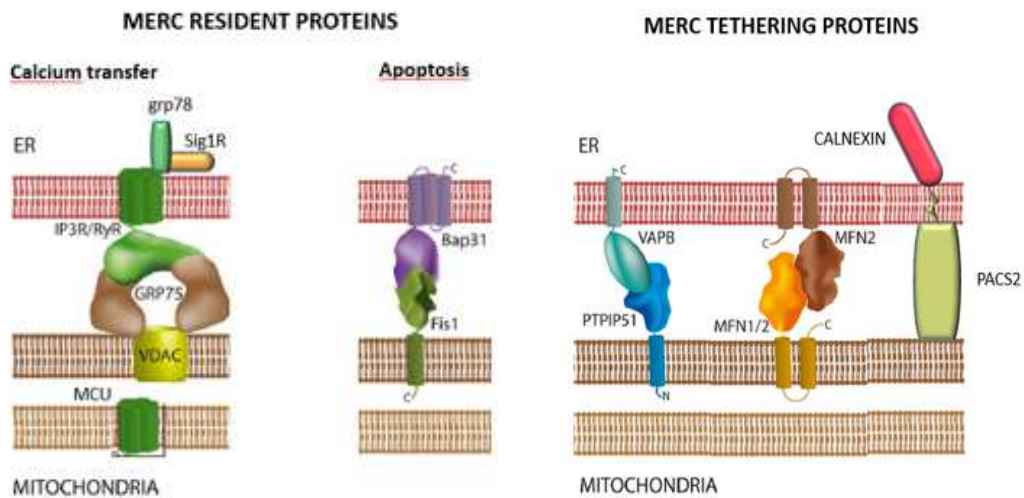


**Figure 8: Representative MERC resident and tethering proteins.** MERC resident proteins are proteins that localizes in the cleft of the MERC and participates in its biochemical activity or functional regulation. The MERC tethering proteins are required for MERC formation and they physically hold together the organelles, possibly, dynamically regulating the MERC thickness. Proteins participating in calcium transfer from ER to mitochondria and in apoptosis can be considered as MERC resident proteins. In mammals, calcium transfer is performed by the cytosolic chaperone glucose-regulated-protein 75 (GRP75), which forms a complex with the ER transmembrane  $\text{Ca}^{2+}$  release channel, the inositol 1,4,5-trisphosphate receptor (IP3R), and the mitochondrial porin voltage-dependent anion channel (VDAC) in the OMM. The ER protein sigma-1 receptor (Sig-1R) also localizes to the ER–mitochondria junctions forming in the ER lumen a  $\text{Ca}^{2+}$ -sensitive chaperone complex with Glycoprotein 78 (grp78) that stabilizes IP3R under calcium depletion. MCU: mitochondrial calcium uniporter, to transfer calcium in mitochondrial matrix. MERC resident proteins involved in apoptosis are mitochondrial Fis1 that was reported to interact with ER Bap31, in order to recruit procaspase-8 to the

MERC facilitating its activation into caspase-8. One example of MERC tethering protein is Mfn2 that can localize on both OMM and ER cytosolic face and form homo and heterotypic interactions with Mfn1. Another MERC tether is the ER phosphofurin acidic cluster sorting protein (PACS2) that is also able to partially mediate calnexin localization interacting with it. Another couple of tethering resident proteins is formed by vesicle-associated membrane protein B (VAPB), an ER resident protein, that binds to the OMM protein tyrosine phosphatase-interacting protein-51 (PTPIP51) and modulates the extent of MERC (modified from Schrader M. et al., 2015).

### **4.3 High Content Screening in Cell Biology**

Cells culture have provided a useful model in understanding many fundamental biological questions. The discovery of RNA interference (RNAi) allowed to perform gene specific functional studies in cell culture. RNAi is a cellular process conserved in fungi, plants and animals. It is thought that RNAi has evolved as a defence mechanism to eliminate double strand RNA (dsRNA) deriving from virus infections (Obbard D.J. et al., 2009). dsRNAs, either introduced into cells or generated by the cells itself, are processed by Dicer, a dsRNA-specific RNase III, to form small interference RNA (siRNAs). These siRNAs, which are kept in the cytosol by binding to exportin60 (Ohrt T. et al., 2006), are then loaded into argonaute 2-containing RNA-induced silencing complexes (RISCs). The relative thermodynamic stability of the two single RNA forming siRNA determines which strand becomes the 'guide', and which will be degraded as pseudo-target. The guide strand is then used by RISC to repeatedly target mRNA recognition, degradation and release. siRNA targeting specificity remains not fully understood (Wilson R.C. et al., 2013). This process is represented in Figure 9.

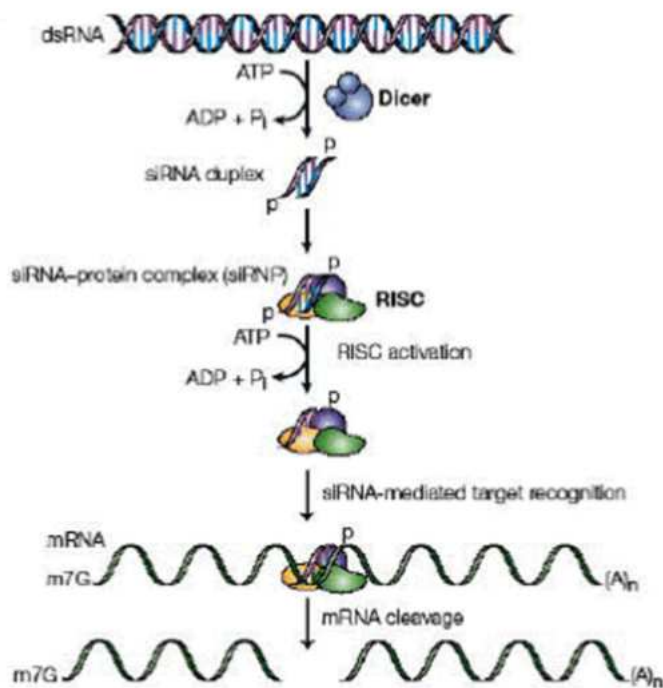


**Figure 9: The siRNA pathway.** Long double-stranded RNA (dsRNA) is digested by Dicer in an ATP-dependant way. Then siRNAs are uptaken by RISC. ATPs are hydrolysed to help unwind of siRNA but the incorporation is ATP independent. The single-stranded antisense strand help RISC to find the target mRNA, and the mRNA is cleaved in the middle of the duplex region (from Dykxhoorn D.M. et al., 2003).

The use of RNAi expanded from small-scale experiments to genome wide screening: the first one was performed in *Caenorhabditis elegans* using dsRNAs (Fire A. et al., 1998). Subsequently, short dsRNAs (shRNA) that mimic siRNAs were shown to trigger a potent and specific genetic downregulation with the same mechanism of RNAi, without activating the immune system (Elbashir S.M. et al., 2001). Various strategies have been developed nowadays to elicit the RNAi pathway and can be optimized in several cellular models. Driven by genome sequence data, RNAi is now widely used in high-throughput screens (HTS) in both basic and applied biology. RNAi has also become a method of election in the development of pharmaceutical compounds, from hit discovery and validation to the analysis of the mechanisms of action of small molecules (Kramer R. et al., 2004).

In parallel with the introduction of the first automated fluorescent imaging systems, the term “High-Content Screening” (HCS) was invented. HCS is defined as a functional screening based on imaging of multiple targets by fluorescent molecules in living cells without altering

physiological conditions (Giuliano K.A. et al., 1997). There are a number of advantages of HCS over other screening technologies. It is a powerful method for addressing many questions in cell biology because, in addition to direct loss of function, can have multiple read out at the same time, such as cell and organelle morphology and cell viability. On the other hand, most HCS based on RNAi are complex and expensive undertakings, requiring significant automation and computing infrastructures, and a combination of disparate skills, ranging from informatics to cell-culture expertise. Although several HCS have already been carried out in both *Drosophila melanogaster* and mammalian cells, this is still an area of huge opportunity especially as new technical advances arise (Krausz E., 2007).

HCS based on RNAi can be used to elucidate a biologically relevant question that is reflected in the assay system of interest. For a precise and meaningful result, this question needs to be well defined, supplemented with a carefully chosen read-out system, followed by an accurate and optimized technical screening procedure. The right cell line should always be defined by the biological question to answer. The read-out system has to be technically stable and robust to avoid misleading background noise, but sensitive enough to detect small changes in the analysed phenotype. The dynamic range of the chosen read-out assay therefore represents the difference between “baseline values” and representative “hit values” that significantly differ from the baseline. Such initial considerations are fundamental as they may predetermine the significance and relevance of potential screening hits (Falschlehner C. et al., 2010).

In recent years, HCS that can provide multi-parametric read-outs, meaning they measure multiple phenotypic features simultaneously, usually by optical microscopy, developed exponentially. Many fluorescence- or chemiluminescence-based assays, by which the activity of a cellular pathway can be investigated, have been developed. HCS based on these fluorescent reporters are typically carried out in arrayed formats using microwell plates with 96- or 384-wells. Although it is more difficult to adapt some assays and cells to the 384-well than to the 96-well format, the 384-well format provides shorter timelines and lower costs. Even if the resolution of these plates is not very high, is still sufficient for the analysis of fluorescent intensity, size, location or morphological changes at the cellular level (Echeverri C.J. et al., 2006). Plastic bottom microtiter plates that reach imaging quality similar to the much more expensive glass bottom plates that had to be used previously, have been

produced. Several High Throughput automated microscopy platforms where laser scanning excitation at various wavelengths is combined with photomultiplier tube detection are now available. The main challenge of microscopy-based HCS remains the storage of large-scale datasets that can easily exceed a terabyte per screen.

#### **4.3.1 Genome Wide Screening with targeted shRNA libraries**

Different RNAi can virtually silence any human, mouse or rat gene, and thus provide a broad potential for finely tuning many biological processes. Importantly, transfection and culture conditions required for efficient silencing sometimes can cause toxicity or perturb cell physiology, altering the readout of the process under scrutiny. Thus, scrupulous optimization of silencing conditions for each individual cell line is required, in order to reach good silencing levels without affecting cell viability.

Most mammalian cell-based RNAi studies rely on siRNAs that are designed to closely mimic endogenous 21bp siRNAs with 2-base overlaps at both 3' ends (Elbashir S.M. et al., 2001) to maximize the possibility of potent target degradation and at the same time minimize the risk of generating off-target effects (Reynolds A. et al., 2004). When it was performed, experimental validation of these libraries has generally yielded to a >70% reduction in target mRNA expression in transformed human cells (Echeverri C.J. et al., 2006). It is worth to note that the silencing threshold necessary to yield a detectable loss of function phenotype depends on the target gene and on the sensitivity of the chosen read-out (Huang F. et al., 2004). The rise of shRNA has led to cheaper libraries that can be delivered with 100% efficiency into nearly any cell type, making this has shRNA approach very powerful. So far, retroviral, adenoviral and lentiviral vectors have been most widely used and several libraries for many model organisms are available. However, given the cell-to-cell variability of expression observed with all shRNA vectors, appropriate controls are necessary (Moore C.B. et al., 2013).

When performing a HTS RNAi screen, the experimenter must define the desired screening paradigm: a systematic screen, targeting each gene individually, or a selection-based screen, using pooled libraries of shRNAs to target many genes at once. The precision of current gene and transcript predictions is fundamental in both approaches. Systematic screening gives the

possibility of working with any group of genes, from a selected subset to the whole genome. This is the most direct approach to RNAi screening, and the most suitable for the range of phenotypes that can be studied. However, the optimization necessary to obtain an assay both sensitive and robust enough in order to provide reproducible results represents a significant challenge (Echeverri C.J. et al., 2006). Moreover, the costs for the elevated amounts of screening reagents and for the instrumentation needed automation are very high. On the other hand, shRNA pools are likely to increase the silencing efficiency and diminish off target effects due to the relatively lower concentration of the individual shRNAs in the respective pool. However, this methodology makes more difficult to associate an observed phenotype to a specific gene. On the contrary, the use of individual shRNA sequences in a screen might facilitate hit evaluation, as it enables target selection on the condition that at least two or more individual shRNAs directed against the respective gene show the same phenotype. Three out of three (3/3) effective shRNAs is rarely observed. More commonly 2/3 effective shRNA are observed. Unfortunately, a high number of 1/3-hits are found, because a certain number of shRNAs shows no effect or exhibits low efficacy. This ratio can also be an indication of an off-target effect. A second independent replicate of the whole screen is therefore recommended for hit confirmation and elimination of false-positives candidates (Krausz E. et al., 2007).

An important issue regarding RNAi screening in general is the possibility of having off-target effects. There are sequence-dependent and independent off target effects and they are controllable by careful experimental design and utilization of appropriate controls. The easiest method for HTS to eliminate sequence-dependent off-target effects is the inclusion of multiple shRNAs targeting the same gene and so causing the same phenotype, as discussed before (Echeverri C.J. et al., 2006). To address sequence-independent off-target effects, necessary controls to be included are the “scrambled” controls, defined as shRNAs without a specific target sequence. These are generally more informative than ‘mock transfection’ in which the silencing reagent is not present, because if scrambled shRNA exhibit a phenotype this can be excluded from the analysis. Moreover, they allow the normalization of all data subsets from different plates into a single coherent data set. Also, positive and negative controls can be introduced if an appropriate read-out is feasible.

Several artefacts can occur during HTS performance and need to be corrected if possible, or verified. The most common artefacts are plate position effects such as edge and positioning effects. Edge effect is due to a different temperature across the plate when the plate is placed in the incubator. The outer wells reach 37°C fastly compared to the inner wells and it has to be addressed if this can cause a different response in the assay readout (Maddox C.B. et al., 2008). It is also possible that particular well positions in the plates affect the silencing efficiency or the read-out system. The overall quality of the obtained results will rely critically on the screen's robustness: this term defines the degree to which all sources of variability affect experimental reproducibility, so a high robustness indicates that an experiment is less perturbed by experimental variables. The miniaturization of the assay system, besides saving time and money, improve the stability of the system and therefore the HCS data quality (Echeverri C.J. et al., 2006).

A common quality criterion for HCS is the  $Z'$ -score that describes the number of standard deviations from the mean. A stable assay should result in a  $Z'$ -score between 0,5 and 1 to enable the separation of hits from the background noise (Zhang G. et al., 2005). A high  $z$ -score reflects a significant deviation of a phenotype from the median of a screen. Moderate phenotypes, reflected by lower  $z$ -scores, can be caused by an incomplete KD of a gene with a strong effect or by a strong KD of a gene with a weak phenotype. Since  $z$ -score is sensitive to outliers, the so-called robust  $z$ -score, where the median and median absolute deviation (MAD), insensitive to outliers, replace mean and standard deviation in the  $z$ -score calculation, is generally considered preferable for RNAi screens (Birmingham A. et al., 2009).

The analysis of raw data from a screen can be complex and time consuming. Computational data analysis methods are commonly used to normalize the data and to correct, for example, for plate position effects. Specific software solutions can be applied for normalization of the screen and for supplying an initial hit list of the strongest phenotypes. In the HCS that we performed cellHTS2, a software package based on the programming language R and the open source platform Bioconductor ([www.bioconductor.org](http://www.bioconductor.org)), specifically designed to analyse RNAi screens capturing both workflow and data analysis (Boutros M. et al., 2006), was used to statistically analyse the obtained data. The final output of the initial data analyses is a list of the strongest candidates in the screen, which can be composed of up to several

dozens of potential hits. As a consequence, secondary assays can be performed with methods independent to those used in the screen to confirm that the observed phenotype is really dependent on the identified candidates. These assays should be specific for the question addressed by the screen, thus eliminating unspecific hits.

#### **4.4 MAMs and Neurodegeneration**

Alzheimer's disease (AD), Parkinson's disease (PD), and Amyotrophic Lateral Sclerosis with Associated Frontotemporal Dementia (ALS/FTD) are neurodegenerative disorders that affect a vast worldwide population. It has been estimated that there are 46 million people in the world with dementia associated with AD and PD (Prince M. et al., 2015). ALS is the motor-neuron disease with the biggest prevalence worldwide with more than 400,000 people affected. Furthermore, ALS is related to FTD by a clinical, genetical and pathological point of view (Ling S.C. et al., 2013). An effective therapy for these neurodegenerative diseases has not yet been developed. It is worth to notice that AD, PD and ALS/FTD present

several features in common, even if the regions of the nervous system involved in the pathology are diverse.

In AD, the main pathological markers are the presence of proteinaceous plaques composed of amyloid beta (A $\beta$ ) peptide in the extracellular matrix in brain and deposits of the microtubule-associated protein Tau within neurofibrillary tangles inside neurons (Goedert M. et al., 2006). A $\beta$  is a 39-43 aminoacids polypeptide and is a natural component of cerebrospinal fluid (CSF) and blood plasma that is soluble under normal conditions, but in pathological conditions it forms insoluble  $\beta$ -sheet-rich fibrillary plaques and diffusible aggregates which are cytotoxic (Sengupta P. et al., 2003). A $\beta$  is originated from the amyloid precursor protein (APP) by proteolytic cleavage performed by two enzymes:  $\beta$ -site APP-cleaving enzyme (BACE1) and the  $\gamma$ -secretase complex. The  $\gamma$ -secretase complex consists of four different proteins: two of these are Presenilins 1 and 2 (PSEN1 and 2) (De Strooper B. et al., 2003). Mutations in APP are causative for some dominantly inherited forms of AD. Moreover, mutations in both PSEN genes also cause familial AD (FAD) (Weggen S. et al., 2012). There is strong evidence that Presenilins mutants linked to AD pathology are catalytic loss-of-function (De Strooper B., 2007).

In the same fashion, accumulation of Tar DNA-binding protein 43 (TDP-43), Fused in Sarcoma (FUS) protein, and dipeptide repeat proteins derived from the C9ORF72 gene are major hallmarks for ALS/FTD: as expected mutations in the genes codifying for these proteins are causative for dominantly inherited forms of the disease (Ng A.S. et al., 2015). The frequency of pathological mutations in the TDP43 gene is approximately 3% in patients with familial ALS as well as 1,5% in sporadic cases (Lattante S. et al., 2013). PD will be discussed in detail in Section 3.4.1. Thus, there is a convergence of pathological features, given by the accumulation of cytotoxic protein aggregates, and evidences of genetics transmission for each one of these three diseases. There is also a significative correspondence in the downstream physiological processes that are damaged in these neurodegenerative diseases, such as mitochondrial damage, Ca<sup>2+</sup> signalling, lipid metabolism, axonal transport, activation of the unfolded protein response (UPR), autophagy and also inflammatory pathways. Since many of these functions are modulated by ER-mitochondria contacts, resolving the role of MAMs in the pathological mechanisms leading

to these disorders may unify several of the previously identified defects that occur during neurodegeneration.

Furthermore, it is now known that ER–mitochondria associations are disrupted in AD, PD, and ALS/FTD (Paillusson S. et al., 2016). PSEN1 and PSEN2, APP and  $\gamma$ -secretase are all enriched in MAMs (Area-Gomez E. et al., 2009; Schreiner B. et al., 2015; Urano Y. et al., 2005). In cell models and patient's fibroblasts from both FAD and sporadic AD (SAD), ER-mitochondria contacts and lipid metabolism related to MAMs were shown to be upregulated. The same upregulation of ER-mitochondria contacts was observed in cells KO for a single Presenilin or double knockout (DKO) for both proteins. Notably, KD of either PSEN1 or PSEN2 is able to reverse phospholipids synthesis defects in Mfn2 KO MEF, meaning they are able to restore a sufficient level of ER-mitochondria contacts (Area-Gomez E. et al., 2012). PSEN1 and PSEN2 interact with IP3Rs and mutations in each gene associated with FAD leads to increased IP3R gating activity and augmented calcium exit from the ER, associated to a closer proximity between the two organelles (Cheung K.H.H. et al, 2011). Slightly different results were performed in cell line expressing PSEN2 mutant, where mitochondria-ER tethering was increased as the  $\text{Ca}^{2+}$  release; while in this case PSEN2 KD is observed a decreased mitochondria-ER proximity and there is no effect for PSEN1 mutant overexpression (Zampese E. et al., 2011). Recently, it has been published that PSEN2 can interact with Mfn2 and that PSEN2 mutants associated with FAD are more effective than the WT form in modulating ER-mitochondria tethering because their binding to Mfn2 in MAMs is favoured (Filadi R. et al., 2016). These studies are apparently contradictory: one group reported that PSEN1 KO increased ER–mitochondria interactions (Area-Gomez E. et al., 2012); whereas another reported that PSEN2 but not PSEN1 overexpression increased these interactions (Zampese E. et al., 2011). A further study showed that PSEN1 mutants were associated with decreased, not increased, ER–mitochondria tethering (Sepulveda-Falla D. et al., 2014). It is well demonstrated that  $\text{A}\beta$  is generated at MAMs and this is consistent with the localisation of Presenilins to these regions of ER. Recently in a cell model of human embryonic kidney 293 (HEK) stably overexpressing APP Swedish mutation, it has been observed that the KD of Mfn2 increases the length of ER stretches in contact with mitochondria and so increasing  $\text{Ca}^{2+}$  transfer from ER to mitochondria. This alteration of ER-mitochondria contacts also leads to a decreased  $\text{A}\beta$  amount due to a reduction of  $\gamma$ -

secretase activity (Leal N.S. et al., 2016). Elevated amounts of PACS2 and Sigma1R, functional proteins in MAMs involved in calcium handling, were measured in both post-mortem analysis of human AD brain and AD mouse models (Hedskog L. et al., 2013). Notably, Sig1R is one of the main player in Tau phosphorylation, thus unraveling the surprising relationship between MAMs and hyperphosphorylated Tau (Tsai S.Y. et al., 2015). Moreover, dysregulation of ER–mitochondria contacts are detected in APP transgenic mouse models. Neurons treated with A $\beta$  peptide exhibit an elevated level of ER–mitochondria contacts, measured by proximity ligation assay, thus further establishing dysregulated MAM signalling as a hallmark of AD (Hedskog L. et al., 2013). Finally, the  $\epsilon$ 4 apolipoprotein (Apo $\epsilon$ 4), linked to an augmented risk of developing SAD compared with the Apo $\epsilon$ 3 allele, has been shown to augment mitochondria-ER proximity (Tambini M.D. et al., 2015). Despite some contradictory results, alterations of MAMs structural and functional feature can account not only for the altered phospholipid, cholesterol and Ca<sup>2+</sup> metabolism observed in AD samples, but also for the excessive A $\beta$  production. Indeed, variations in the MERCs lipid bilayer composition and in the lipid rafts-like structure could affect at structural level the interaction of  $\gamma$ -secretase complex with its substrate, thus enhancing the processing of longer A $\beta$  forms (Uemura K. et al., 2009).

MAMs stability and signalling have been found altered also in several ALS/FTD forms. The P56S mutant form of VAPB protein is enriched at the MAM and is associated with the severe familial ALS type 8 (Nishimura A.L. et al., 2004). The interaction of VAPB with PTPIP51 tightens the tickness at the ER-mitochondria contact sites and results in increased calcium transfer from ER to mitochondria (De Vos K.J. et al., 2012), as discussed in Section 3.2.2. TDP-43 is a negative modulator of this interaction, and a decrease in ER–mitochondria proximity, but also a dramatic reduction of Ca<sup>2+</sup> exchange between the two organelles has been detected when both WT and familial ALS/FTD TDP-43 mutants have been overexpressed in mouse models and motor neuron cell lines (Stoica R. et al., 2014). Moreover, VAPB P56S mutant completely abolish the interaction of Miro1 with tubulin, impinging anterograde axonal transport of mitochondria in rat cortical neurons. This phenotype was reversed by the co-expression of a Miro1 mutant not responding to calcium regulation, stressing the importance of the regulation of calcium signalling at MERCs also in relation to mitochondrial transport (Morotz G.M. et al., 2012). Of note, it has been

previously shown that fibroblasts derived from VAPB P56S patients, as well as neuronal cultures, present intracellular aggregates composed by VAPB and Sigma1R (Hayashi T. et al., 2007). Notably, Sigma1R mutations are also related with ALS/FTD (Al Saif A. et al., 2011; Luty A.A. et al., 2010). It has been shown that is possible to obtain a reduction in VAPB aggregation by Sigma1R activation by drug treatment, leading to neuroprotection (Prause G. et al., 2013); conversely loss of Sigma1R has been shown to reduce ER–mitochondria junctions (Bernard-Marissal N. et al., 2015). The protein linking VAPB to TDP-43, is Glycogen synthase kinase 3 $\beta$  (GSK-3 $\beta$ ) that seems to act as a negative regulator of the VAPB–PTPIP51 binding. Activation of GSK-3 $\beta$  reduces the binding of VAPB to PTPIP51 and so ER-mitochondria contacts; whereas its inhibition increases this binding. During disease, the activation of GSK-3 $\beta$  by mutated TDP-43 can abolish the link between VAPB to PTPIP51, leading to decrease in ER-mitochondria proximity (Stoica R. et al., 2014) (Figure 10).

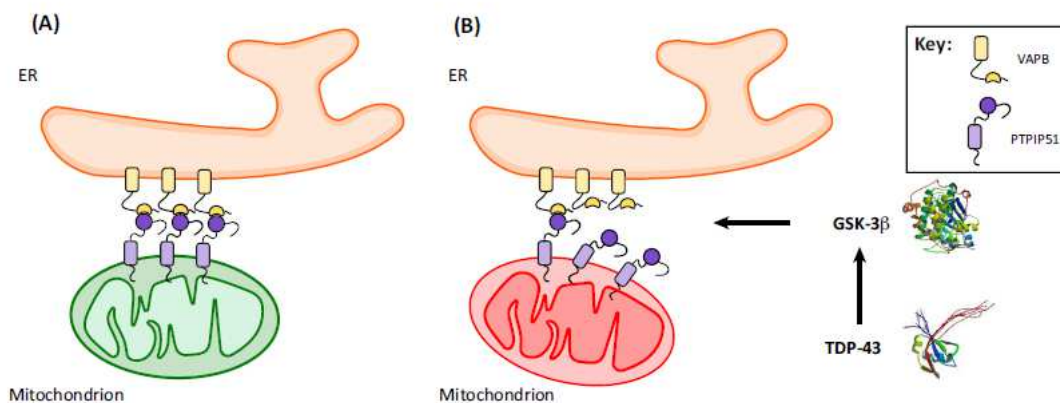


**Figure 10: Tar DNA-Binding Protein 43 (TDP-43) Loosens ER–Mitochondria Associations in Amyotrophic Lateral Sclerosis with Associated Frontotemporal Dementia(ALS/FTD).** (A) Normal situation. PTPIP51 is associated with VAPB at MAMs regulating ER-mitochondria contacts. (B) Disease situation. TDP-43 induces activation of glycogen synthase kinase 3 $\beta$  (GSK-3 $\beta$ ), which then disrupts binding of vesicle-associated membrane protein-associated protein B(VAPB) to protein tyrosine phosphatase interacting protein 51 (PTPIP51) to reduce ER–mitochondria associations and Ca<sup>2+</sup> exchange between the two organelles (from Paillusson S. et al., 2016).

#### **4.4.1 Parkinson Disease and MAMs**

Parkinson's disease (PD) is the second most common neurodegenerative disorder after AD, affecting about 2% of the worldwide population older than 60 years (Gribkoff V.K. et al. 2016). Generally, pathological onset before age 20 is defined as juvenile-onset; onset between 20 and 50 years of age is classified as early-onset; and onset after age 50 is referred as late-onset. The overall age- and gender-adjusted incidence rate is 13.4 per 100,000, with men being more affected than women (19 vs. 9.9 per 100,000). The incidence of PD is not influenced by ethnicity, however it seems less diffused among African Americans (Van Den Eeden S.K. et al., 2003).

The cardinal clinical features of PD include resting tremor, stiffness of the muscles (rigidity), slowness of movements (bradykinesia) and balance disturbance (Rodriguez-Oroz et al., 2009). In addition to the typical motor symptoms, various non-motor features may develop, such as autonomic dysfunctions, sleep disturbances, depression and anxiety, cognitive impairment and olfactory loss, indicating a more widespread degenerative process (Goldman J.G. et al., 2014).

A definitive diagnosis of PD can be obtained only by post mortem analysis of brain tissue based on two decisive features: degeneration of neurons in the substantia nigra pars compacta (SNpc) that are responsible for dopamine (DA) production, that leads to the strong depletion of DA inside the striatum, and characteristic intra-neuronal inclusions termed as Lewy Bodies (Alexander G.E., 2004). Lewy Bodies are proteinaceous aggregates found inside neuronal cell body that are enriched in  $\alpha$ -synuclein, ubiquitin, neurofilaments and molecular chaperones (Spillantini M.G. et al., 1997). Pharmacological treatment with DA can slow the progression of the motor symptoms, but its efficacy decays over time (Savitt J.M. et al., 2006). To date, there are no therapies that directly target the underlying disease mechanisms or stop PD progression.

The sporadic form of PD, accounting for more than 90% of the cases, is seen as a complex multifactorial disorder where both environmental factors and genetic susceptibility provide a significant contribution. A number of environmental risk factors have been evaluated for their role in disease susceptibility: smoking has consistently been reported to result in a 50% of decrease in the risk of developing PD. Serious head trauma has also been found in multiple studies to increase the risk of PD. (Lai B.C. et al., 2002). To unravel the mechanisms of

PD a series of experimental models were developed and used in different species, but the two most common toxin-induced PD models are the 6-hydroxy-dopamine (6-OHDA) model and the 1-methyl-4-phenyl-1,2,3,6-tetrahydropyridine (MPTP) model (Schoder A. et al., 2004). Since its first description in 1959, 6-OHDA has played a fundamental role in preclinical research on PD. 6-OHDA is a compound structurally similar to catecholamines, DA and noradrenaline, and for this it can act on catecholaminergic neurons (Simola N. et al., 2007). It has been shown that 6-OHDA injection unilaterally into the SN of a rat to obtain the so called "6-OHDA Ungerstedt model" of rotation is able to mimic the pathological features of PD (Ungerstedt U. et al., 1970). Thus, oxidation of 6-OHDA by monoamine oxidase (MAO-A) generates hydrogen peroxide ( $H_2O_2$ ) which, besides being highly cytotoxic *per se*, triggers the production of oxygen radicals (Cohen G., 1984). In addition, 6-OHDA can self-oxidate producing more  $H_2O_2$ , reactive oxygen species (ROS) and catecholamine quinones which strongly bind to endogenous nucleophilic groups (Palumbo A. et al., 1999). An augmentation in levels of ROS and other reactive species, triggered by 6-OHDA, causes a fast reduction of cellular antioxidant enzymes, consequently resulting in a broad neurotoxicity causing abnormalities in cell structure and metabolism and eventually leading to neuronal damage (Blum D. et al., 2001).

In 1980s, a rapid-onset, dopamine-responsive parkinsonism was observed in users of heroin that were also relatively young. The toxin causing the outcome of the pathology was identified as MPTP, a compound that after metabolic processing is preferentially reuptaken at synaptic terminal sites. The inhibition of complex I of the mitochondrial electron transport chain caused by MPTP is the ultimate cause of the pathology onset, thus implicating mitochondrial dysfunction as a notable cause of PD. Subsequently, it was shown that activity of complex I is selectively reduced also in the SNpc of patients with idiopathic PD as well (Schapira A.H. et al., 1989). As oxidative stress had been obviously linked to the development of MPTP-induced parkinsonism, it was straightforward to focus on environmental oxidants and inhibitors of mitochondrial respiration to search for valuable PD models (Garrett E. et al., 2004). The mechanisms of 6-OHDA and MPTP are represented in Figure 11. Both Paraquat (N, N'-Dimethyl-4,4'-bipyridinium dichloride) and Rotenone, two pesticides, are strong inhibitors of mitochondrial complex I, and both have shown to be potentially neurotoxic (Subramaniam S.R. et al., 2013). While neuronal toxicity of Paraquat

is not specific for dopaminergic neurons, Rotenone has been shown to generate an excellent model of PD in rodents when dispensed chronically in low doses (Greenamyre J.T. et al., 2003). However, administration of rotenone leads to high mortality in rats and, somehow, is difficultly reproducible because neurodegeneration has also been detected in non-dopaminergic systems (Blesa J. et al., 2014).

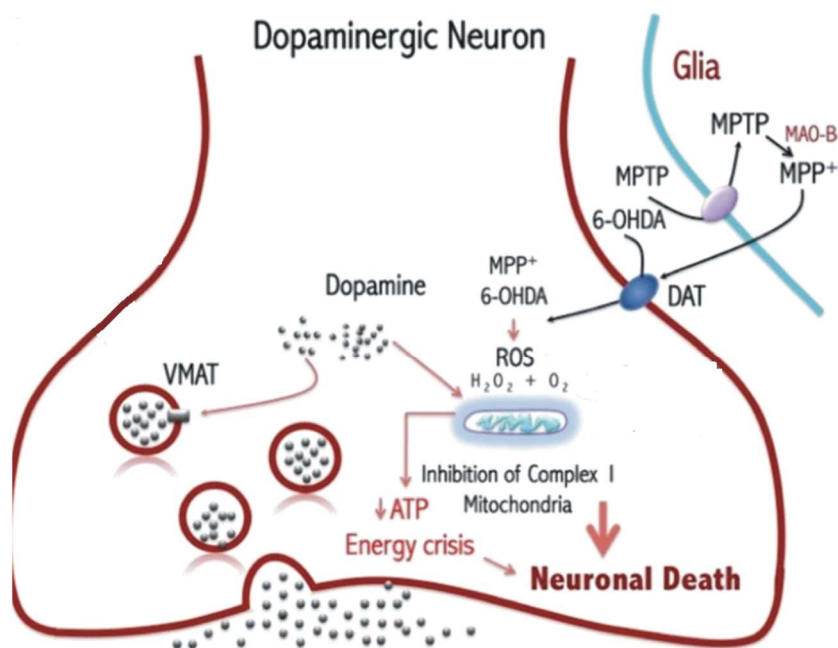


**Figure 11: Neurotoxic mechanisms of dopamine (DA) and neurotoxins used to mimic PD in the dopaminergic neuron.** DA and the neurotoxins 6-hydroxydopamine (6-OHDA) and 1-methyl-4-phenyl-1,2,3,6-tetrahydropyridine (MPTP), cause reactive species of oxygen (ROS) affecting the mitochondrial function, which leads energy crisis and neuronal death. MPTP is first incorporated into the glial cells and metabolized to MPP<sup>+</sup>, this metabolite can cross the membrane through the DA transporter (DAT) to reach intracellular compartments in dopaminergic neuron, while 6-OHDA can directly cross through DAT. vesicular monoamine transporter (VMAT) (modified from Rangel-Barajas C. et al., 2015).

For many years PD was thought to be strictly influenced by environmental factors without a substantial genetic contribution to disease etiology, but in 1996 the mapping and the subsequent identification of the first mutations responsible for PD indisputably showed that PD may be hereditary (Polymeropoulos M.H. et al., 1996). In the actual PD genetic terminology 18 specific chromosomal locus, are named PARK to evidence their assumed

relationship with PD etiology and numbered based on their identification date (Klein C. et al., 2012). Until now, a number of loci associated to PD have been identified, and for six of them, the corresponding genes have been characterized. Four loci (Park1/4, Park3, Park5 and Park8) have been associated with autosomal dominant forms of PD, whereas Park2, Park6, Park7 and Park9 have been associated with autosomal recessive forms. Although no corresponding gene is known for loci Park3 and Park9, the other loci have been associated to  $\alpha$ -synuclein gene (Park1/4), Parkin (Park2), UCHL1 (Park5), PINK1 (Park6), DJ-1 (Park7) and LRRK2 (Park8), respectively (Ryan B.J. et al., 2015). These loci and the genes with which they are associated are summarized in Table 1.

Locus Name	Gene Symbol	Protein Product	Mode of Inheritance	Types of Mutations	% of Affected Individuals
PARK 1/4	SNCA	$\alpha$ -synuclein	Dominant	Missense/Gene multiplications	Rare
PARK2	PRKN	Parkin	Recessive	Missense, non-sense, frameshifts insertions, deletions, duplications	50% early onset PD
PARK5	UCHL1	Uchl1	Dominant	Missense mutation	one family
PARK6	PINK1	PTEN-induced putative kinase	Recessive	Missense, non-sense, frameshifts insertions, deletions,	1-7% early onset PD
PARK7	DJ-1	Protein DJ-1	Recessive	Missense, frameshifts, deletions	Rare
PARK8	LRRK2	Leucine-rich repeat kinase 2	Dominant	Missense	Most common cause of familial PD

**Table 1: Causative genes for Parkinson Disease** (modified from Pankratz N. et al., 2007).

SNCA was the first gene with mutations reported to cause autosomal-dominant PD in an Italian family, the Contursi cohort. Patients with SNCA mutations usually have early-onset PD (Polymeropoulos M.H. et al., 1997). Although, mutations in SNCA are generally rare and to date only five different missense mutations as well as duplications and triplications of the entire gene have been observed (Ferreira M. et al., 2016). The first identified mutation, A53T, is so far the most common (Klein C. et al., 2012). Other identified mutations are A30P and E46K (Pankratz N. et al., 2007). More recently, two new point mutations have been

reported: H50Q and G51D (Appel-Cresswell S. et al., 2013; Lesage S. et al., 2013). Intriguingly, an interrelationship between the clinical symptoms and the level of gene expression has been postulated, given that triplications of SNCA gene are related with an earlier onset, more severe symptoms and faster disease progression compared to duplications (Fuchs J. et al., 2007; Ross O.A. et al., 2008). However, in contradiction, three SNCA duplications were found in a sample of 906 screened subjects (<1%): only one of the three positive patients had a familiar cases of PD. Importantly, in all the three families, there were asymptomatic individuals who carried the duplicated allele, indicating an incomplete penetrance of SNCA duplicated allele, linking it to sporadic PD (Ahn T.B. et al., 2008). The SNCA gene is composed of six exons codifying a 140 aminoacids cytosolic protein expressed in quite large amounts:  $\alpha$ -synuclein, described as a component of Lewy Bodies (as previously discussed in this section), thus establishing a link between sporadic and familial forms of PD (Spillantini M.G. et al., 1997).  $\alpha$ -synuclein consists of three domains: the amino-terminal region (aa 7–87) contains seven imperfect repeats, each 11 amino acids in length, and is partially overlapping with a central hydrophobic domain (aa 61–95), so-called NAC (non-A $\beta$  component), and an acidic, negatively charged carboxy-terminal domain (aa 96–140) (Stefanis L., 2012). It is evident that all five missense mutations affect the amino-terminal domain. Although the native conformation of the protein is almost completely unfolded with very few elements of secondary structure, once it interacts with the phospholipid present in membranes by the repeats in the N-terminal,  $\alpha$ -synuclein changes its conformation into a  $\alpha$ -helix rich structure (Giasson B.I. et al., 2001). Intriguingly, the protein presenting one of the three-point mutations tend to form stable  $\beta$ -sheets and so intensify the formation of toxic aggregates. For this reason, the current hypothesis is that the missense SNCA mutants are toxic gain of function, and so lead to PD (Bertoncini C.W. et al., 2005). The domain and the 3D structure of  $\alpha$ -synuclein with the described point mutations are represented in Figure 12.

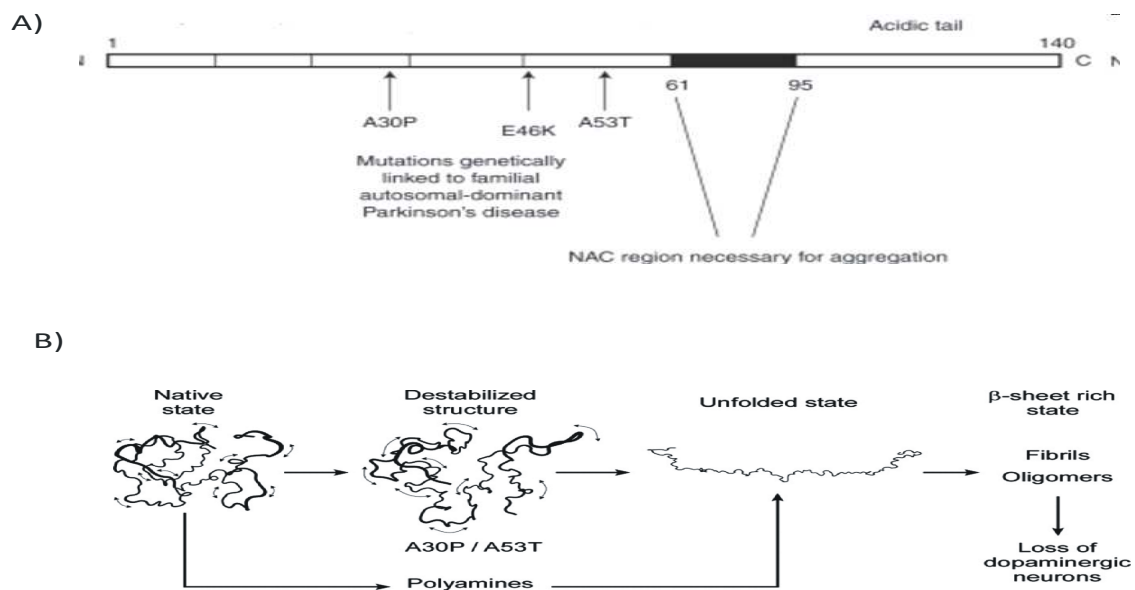


**Figure 12: Linear and 3D protein structure of  $\alpha$ -synuclein with its pathological mutations.**

A)  $\alpha$ -synuclein consists of three domains: the amino-terminal region (aa 7–87) contains seven imperfect repeats, each 11 amino acids in length, and is partially overlapping with a central hydrophobic domain (aa 61–95) so-called NAC (non-A $\beta$  component), and an acidic, negatively charged carboxy-terminal domain (aa 96–140) (from Stefanis L., 2012). B) The two familial Parkinson's disease associated mutants A30P and A53T perturb the long range interactions essential for the native state of  $\alpha$ -synuclein. Long range interactions characterize the auto-inhibited native state of  $\alpha$ -synuclein, maintaining the protein in a soluble innocuous state. Mutants can overcome more easily the energetic barrier for self-association, leading to an increased tendency to oligomerize. Polyamine binding and high temperature, conditions that *in vitro* enhance aggregation, induce a completely unfolded structure (from Bertoni C.W. et al., 2005).

The co-segregation of PD with a I93M mutation in ubiquitin carboxy-terminal hydrolase-L1 (UCHL1) (Park5), was observed in a couple of German sibling. The clinical symptoms were comparable with the ones observed in idiopathic PD, including as a response to dopamine and age of onset at 49 and 50 years (Leroy E. et al., 1998). Hundreds of PD patients were screened, but to date no patients presenting I93M or any other mutations in UCHL1 have been reported (Healy D.G. et al., 2006) and no additional families have been reported so far (Ferreira M. et al., 2016).

The last gene associated with autosomal dominant PD, LRRK2 (Park8) will be discussed deeply in the next section.

The second identified PD gene was Parkin (Park2) and it was also the first gene associated to autosomal recessive PD. In autosomal recessive forms, the onset is between 30 and 40 and the progression is generally slow (Olszewska D.A. et al., 2015). However, some of the patients carrying Parkin mutations show a very early onset even in childhood: homozygous mutations in Parkin are in fact the most common reason for juvenile PD (Kitada T. et al., 1998). A large number and broad variety of Parkin mutations has been reported for all 12 exons of the gene (Lohmann E. et al., 2003). Parkin is a E3-ubiquitin protein ligase containing a ubiquitin-like (Ubl) domain at the N-terminus, RING-between-RING (RBR) domains at the C-terminus, and an atypical RING domain, RING0, in its linker region (Arano T. et al., 2015). Parkin participates in the degradation of specific substrates, including  $\alpha$ -synuclein, and is believed that mutations in Parkin abolish its fundamental ubiquitination activity. Parkin structure is represented in Figure 13.

Mutations in the phosphatase and tensin homolog (PTEN)-induced putative kinase 1 (PINK1) (Park6) gene are the second most common cause of autosomal recessive early onset PD, but are also reported in 2-4% of sporadic cases (Kumazawa R. et al., 2008). Point mutations, frameshift mutations and missense mutations have been found throughout the gene. Patients with PINK1 mutations present common points with sporadic late onset PD; but they can also present atypical symptoms such as dystonia at onset, sleep benefit, and psychiatric disturbances. It is thought that PINK1 mutations exhibit a high penetrance (Bonifati V. et al., 2005). PINK1 is a 581 amino acid protein kinase that is broadly expressed. It is composed of an amino-terminal 34 aa mitochondrial targeting sequence followed by a transmembrane domain, a conserved serine–threonine kinase domain (aa 156–509), and a carboxy-terminal autoregulatory domain (Cardona F. et al., 2011), represented in Figure 13. Two thirds of the reported mutations in PINK1 are loss of function affecting the kinase domain, indicating the fundamental role of PINK1's enzymatic activity in the pathogenesis of PD (Wasti A.Z. et al., 2015).

Parkin and PINK1 act within the same cellular pathway which is involved, via targeted degradation of dysfunctional mitochondria, in the quality control of the organelle network, with PINK1 upstream of Parkin (Narendra D. et al., 2008). Under physiological conditions with normal mitochondrial membrane potential, PINK1 is fastly eliminated and scarcely detectable; in contrast, with a reduction in mitochondrial membrane potential, PINK1

accumulates on the OMM cytosolic face, acting as a molecular indicator of damaged mitochondria (Okatsu K. et al., 2015). PINK1 then can recruit Parkin to damaged mitochondria and activate it. PINK1 is able to phosphorylate both Ser65 in the Ubl domain of Parkin and the ubiquitin present on OMM: the subsequent interaction between phospho-ubiquitin and phospho-parkin consent the conformational changes needed to expose the active catalytic site of Parkin in the cytosol, thus activating it, and so allowing the degradation of damaged mitochondria (Matsuda N. et al., 2016). Recent studies indicated also a role for PINK1/Parkin in the biogenesis of mitochondrial-derived vesicles, that cargo mitochondrial content to lysosomes in an autophagy-independent manner (Mc Lelland G.L. et al., 2014). PINK1 protein structure and the mechanism of action with Parkin is depicted in Figure 13.

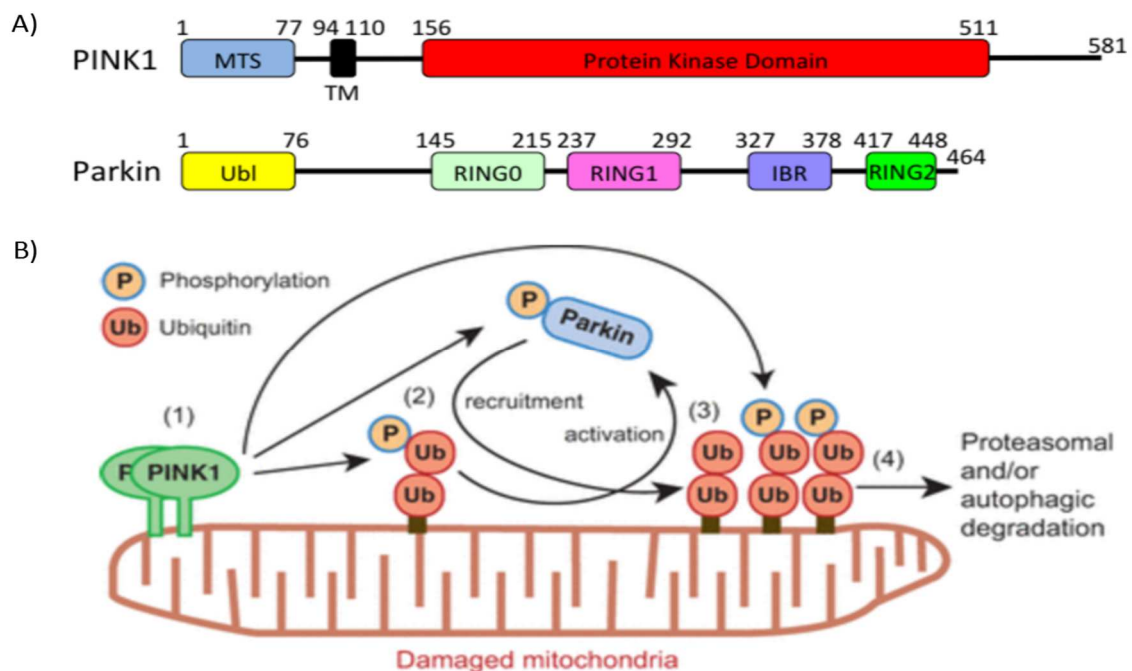


**Figure 13: PINK1 and Parkin structures and mechanism of action.**

A) Schematic structures of PINK1 and Parkin proteins MTS: mitochondrial targeting sequence, TM: transmembrane region, Ubl: ubiquitin-like domain, RING: really interesting new gene domain, IBR: in between RING domain. Numbers indicate the positions in the amino acid sequence (from Aranu T. et al., 2015). B) Accumulated PINK1 on damaged mitochondria (1) phosphorylates Parkin and ubiquitin, which (2) induces Parkin activation and its recruitment to the phosphorylated ubiquitin chain. Activated Parkin produces more ubiquitin chain (3), and the resultant ubiquitin is phosphorylated by PINK1 in a positive feedback cycle.

Parkin thus functions as an amplifier of the (phospho-)ubiquitin chain on depolarized mitochondria (4) for degradation (from Matsuda N. et al., 2016).

Daisuke-Junko 1 (DJ-1) is the last gene related to autosomal recessive PD, and it is found mutated in around 1–2% of early onset PD cases (Pankratz N. et al., 2006). DJ-1 associated PD cases are uncommon and very small number of patients have been described; nevertheless approx. 10 point mutations and exonic deletions have been reported (George J.L. et al., 2009). DJ-1 codifies for a 189aa ubiquitous protein conserved in eukariotes that is involved in oxidative stress detection (Taira T. et al., 2004), resulting in oxidation of cysteine residue at position 106 (Canét-Aviles R.M. et al., 2004). It is believed that once DJ-1 is oxidized it can function as a chaperone that includes among its substrates also  $\alpha$ -synuclein, and acts to prevent protein fibrillogenesis, aggregation, and misfolding (Shendelman S. et al., 2004). DJ-1 is found as dimer in physiological conditions (Macedo M.G. et al., 2003), and it seems that the majority of DJ-1 mutants related to PD are able to heterodimerize with wild-type DJ-1 (Takahashi-Niki K. et al., 2004). In addition, the mutated proteins are frequently not properly folded, unstable, and fastly degraded by the proteasome, this of course lead to a dramatic reduction in the neuroprotective and antioxidant role exerted by the protein (Malgieri G. et al., 2008).

Both toxic and genetic models of PD point to an important role for mitochondria in PD pathogenesis: from inhibition of complex I to alterations in mitochondrial DNA, mitochondrial dynamics, apoptosis, mitophagy and MERCs, leading to the so called “mitochondrial hypothesis” for PD etiology (Franco-Iborra S. et al., 2015). Moreover, as discussed in Section 3.4., many altered cellular processes in neurodegeneration are regulated by MERCs, so the relationship between PD and ER-mitochondria dynamics will be analysed in the next paragraph.

$\alpha$ -synuclein can also localize at MAMs (Guardia-Laguarta C. et al., 2014) where it increases the calcium exchange from the ER to the mitochondria, and conversely overexpression of  $\alpha$ -synuclein has been reported to increase calcium transfer between the two organelles, pairing with an up-regulation of mitochondria–ER contacts in human cells. As expected, a KD of  $\alpha$ -synuclein reduces ER-mitochondrial transfer (Cali T. et al., 2012). Remarkably, PD-linked  $\alpha$ -synuclein mutants are not localized at MAMs, leading to a reduced formation of ER-

mitochondria contacts (Guardia-Laguarta C. et al., 2014) likely impinging the interaction with lipid rafts for A30P mutant, or through reduced amounts of total  $\alpha$ -synuclein for A53T mutant (Fortin D.L. et al., 2004).

Parkin substrates include numerous proteins localised at MERCs, as Mfn2 (Gegg M.E. et al., 2010) and Miro1 (Liu S. et al., 2012). In cultured rat neurons, glutamate excitatory stimulation triggers the accumulation of Parkin at mitochondria, ER and at ER-mitochondrial junction, without the activation of mitophagy (Van Laar V.S. et al., 2014). Parkin overexpression is associated with an increase in ER and mitochondria contacts both from a physical and a functional point of view, stimulating ATP production and calcium transfer. Conversely, acute Parkin depletion has the opposite effect, altering mitochondrial morphology in cell lines (Calì T. et al., 2013). However, it has been recently reported that the ER-mitochondria contacts, measured by EM and confocal microscopy, are increased in primary fibroblasts derived from Parkin KO mice and patients carrying Parkin mutations. The same phenotype has been observed in neurons derived from iPSc of a patient with Parkin mutations. Higher levels of Mfn2 have been found at MAMs from Parkin KO tissues, and Mfn2 downregulation is able to restore the normal calcium transfer between ER and mitochondria (Gautier C.A. et al., 2016). A role for PINK1 in ER-mitochondrial communication has not been reported. However, PINK1 participates in mitochondrial transport, a process that is regulated also at MERCs level (Liu S. et al., 2012). PINK1, via Parkin, drives to proteasomal degradation Miro1/2, the complex necessary for mitochondria transport along the axons, and Mfn1/2 (Tanaka A. et al., 2010; Wang X. et al., 2011). DJ-1 is able to regulate mitochondrial calcium levels by enhancing ER-mitochondria tethering. Reduced DJ-1 levels lead to mitochondrial fragmentation and to reduced mitochondrial calcium uptake in stimulated cells, indicating that damaged ER-mitochondrial connection may have a role in mitochondrial dysfunction observed in PD (Ottolini D. et al., 2013). Parkin, DJ-1 and PINK1 can all bind grp75 (Li Y. et al., 2005; Davison E.J. et al., 2009), a finding that could, at least partially, explain the defects in mitochondrial  $\text{Ca}^{2+}$  transfer reported in PD patients.

Overall, these findings converge to suggest that disturbances of ER-mitochondria contact might play a critical role in PD pathogenesis.

#### 4.4.2 LRRK2: Genetic and Structure

In 2002, Funayama and colleagues set a connection between PD and a region on chromosome 12 containing 116 genes by studying a large Japanese family, the Sagami-hara kindred, with autosomal-dominant parkinsonism (Funayama M. et al., 2002). However, only in 2004 mutations of the gene for Leucine-Rich Repeat Kinase 2 (LRRK2) were identified as the underlying genetic cause of PD associated to chromosome 12 locus (Paisan-Ruiz C. et al., 2004). The genetic region was termed Park8 and the causative gene for the disease encodes for protein LRRK2, named also dardarin from “dardara” which means tremor in basque (Paisan-Ruiz C. et al., 2004). Mutations in the gene encoding for LRRK2 are the most frequent cause of familial PD (Singleton A.B. et al., 2013). The clinico-pathological features of PD related to LRRK2 mutations are nearly identical to idiopathic PD based on age of onset, presence of Lewy bodies and responsiveness to dopamine treatment (Kalia L.V. et al., 2014). These findings, coupled with the discovery that LRRK2 polymorphisms are related with augmented risk for onset of sporadic PD during life (Nalls M.A. et al., 2014), indicated that LRRK2 can be a very good model for a deep understanding of the molecular mechanisms of PD.

The precise physiological role of LRRK2 has not yet been clarified, even though it is involved in a plethora of cellular processes (Wallings R. et al., 2015). LRRK2 is a 2527aa protein, conserved from *C. elegans* to humans (Liu et al., 2011), comprising two different enzymatic core domain. The GTPase domain, composed by a Ras of complex (ROC) domain with a spacer domain called C-terminal of the Roc-domain (COR) at its end, is followed by the kinase domain, member of the serine/threonine kinase family. This enzymatic core is encompassed a series of by protein-protein interaction domains such as the armadillo (ARM), the ankyrin (ANK) and the leucine rich repeat (LRR) domains at the LRRK2 N-terminal (Marin I., 2006). At C-terminal is found the WD40 domain that has an important role in protein folding regulating LRRK2 kinase activity (Rudenko I.N. et al., 2012) (Figure 14).

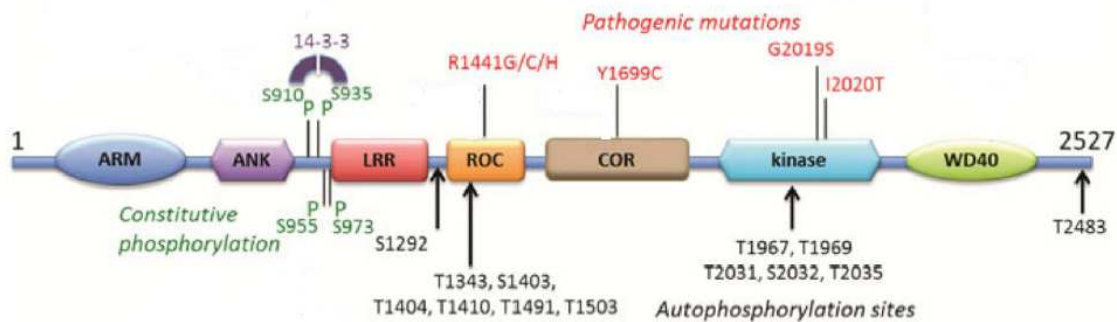


**Figure 14: LRRK2 domain structure, pathogenic mutations, constitutive and auto-phosphorylation sites.** LRRK2 is a 2527aa protein with two enzymatic domains at its core. The GTPase domain, composed of a Ras of complex (ROC) domain ends with a spacer domain called C-terminal of the Roc-domain (COR), followed by the kinase domain, a serine/threonine kinase. This enzymatic core is surrounded by protein-protein interaction domains such as the armadillo (ARM), the ankyrin (ANK) and the leucine rich repeat (LRR) domains at the LRRK2 N-terminal. The LRRK2 C-terminal terminates with the WD40 domain. Pathogenic mutations and susceptibility polymorphisms of LRRK2 are shown in red, constitutive phosphorylation in green and a selection of auto-phosphorylation sites is shown in black (modified from Wallings R. et al., 2015).

Because of its double enzymatic core, LRRK2 is part of the ROCO protein family: only three ROCOs proteins are found in humans except of LRRK2, there are leucine-rich repeat kinase 1 (LRRK1), death-associated protein kinase 1 (DAPK1), and malignant fibrous histiocytoma-amplified sequences with leucine-rich tandem repeats 1 (MASL1). Human ROCOs are able to bind and hydrolyze guanine nucleotides thanks to their ROC domain and this interaction seems pivotal for formation of protein complexes and kinase activity of the same proteins (Civiero L. et al., 2014), indicating that ROC domain is critical for ROCO function regulation. Even though ROCO proteins have been identified more than 10 years ago, their physiological role remains obscure as well as their molecular mechanism of action. The kinase domain of LRRK2 is highly homologue to the one of MLK subfamily of mitogen-activated protein kinase kinase kinase (MAPKKK) (Wang L.H. et al., 2004) and it is very closely related to RIP kinases (Paisan-Ruiz C. et al., 2013). The Roc domain of LRRK2 is a member of small G-proteins family, which are GTP binding proteins that are continuously shifting from an active GTP- and inactive GDP-bound state (Vetter I.R. et al., 2001). The phosphate-binding motif (P-loop) region is the part in the ROC domain able to bind GTP (residues 1341–1348, GNTGSGKT). GTP is also hydrolyzed at ROC domain at a slow rate

thanks to a catalytic Switch II motif (residues 1394–1398, DFAGR) (Biosa A. et al., 2013). The Switch II motif of LRRK2 is characterized by an Arginine (R) residue at position 1398 fundamental for the GTPase activity, while another positively charged Glutamine (Q) residue is found in the same position in most of other small GTPases. In the other ROCO proteins LRRK1 and MFHAS1, at residue 1398 there is a Pro (DIGGP) or Asp (DLAGD) respectively (Marin I. et al., 2008), thereby pointing out the existence of different mechanism of regulation in ROCO proteins compared with other small GTPase.

LRRK1 is the protein most similar to LRRK2, but even if rare variants of LRRK1 have been suggested to be associated with PD, there is no genetic evidence for causal role of LRRK1 in the disease (Schulte E.C. et al., 2014). LRRK1 shows a comparable domain organization with LRRK2 (Civiero L. et al., 2012), but it is reported that each one has a specific subset of interactors and is involved in distinct cellular process (Reyniers L. et al., 2014).

In the brain, LRRK2 is expressed in neurons, astrocytes and microglia (Miklossy J. et al., 2006). By means of in situ hybridisation and immunohistochemistry, it has been detected that in normal brain LRRK2 is found in various neuronal populations such as cerebral cortex, caudate-putamen and hippocampus, as well as in dopaminergic neurons of the SNpc (Higashi S. et al., 2007). It is also expressed in other tissues such as in liver, lung, kidney, heart and immune system (Bae J.R. et al., 2015). Inside the cell, LRRK2 is localized mostly in the cytoplasm but is enriched in lipid raft, early endosomes, lysosomes, synaptic vesicles and plasma membrane as well as in the Golgi complex (Hatano T. et al., 2007) endoplasmic reticulum (Vitte J. et al., 2010) and outer mitochondrial membrane (Biskup S. et al., 2006).

More than 100 LRRK2 genetic variants have been described, but only six mutations (R1441C/G/H, Y1699C, G2019S, I2020T) are linked to PD pathology and all of them are biochemically active (Cookson M.R., 2015). Pathological mutations and their position in LRRK2 are represented in Figure 14.

The most common LRRK2 mutation is G2019S and it is most widespread in Middle East, Portugal, Spain and Italy with a clear north-south gradient in Europe (Diéterlen F. et al., 2010). In Ashkenazi Jews the frequency is 29,7% in familial cases and 13,3% in sporadic PD and can reach approximately 40% in both sporadic and in familial cases in North African Berbers (Olszewska D. et al., 2015). The G2019S is a gain of function mutation that occurs

in the kinase domain, causing a two-fold increase in the protein kinase activity (Rudenko I. et al, 2014). The R1441C, R1441G and R1441H mutations occur in the ROC GTPase domain of LRRK2; the R1441G mutation is particularly frequent in the Basque population where it causes more than 40% of familial PD cases (Gorostidi A. et al., 2009). The Y1699C mutation is found in the COR domain, between the ROC and kinase domains (Melrose H., 2008). The R1441C/G/H mutations exhibited reduced GTP hydrolysis with no or negligible consequences on steady-state GTP binding capacity of the protein (Lewis P.A. et al., 2007; Liao J. et al., 2014), as did the Y1699C mutation (Daniels V. et al., 2011). It has also been shown that R1441C and Y1699C mutant proteins exhibit an altered cellular localisation accumulating within discrete cytosolic pools, resembling inclusion bodies that were hypothesized to be aggregates of misfolded protein (Greggio E. et al., 2006). The disease-related I2020T mutation affects the kinase domain and it exhibits a considerable 40% increase in auto-phosphorylation (Gloeckner C.J. et al., 2006). These studies account for the important role of both enzymatic domains and functions of LRRK2 in PD pathogenesis and indicate a communication between one domain and the other.

Besides its known role in PD, increasing findings indicate that LRRK2 can be involved also in other apparently unrelated human diseases, such as inflammatory diseases, leprosy, and several types of cancer (Bae J.R. et al., 2015). This raises the intriguing hypothesis that LRRK2 may play specific roles based on cell types and tissues where is expressed. This portrait could be possible only with the existence of molecular mechanisms that consent to the same LRRK2 protein to act in different ways in different tissues based on LRRK2 splicing variants, or on tissue-specific expression of LRRK2 activators, substrates and interactors. There is a scarce knowledge on LRRK2 splicing: only one study performed in mice evidenced the existence of 2 splicing variants of LRRK2 in primary neurons, astrocytes and microglia, but further investigations are necessary (Giesert F. et al., 2013). It is much more known that LRRK2 exhibits a large plethora of interactors, due to its peculiar domain structure and LRRK2 interactors will be discussed in the next session 3.4.3.

The main objective of academia and industry is in the development of kinase inhibitors to be used as drugs for treating PD related to LRRK2. Several highly specific LRRK2 kinase inhibitors that can cross the blood brain barrier were created but have still to be optimized in order to be acceptable drug candidates for therapeutic use (Deng X. et al., 2011). However,

accumulation in peripheral tissues, especially in kidneys and lungs, and related drug induced toxicity are still a strong and common problem for all LRRK2 kinase inhibitors (Estrada A.A. et al., 2015). Fundamentally, for clinical use, the long-term benefits of LRRK2 inhibitor treatment should outcome the advantages of the already existing symptomatic treatments for PD (Rudenko I.N. et al., 2012). In this picture, it will be important to expand the search for LRRK2 inhibitors also for other domains besides the kinase domain for example the N- and C-terminus, the GTPase activity of ROC, and taking also in account LRRK2 localization, dimerization, or allosteric modifications of the kinase domain, might significantly improve therapeutic benefits (Lee B.D. et al., 2012). Recently, the first GTP binding inhibitors, compounds 68 and 70, were developed and they were shown to inhibit both GTPase and kinase activity of LRRK2 *in vitro* as well as *in vivo* and consequently reducing neurodegenerative effects in human cell lines and in rodent tissues (Li T. et al., 2014).

#### **4.4.3 LRRK2 Interactome: Partners and Cellular Functions**

The precise molecular mechanism by which the catalytic activity of LRRK2 is controlled is unclear but at least three different processes: dimerization correlated with cellular localization, intramolecular interactions, and binding of substrate to the N- and C-terminal domains seem to be crucial.

LRRK2 is mainly detected as a dimer *in vivo*. Dimerization is due to the interaction between different regions of LRRK2, comprising the ROC domain and lots of points included in the LRR domain (Deng J. et al., 2008). LRRK2 is found in the monomer form, and so nearly inactive, in the cytosol whereas it become mostly dimeric and activated when localized at cellular membranes (Berger Z. et al., 2010). LRRK2 enriched in membranes exhibits an increased molecular mass as well as a 8,4 fold increase in kinase activity respect to cytosolic LRRK2 (Sen S. et al., 2009). LRRK2 double enzymatic core suggests that these two activities could affect each other. Auto-phosphorylation of particular residues (Figure 15) within the ROC domain have been reported to control interaction with GTP (Webber P.J. et al., 2011) especially at T1410 (Pungaliya P.P. et al., 2010) and at Ser1292: this has been proposed as a potential measure for LRRK2 kinase activity (Sheng Z. et al., 2012). On the other hand, hydrolisation of GTP by ROC domain has been shown to enhance LRRK2

kinase activity (Guo L. et al., 2007). In addition, GTP binding is also fundamental the protein kinase activity of LRRK2 (Ito G. et al., 2007). Interestingly, blocking LRRK2 dimerization by means of pathological mutations has an additional effect on auto-phosphorylation levels prolongating kinase activity, thus suggesting that both enzymatic functions are critically influenced dimerization (Deng J. et al., 2008). Together the results may indicate that the ROC-COR domain is modulating kinase activity, the kinase is regulating the GTPase activity of ROC, and both functions are necessary for regulation of LRRK2 cellular localization (Rosenbusch K.E. et al., 2016). LRRK2 dimerization and activation is also controlled by the protein-protein interaction domains retrieved at the N- and C-terminal of the protein. Cellular studies with LRRK2 and related Roco proteins lacking the N- or C-terminus domain, evidenced their importance for signalling *in vivo* (van Egmond W.N. et al., 2010). Deletion of the WD40 repeats brings to reduced dimer levels paired with reduced kinase activity and altered protein localization (Jorgensen N.D. et al., 2009).

Over the last 10 years, many signalling transduction pathways have been related to LRRK2. Among these, LRRK2 has shown to be able interact with and phosphorylate Mitogen Activated Protein Kinase MAP2K 3-4-6 and potentially -7 *in vitro* activating them (Gloeckner C.J. et al., 2009). The ROC-COR domain of LRRK2 was reported to bind with Dishevelled proteins 1, 2 and 3 (DVL1-3), main mediators of the Wntless (Wnt) signalling pathway; interestingly LRRK2 pathogenic mutations were sufficient deteriorate this interactions (Sancho R.M. et al., 2009). This interplay has been better characterized and LRRK2 is now believed to have a role in the classical Wnt cascade interacting with DVL1-3 and other proteins, therefore increasing the Wnt signaling cascade (Berwick D.C. et al., 2012).

LRRK2 was reported to regulate Nicotinic Adenine Acid Dinucleotide Phosphate (NAADP) receptors, with subsequent activation of a calcium signalling cascade, due to the Calcium/calmodulin-dependent protein kinase kinase  $\beta$  (CaMKK- $\beta$ ), that would in the end led to activation of Adenosine Monophosphate activated Protein Kinase (AMPK) coordinating in this way different cellular pathways related to nutrient homeostasis and energetic balance (Gomez-Suaga P. et al., 2012).

Phosphorylation of the eukaryotic initiation transcription factor 4E Binding Protein (4E-BP) by LRRK2 was observed in humans and *Drosophila melanogaster* (Imai Y. et al., 2008).

4E-BP is a downstream effector in the Target of Rapamycin (TOR) pathway and its dephosphorylation during nutrients deprivation reduces protein synthesis (Kumar A. et al., 2010). Also 14-3-3 proteins that have shown to be LRRK2 interactors and are involved in the control of LRRK2 cellular distribution (Nichols R.J. et al., 2010). 14-3-3 proteins can also bind a huge number of target substrates, therefore activating many different signalling pathways, such as AMPK and the TOR.

Different studies demonstrated the role of LRRK2 kinase activity in the stimulation and maintenance of neurite outgrowth. It is generally thought that LRRK2 G2019S mutation can dramatically block neurite outgrowth and branching (MacLeod D. et al., 2006). The explanation for this could be the regulation of LRRK2 by cytoskeletal elements. A high throughput screening to unravel LRRK2 interactome found proteins belonging to the actin family and to the actin-regulatory network as LRRK2 substrates, in line with the observation that LRRK2 is able to regulate actin polymerization *in vitro* (Meixner A. et al., 2011). LRRK2 pathogenic mutant were also found to decorate microtubules in various cell models (Kett L.R. et al., 2012). Additional studies showed that LRRK2 can regulate cytoskeletal dynamics. The depolymerization of actin filaments, a process mediated by the GTPase Rac1, was increased in cell lines after LRRK2 KD or expression of mutant LRRK2 (Chan D. et al., 2011). In neuronal cells from R1441G mutant transgenic mice, as well as in G2019S mutant fibroblasts, LRRK2 make the actin cytoskeleton more prone to depolymerizing agents (Caesar M. et al., 2015). LRRK2 was also reported to phosphorylate moesin (Jaleel M. et al., 2007), a protein involved in regulation of actin and microtubule architecture: G2019S transgenic and LRRK2 KO mice evidenced an augmented actin polymerization in the filopodia that behave as a physical barrier that blocks microtubule protrusions and causes the inhibition of growth of neuronal processes (Parisiadou L. et al., 2009).

The GTPase domain of LRRK2 was shown to pull-down  $\alpha/\beta$  tubulin from cell lysates (Gandhi P.N. et al., 2009) and LRRK2 was co-precipitated with  $\beta$ -tubulin from WT mouse brain extracts, and finally recombinant LRRK2 has been reported to phosphorylate  $\beta$ -tubulin *in vitro* (Gillardon F., 2009). LRRK2 binding to tubulin has been linked to modulation of microtubule stability and acetylation (Law B.M. et al., 2014). The stabilization of microtubules by LRRK2 may be due to LRRK2 binding to protein tau associated with microtubules, as it has been shown that LRRK2 is able to phosphorylate tau in the presence

of tubulin, therefore modifying microtubule-tau binding dynamics, while *in vivo* Tau is observed to be hyper-phosphorylated in brains from R1441G transgenic mice (Kawakami F. et al., 2012).

Strong evidence indicates a role for LRRK2 in various secretory and endocytic pathways. In detail, LRRK2 regulates synaptic vesicle trafficking binding to pre-synaptic proteins such as syntaxin, synaptic vesicle glycoprotein 2A (SV2A), N-ethylmaleimide-sensitive factor (NSF), and Synapsin I (Piccoli G. et al., 2011). LRRK2 was shown to modulate synaptic vesicles endocytosis via association with Rab5b: KD of LRRK2 significantly decreased synaptic vesicle endocytosis (Matta S. et al., 2012). In *Drosophila melanogaster*, LRRK2 was reported to phosphorylate endophilin A (EndoA), so reducing EndoA affinity for membranes and influencing membrane tubulation regulated by EndoA. The G2019S mutation has also been reported to prevent synaptic endocytosis (Shin N. et al., 2008). The LRRK2 pathogenic mutations, G2019S, R1441C and Y1699C displayed augmented Golgi clearance, but the mutation that decrease GTP binding, the T1348N, or the kinase-inactive K1906M mutation abolish Golgi clearance, indicating that both kinase and GTPase activities are required for performing this pathways (Beilina A. et al., 2014). Finally, the G2019S and R1441G mutations tend to increase the expression of dopamine receptor D1 on the membrane surface (Migheli R. et al., 2013). In conclusion, pathological LRRK2 activity might influence vesicle trafficking and release. Along this line, Lrrk2 has been shown to interact with different members of Rab proteins, the Ras family of small GTPases that modulate intracellular vesicular transport, and is composed by ~70 members in humans. They act as molecular switches in the tethering, docking, fusion, and rearrangement of intracellular membranes. Rab7 was found in complex with LRRK2 to promote clearance of Golgi-derived vesicles via the autophagy. Human LRRK2 can interact with Rab7L1, an important player of the autophagic-lysosomal pathway, ablation of Rab7L1 summarizes the dopaminergic neuron depletion verified with LRRK2-G2019S mutation and Rab7L1 overexpression is able to recover mutant LRRK2 phenotypes (MacLeod D.A. et al., 2013). Moreover, LRRK2 binding to Rab5 might also influence the early phase of autophagosome formation (Ravikumar B. et al., 2008). Recently, Rab10 has shown to be the strongest *bona fide* substrate of Lrrk2 kinase in cells. The phosphorylation of Rab10 takes place on a conserved threonin residue, and the same happens for Rab3a and Rab8a. Pathogenic Lrrk2

G2019S mutation increases Rab phosphorylation and this strongly decreases Rab affinity for their regulatory proteins causing the accumulation of inactive Rabs in the membranes, thus establishing Lrrk2 as an important regulator in Rab homeostasis, which is likely contributing to PD development (Steger M. et al., 2016).

Variuos studies correlates PD associated with LRRK2 mutations to mitochondrial defect and alterations in autophagy. In fibroblasts from PD patients carrying the G2019S mutation an anomalous mitochondrial morphology has been detected (Mortiboys H. et al., 2010) and primary mouse cortical neurons expressing either G2019S or R1441C LRRK2 mutations are characterized augmented levels of mitophagy related with abnormal calcium levels (Cherra S.J. et al., 2013). It has been reported that LRRK2 overexpression led to the localization of Drp1 to the mitochondria surface (Wang X. et al., 2012), and co-expression of DLP1 with LRRK2 led to increased levels of oxidative stress, Drp1 recruitment to the mitochondria and induction of mitochondria clearance. Furthermore, expression of LRRK2 G2019S and R1441C in neurons caused mitochondrial fragmentation and enhanced their interaction rate with Drp1, leading also to an increased level of ROS (Niu J. et al., 2012). These findings may indicate that LRRK2 could be involved in mitochondrial homeostasis, likely by a Drp1-dependent, mitochondrial quality control. LRRK2 can bind also to dynamin-related proteins that control mitochondrial fusion such as Mfn1, Mfn2 and OPA1. It has also been reported that LRRK2 partially colocalize with endosomal dynamin-1, Mfn1, Mfn2 and OPA1 at mitochondrial membranes. The subcellular localization and the complexes formation of dynamin GTPases are not influenced by Lrrk2 expression variation in mouse brain, on the contrary levels of OPA1 short form are reduced in brains from patients carrying G2019S mutation (Stafa K. et al., 2014). However, it still not fully clarified if LRRK2 is involved in the maintenance of mitochondrial integrity, and if mitochondrial alteration is a primary pathogenic event in PD associated with LRRK2, or if it occurs only as a secondary consequence (Wallings R. et al., 2015).

Autophagy started to be related to LRRK2 when it was reported that expression of LRRK2 G2019S in in SHSY5Y cells caused the shortening of neurite length and increased the number of autophagic vacuoles. Inhibition of macroautophagy through KD of important autophagy genes was sufficient to reduce the toxicity caused by G2019S LRRK2 overexpression (Plowey E.D. et al., 2013). A subsequent study postulated that LRRK2 is

localized to autophagic vesicles and multivesicular bodies. Moreover, KD of LRRK2 was found sufficient to trigger macroautophagy in HEK293 cells (Alegre-Abarategui J. et al., 2009). The pathways modulating and correlating mitochondrial dysfunction mediated by Lrrk2 in PD and aberrant autophagy are only partially understood, but most very possibly rely the activation of AMPK, MAPK and NAADP (Rosenbusch K.E. et al., 2016).

## 5 Results

### **A genome wide high content imaging screen identifies a novel function for the Parkinson's disease gene LRRK2 as endoplasmic reticulum-mitochondria tether**

Annalisa Serafini<sup>1</sup>, Sowmya Lakshminarayanan<sup>1,2</sup>, Emilie Schrepfer<sup>1,2</sup>, Elena Marchesan<sup>1</sup>, Laura Civiero<sup>1</sup>, Elisa Greggio<sup>1</sup>, Elena Ziviani<sup>1,3</sup>, and Marta Giacomello<sup>1,3</sup>, Luca Scorrano<sup>1,2</sup>

*1 Dept. of Biology, University of Padova, Via U. Bassi 58B, 35121 Padova, Italy;*

*2 Dulbecco Telethon Institute, Venetian Institute of Molecular Medicine, Via Orus 2, 35129 Padova, Italy;*

*3 Fondazione Ospedale San Camillo, IRCCS, Lido di Venezia, Venezia, Italy*

Address correspondence to

Marta Giacomello [marta.giacomello@unipd.it](mailto:marta.giacomello@unipd.it) or Luca Scorrano. Email:

luca.scorrano@unipd.it

## Summary

The close juxtaposition between mitochondria and Endoplasmic Reticulum (ER) participates in several processes such as lipid and Ca<sup>2+</sup> homeostasis. Mitofusin2 (Mfn2) was the first recognized mitochondria-ER structural tether in mammalian cells, but the molecular identity of the other tethers remains unknown. Here we show that Parkinson's disease (PD)-associated gene leucine rich repeat kinase 2 (LRRK2) is a previously uncharacterized ER-mitochondria tether. A genome wide high content screen (HCS) based on the changes in basal and maximal FRET values of a FRET ER-Mitochondria proximity probe (FEMP) expressed in mouse embryonic fibroblasts transduced with lentiviral particles carrying shRNAs targeting the whole murine genome identified 147 potential tethers, including 4 hits known to localise at both mitochondria and ER. Pathway prediction analysis identified among the potential tethers a network of genes associated to PD among which LRRK2 emerged as a top candidate due to its known localization at both mitochondria and ER. Subcellular fractionation experiments revealed that LRRK2 localized mostly in ER and mitochondria associated membranes (MAMs). Accordingly, levels of ER-mitochondria proximity were reduced in LRRK2<sup>-/-</sup> cells. ER-mitochondria juxtaposition and communication in was fully restored by reintroduction in LRRK2<sup>-/-</sup> cells of wt but not of the familial PD associated mutant G2019S LRRK2. Hence, LRRK2 participates in ER-mitochondria tethering and its PD associated mutations impair interorganellar juxtaposition and communication.

## **Introduction**

The existence of points of close proximity between cellular organelles has been known for many years, but only recently their importance in regulation of key cellular processes and functions has been appreciated. The contacts forming between ER and mitochondria (MERCs) are the most extensively studied from their discovery in 1990 (Vance J.E. et al., 1990) and the subsequent functional evidence of their fundamental role in the calcium transfer between the two organelles (Rizzuto R. et al., 1998). It is now known that MERCs are implied in lipid biosynthesis, autophagosomes formation and biogenesis, immune response, metabolic adaptations and their defects have been related also to several pathologies, in particular to neurodegenerative disorders (Paillusson S. et al., 2016).

The close apposition of the cytosolic face of OMM with the smooth or the rough ER membrane that can be clearly observed by electron microscopy is defined as MERC (Giacomello M. et al., 2016). In both cases, the length of the apposed surface between the two membranes is around 100 nm (Sood A. et al., 2014), and they are not fusing keeping a distance/thickness between them of ~10 to ~80nm. It has been proposed that at the interface between these two organelles there are proteins specifically devoted to tightly regulate the distance between the organelles membranes. This hypothesis has been strengthened by the observation of electron dense aggregates between ER and mitochondria visualized in electron microscopy images (Csordas G. et al., 2006), and by the identification of proteins in biochemical fractionation of such interorganelle compartment. In recent years, some proteins have been identified tethering ER and mitochondria. One of these proteins is phosphofurin acidic cluster sorting protein (PACS-2), a multifunctional protein localised at ER, whose depletion leads to mitochondria fragmentation and uncoupling from the ER driven by Bap31 (Simmen et al., 2005). Mitofusin 2 (Mfn2), a protein originally known to be involved in mitochondrial fusion, was the first recognized structural tether between ER and mitochondria (de Brito O. et al., 2008). This protein belongs to dynamin related GTPase family and, being localized on both OMM and cytosolic side of the ER, is able to form homotypic and/or heterotypic interactions with Mfn1 (de Brito O. et al., 2008). Depletion of

Mfn2 causes an increased MERC thickness, so reduced ER-mitochondria contacts, thus reducing  $\text{Ca}^{2+}$  exchange from ER to mitochondria (de Brito O. et al., 2008). The observed partial reduction in ER-mitochondria contact after Mfn2 ablation, leads to the hypothesis that others proteins besides Mfn2 must exist that maintain the residual tether (de Brito O. et al., 2008). Of note, studies claiming the opposite role for Mfn2 in MERCs formation have recently been published (Cosson P. et al., 2012; Filadi R. et al., 2016), but these findings could be conciliated by the influence that the nutritional status and the culture conditions of the cells can exert on MERCs plasticity (Naon D. et al., 2016).

Aim of this project is to identify proteins that compose/modulate the juxtaposition between the two organelles. To achieve this objective, we have performed two replicates of a genome wide high content screen (HCS), in mouse embryonic fibroblasts (MEFs), by means of a modified version of a FRET based probe (FEMP) developed in our laboratory (Naon D. et al., 2016). Our probe allows the measurement of the proximity between the two organelles both in basal physiological conditions, defined as “basal MERC index”, and at the maximum proximity that can be achieved in a particular cell, namely the “maximum MERC index”. Bioinformatic analysis on the obtained data evidence that several different pathways are involved in the modulation of MERCs formation. Most importantly, 13 hits proteins reported to locate at both ER and OMM, so with the potential ability to form a bridge between the two organelles as Mfn2, emerged from our screen to influence both the basal and the maximum MERC index. While 30 and 16 proteins, always reported to be localized in both OMM and ER, have been found to modulate only the basal or the maximum MERC index respectively. Among the proteins modulating the maximum MERC index, the hit leucine rich repeat kinase 2 (LRRK2), whose mutations are the main cause of familial dominant forms of Parkinson’s disease (PD), emerged as a tether. We show that this protein is enriched at MAMs and its knock out reduces ER-mitochondria proximity, as expected for a tether. Accordingly, reintroduction of wt protein in  $\text{LRRK2}^{-/-}$  cells is able to completely restore ER-mitochondria juxtaposition, but this is not the case for the LRRK2 familial PD-associated mutants.

Our results, although not complete, represents the most extensive to date list of the regulators of MERCs formation and evidences the importance of the ER-mitochondria contact sites both in physiology and pathology.

## Results

### **A High Content Screen based on FRET to assess the modulators of ER-mitochondria contacts**

To unravel the proteins that bridge mitochondria and ER, we performed a genome-wide High Content screen (HCS) based on a FRET ER-mitochondria probe (FEMP) developed in our laboratory (Naon D. et al., 2016). In this probe, two fluorescent proteins, YFP and CFP, are targeted to the outer mitochondrial membrane (OMM) and to the ER respectively and equimolarly expressed under the control of the CMV promoter in the plasmid backbone. FRET occurs only at a distance of ~15nm between the membranes of two organelles and with our FEMP we are able not only to measure the FRET occurring at any given timepoint in physiological condition, but also the maximum possible FRET that can occur. This is possible because each fluorescent protein is also associated with one functional domain: “FK506 binding protein” (FKBP) or the “FKBP Rapamycin-binding domain” (FRB); these domains are able to heterodimerize upon addition of Rapamycin (Figure 1A). Since the binding and stabilization of FKBP-FRB is quite rapid, our FEMP construct provides also the advantage of measuring the total number of possible contacts in a short period of time. Of note, the targeting of the two fluorescent proteins is very specific and provides direct evidences in term of proximity, unlike other conventional tools that are targeted to the lumen of the organelles. Variation in the FRET ratio values would correspond to modifications in ER-mitochondria juxtaposition: we can therefore hypothesize that knockdown of proteins that keep the two organelles closer, herein named “tethers” will result in a decreased FRET intensity; while knockdown of the ones that keep the two organelles apart, defined as “spacers”, will have as output an increased FRET intensity (Figure1B).

We perform two replicates of a High Content Screen (HCS) in which wild type MEFs seeded in 384 well plates and transduced with shRNA lentiviral particle were transfected with our

FEMP construct (Figure 1C). 24 hours post transfection, cells were imaged and FRET Ratio values recorded twice: before and after addition of rapamycin. (Figure 1C). We imaged samples upon fixation after 15 minutes incubation with rapamycin. We decided to fix the sample due to the time for the acquisition employed by the microscope itself, in order to have all the wells in the plate acquired in the same condition, and we verified that fixation doesn't alter the detected values for both basal and maximum MERC index (data not shown). The timepoint of 15 minutes was chosen after monitoring the kinetic of FEMP: it can be clearly observed that a plateau for FRET intensity is reached (Figure 2B). We also determined that no positional effect was observed across the 384 well plate in wild type MEFs expressing FEMP (Figure 2C).

We analysed all the 384 wells present in each plate, each well is automatically divided in several fields and we choose the same six fields to be analysed per well (Figure 3A): the cell population detected in each well is then analysed using a high content image analysis system that automatically draw cellular boundaries and regions of interest (Figure 3B): this process provided us the raw data for the HCS. As detailed in Materials and Methods, we defined two indexes in order to quantify ER-mitochondria contacts: "Basal MERC index" representing the contacts at any given time point, and "Maximum MERC index" that mirror the maximum possible contacts that can occur in a cell.

### **Statistical analysis of obtained HCS data unravels novel ER-mitochondria contacts modulators**

Raw data for Basal and Maximum MERC index obtained for each replicate were processed through a careful statistical analysis by means of the cell HTS2 package in R program (Boutros et al., 2006). Robust Z score normalization was performed at single plate and experiment level (Figure 4A). For plate level normalization, as detailed in Materials and Methods, we obtained a list of tethers and spacers for Basal and Maximum MERC index in replicate 1 and replicate 2. As represented in Figure 4B, in particular for tethers we have 1685 candidates for Basal MERC index replicate 1 and 3271 candidates for Basal MERC index replicate 2; 2129 candidates for Maximum MERC index replicate 1 and 4185 candidates for Maximum MERC index replicate 2. For spacers, we have 1170 candidates for

Basal MERC index replicate 1 and 4405 candidates for Basal MERC index replicate 2; 1398 candidates for Maximum MERC index replicate 1 and 3272 candidates for Maximum MERC index replicate 2. For tethers and spacers, we selected the common genes between the two replicates for Basal and Maximum MERC index: for tethers we obtained 830 candidates in common between the two replicates for Basal MERC index, and 724 candidates for Maximum MERC index; for spacers we obtained 755 candidates in common between the two replicates for Basal MERC index, and 126 candidates for Maximum MERC index. To conclude, we look for candidates affecting both Basal and Maximum MERC index: for tethers we ended up with 205 strongest candidates affecting both the indexes, 625 candidates influencing only the Basal MERC index and 519 candidates affecting only the Maximum MERC index; for spacers we ended up with 59 strongest candidates affecting both the indexes, 696 candidates influencing only the Basal MERC index and 67 candidates affecting only the Maximum MERC index.

We analysed the distribution of the Z score associated to the 205 tethers and 59 spacers obtained before for basal and maximum MERC index (Figure 4C). More than 85% for the basal MERC index and more 90% for the maximum MERC index are distributed as expected.

The full lists of tethers and spacers affecting both Basal and Maximum MERC indexes (205 tethers+59 spacers), or affecting only the basal MERC index (625 tethers+696 spacers) or modulating only the Maximum MERC index (519 tethers+67 spacers) obtained from the primary screen were analysed through the web interface of Mitominer (Smith A.C. et al., 2016) with the aim to identify proteins located in both OMM and ER, more likely to be structural components of the ER-mitochondria contacts sites. (Table 1,2,3). We obtained 13 proteins affecting both the indexes, 30 proteins affecting only the Basal MERC index and 16 proteins affecting only the Maximum MERC index reported to be localized in both ER and mitochondria membranes.

### **Bioinformatics analysis of the candidate lists discloses different protein classes modulating ER-mitochondria proximity**

To gain additional knowledge on the cellular protein classes that control ER-mitochondria contacts, we undertook a system biology approach and performed pathway enrichment analysis. The three lists of candidates, as detailed above, were submitted to the Panther database. By means of over-representation analysis in Panther database, which evidences cellular pathways that are significantly enriched amongst the list of submitted genes, the three gene lists (common tethers and spacers, tethers and spacers affecting only basal MERC index, tethers and spacers affecting only maximum MERC index) were classified for the respective protein classes, which they belong to (Figure 5). While most of protein classes were common to all the three groups, some protein classes were differentially represented. The common pathways highlighted by this analysis provide us new insights on how ER and mitochondria communication is modulated by different signalling pathways.

### **Parkinson's associated gene LRRK2 identified as a new ER-mitochondria tether**

One of the sixteen proteins that were predicted to be localised in both OMM and ER affecting only the maximum MERC index Leucine Rich Repeat Kinase 2 (LRRK2), a protein presenting a double enzymatic core with both serine threonine kinase and GTPase activities, whose mutations are the most common cause of familial Parkinson's disease (PD). Decreased the maximum MERC index is detected in LRRK2<sup>-/-</sup> MEF when compared to WT, as expected for a tether (Figure 6A, 6B). Reintroduction of WT protein in knock out cells (LRRK2<sup>-/-</sup>+LRRK2) is able to completely rescue the phenotype (Figure 6B). While interestingly reintroduction of three different pathological mutants (LRRK2<sup>G2019S</sup>, LRRK2<sup>R1141C</sup>, LRRK2<sup>Y1669C</sup>) is not recovering the ER-mitochondria contact levels (Figure 6C, 6D). If we reintroduce two other LRRK2 mutants (artificially created in laboratory, not found in pathology), namely LRRK2<sup>D1994A</sup>, where the kinase activity is completely abolished, and LRRK2<sup>T1348N</sup> unable to bind GTP, the ER-mitochondria proximity is fully restored (Figure 7). Biochemical fractionation of WT MEFs also indicated that LRRK2 is present in MAMs and enriched in ER, thus confirming the primary screen data (Figure 8). These results are confirmed also in primary MEF. In LRRK2 and LRRK2<sup>-/-</sup> cells, ER-mitochondria contacts were measured by means of confocal microscopy and the overlap

between the two organelles analysed with Mander's coefficient, a reduction of ~30% in LRRK2<sup>-/-</sup> compared to WT is observed (Figure 9A, 9B). Similar results are observed in maximum MERC index analysis after transfection with our FEMP construct (Figure 9C, 9D), although not significant due to the fact that only two replicates of the experiment are to date available. Reintroduction of LRRK2 WT protein in LRRK2<sup>-/-</sup> show a tendency to rescue the normal phenotype. Moreover, two selective inhibitors of LRRK2 kinase activity to WT cells: GSK2578215A, indicated as GSK, or PF-06447475, indicated as PF (as detailed in Materials and Methods), have been added to WT cells and they cause a strong impairment in ER-mitochondria contacts.

## Discussion

Several important cellular processes that are regulated by different molecular pathways take place at ER-mitochondria interface. Despite this finding, only few proteins have been identified as modulators of ER-mitochondria communication and the overall nature of the complexes that tethers the two organelles together has yet not been fully clarified. Aim of this study was to identify proteins that modulate the distance between ER and mitochondria that were classified in two classes: “tethers” if keeping the two organelles closer, “spacers” if keeping the two organelles apart. Through rigorous statistical analysis of two replicates of a FRET probe based HCS and the utilization of two different indexes, basal and maximum MERC index, we classified genes as tethers and as spacers affecting both parameters or only one of the considered indexes. Confidence in our approach and in the chosen cut-off limits is sustained by the finding of previously reported regulators of MERCs function among the lists, including mTOR (FRAP1) affecting the maximum MERC index, and PSEN2 (Betz C. et al., 2013; Area-Gomez E. et al., 2009) affecting the basal MERC index (Table 2,3). The contexts in which these proteins were found to modulate ER-mitochondria contacts is different - while mTOR has shown to be associated to MAMs upon metabolic stress, PSEN2 is localized to MAMs in normal physiological conditions, and alteration of the protein, as for example familial mutations causing Alzheimer disease impinge also on MAMs structure and functions, although the exact role of PSEN2 in MAMs is not completely understood. Of note also nicastrin (NCSN), another component of  $\gamma$ -secretase complex as PSEN 2 has been found in our screen as a protein localized in both ER and mitochondria affecting only the

basal MERC index. The fact that we found these proteins as “hits” is an indication of the high robustness of our screen.

Generally, the same pathways influence both the basal and maximum MERC indexes as indicated by Panther database analysis, although differently enriched (Figure 5). In proteins affecting only the maximum MERC index, the protein classes “storage proteins” and “membrane trafficking proteins” are not present, while they are enriched in the other two groups. Conversely, “structural proteins” and “transmembrane receptor adaptor proteins” classes are not found in the common tethers and spacers, but are present in the other two groups.

One protein of particular interest that showed up as ER-mitochondria tether is LRRK2. Of note, based on our selection criteria we considered LRRK2 as a tether affecting only the maximum MERC index: this is due to the fact that in basal MERC index replicate 2 the number of effective shRNA was 2 instead of our cut-off 3, while in basal MERC index replicate 1 the cut-off selection was passed, so this is a further consideration of the strength of our candidate, besides its reported localization at both ER and mitochondria. Our biochemical analysis indicates that in MEFs LRRK2 is enriched at MAMs and that its ablation increases the distance between mitochondria and ER, that can be rescued by reintroduction of LRRK2 WT protein, suggesting new physiological role for LRRK2 as a tether of ER and mitochondria. Mutations of LRRK2 are the main cause of familial forms of PD: to date there are six known pathological mutations and here we analysed three of them in relation to ER-mitochondria contacts. LRRK2<sup>G2019S</sup> is the most common LRRK2 mutations and is associated with increased kinase activity of the protein; LRRK2<sup>R1141C</sup> and LRRK2<sup>Y1669C</sup> are mutations that reduce the GTPase activity of the protein, but affecting different part of the GTPase domain: particularly LRRK2<sup>R1141C</sup> affect the ROC domain, while LRRK2<sup>Y1669C</sup> is in the COR domain (Wallings R. et al., 2015). The apparent discording finding that reintroduction of LRRK2<sup>T1348N</sup>, a mutant unable to bind GTP, is restoring ER-mitochondria contacts while LRRK2<sup>R1141C</sup> and LRRK2<sup>Y1669C</sup> are not able to rescue the phenotype, can be explained by the fact that the last two mutants present also a different cellular localization: particularly they are reported to form cytosolic aggregates instead of being localized to membranes (Nichols R.J. et al., 2010). For the kinase activity, we observed that a gain of function, as for LRRK2<sup>G2019S</sup>, is detrimental for the maintenance of ER-

mitochondria proximity, as the selective pharmacological inhibition of LRRK2 kinase activity, but this is not observed for the kinase inactive LRRK2<sup>D1994A</sup>. This can be explained by the fact that LRRK2 inhibitors could alter the protein localization or the interaction with other molecular partners in a different way compared to LRRK2<sup>D1994A</sup>. It has to be also considered that the mechanisms controlling LRRK2 cellular localization are not yet been identified and that the two enzymatic activities of the protein can modulate each other. It would be interesting to measure ER-mitochondria contacts after treatment with LRRK2 kinase inhibitors in MEF expressing LRRK<sup>G2019S</sup> to see if there is a complete restoration of organelles proximity and to confirm our findings also in neurons.

Further characterisation of LRRK2, particularly to understand which is/are the interacting partners especially on mitochondria surface will provide us further insight into MAMs composition and organization, and in understanding the molecular mechanism involved in Parkinson disease in order to develop new therapeutic strategies.

## **Experimental procedure**

### **Molecular biology**

pEGFP-N1 YFP-Akap1 (34-63)-FKBP and pEGFP-C3 CFP-HA-FRB-Sac1 (ER)-CFP were kindly provided by G. Hajnoczky (Csordas G. et al., 2010). The modified FEMP was produced as previously described (Naon D. et al., 2016).

All the LRRK2 constructs were kindly provided by Prof. Elisa Greggio. These are 3x-flag-tagged constructs cloned into pCHMWS plasmid, as previously described (Daniels V. et al., 2011).

### **Cell culture**

WT MEFs transformed by SV40 were cultured as described before (de Brito O. et al., 2008).

Immortalized and primary MEF WT and KO for LRRK2 were kindly provided by Prof. Elisa Greggio.

Media utilized for the screen was purchased from Life Technologies and supplemented as reported: Complete DMEM (DMEM high glucose; Life technologies #12800-082)

supplemented with 10% Fetal Bovine Serum (FBS), 1X Pencillin/Streptomycin 100 $\mu$ M and 1X non-essential amino acids (Gibco, REF:11140-035). The same medium without FBS was used to perform transfection.

Cells were kept in incubators at 37°C and 5% CO<sub>2</sub>.

### **High content genome wide shRNA library**

A murine shRNA ready-to-use lentiviral library was purchased from Sigma (MISSION™ shRNA lentiviral particles) and kept at -80°C. More than 10,000 genes were present in the library, arranged in a 384 wells-plate format. For each gene were present 4 or 5 unique shRNAs.

### **Automated shRNA screening**

WT MEFs were thawed from frozen stocks and cultured for 2-3 days before being used in HCS and used no longer than 10 passages. On day 1, upon harvesting with Trypsin 0.25% EGTA, cells were plated in a 384 well plate (μclear-plate black, 384 well REF 781091, Greiner Bio One) at a density of 900 cells per well in a final volume of 90 $\mu$ l. All the steps of plating and addition/removal of solutions were performed by means of an automated system (BiotekprecisionXS) with dedicated plastic ware (starlab natural tips, #E1079-2410), at least is not different specified.

The day after plating, cells were transduced with lentiviral particles. After incubation with 8 $\mu$ g/ml polybrene for 30 minutes, transduction was performed by addition of 5 $\mu$ l shRNA lentiviral particles (BiotekprecisionXS microplate sample processor, starlab sterile filter tips, # E1079-2418). For each plate, empty wells randomly distributed within the library plates were filled with control shRNAs: non targeting controls (scrambled, Scr) and positive controls (shRNAs targeting PACS2 and Mfn2) placed always in different wells to avoid positioning artifacts. After transduction, the plates were centrifuged at 500g for 15minutes before being placed again in the incubators.

24 hours post transduction, 80µl of medium containing the lentiviral particles were removed and 50µl of fresh complete DMEM were added in each well. Transfection complex was prepared in FBS free DMEM with a 1:3 ratio of FEMP cDNA: Genjet lipid Transfection reagent (Signagen, #SL100488), according to the manufacturer instructions. The transfection mixture was dispensed at a concentration of 100ng/well by means of an electronic multichannel pipette 16 channels (Integra electronics).

Imaging was performed 24 hours after transfection. After imaging in resting conditions, the medium was removed from the 384 wells plate and fresh Complete DMEM containing Rapamycin at a final concentration of 100nM was added and let incubate for 15 minutes at RT. Post incubation, the Rapamycin-containing medium was removed and cells were fixed by addition of 70µl of 1% Formaldehyde without methanol (diluted with PBS1x, pH 7.4 from a stock of 37% formaldehyde) incubating for 10 minutes at RT. Subsequently, formaldehyde is removed and 90µl of PBS1x are added in each well. The second image acquisition upon Rapamycin addition is performed in presence of PBS1x.

### **Image acquisition and processing**

Image acquisition was performed in the Operetta High content imaging system (Perkin Elmer) and the settings were established with the Harmony 3.5 software. Images were acquired with 20X objective (high working distance) that allows the acquisition of the entire 384 well plate. The following filters were utilized: CFP (ex 410-430, em 460-500), YFP (ex 490-510, em 520-560) and YFP<sub>FRET</sub> (ex 410-430, em 520-560). After acquisition, images were analysed using Perkin Elmer Harmony 3.5 image analysis software.

### **Image analysis**

High throughput image analysis was performed with the Harmony image analysis software 3.5.2 (Perkin Elmer). A custom workflow was set (Figure 3). Image segmentation and drawing of the Regions of Interest (ROIs) corresponding to single cell was based on YFP channel intensity. The following parameters were chosen to identify cell boundaries:

$$\text{Area} > 150 \mu\text{m}^2;$$

Splitting coefficient: 0.30;

Common threshold: 0.20.

For each ROIs, a CFP intensity is estimated and used to select a CFP-positive subpopulation. Based on this procedure, only cells expressing both CFP and YFP were considered for the final HCS analysis. A background ROI was then automatically drawn around every cell boundary to estimate the background intensity of each channel. For each ROIs, YFP, CFP and FRET intensities were measured and background subtracted. Finally, the basal and maximum MERC indexes were calculated as follows:

$$\text{Raw FRET intensity} = \frac{FYFP_{cell} - FYFP_{bg}}{FCFP_{cell} - FCFP_{bg}}$$

Calculated in resting condition ( $FRET_{basal}$ ) and after Rapamycin addition ( $FRET_{max}$ )

$$\text{Maximum MERC index} = \frac{FRET_{max} - FRET_{basal}}{FRET_{basal}}$$

$$\text{Basal MERC index} = \frac{FRET_{max} - FRET_{basal}}{FRET_{max}}$$

### **Statistical analysis of the data obtained from HCS**

For each replicate of the screen, data from all the plates were pooled together and normalised to the overall experiment for both basal and maximum MERC index. CellHTS2 package R program (Boutros et al., 2006) was utilized to calculate Robust Zscore for normalisation since it is not dependent to controls and to outliers, which are essentially the candidate genes of interest (Birmingham et al., 2009; Malo et al., 2006). We decided to analyse the data previously obtained in two ways: plate-level and experiment-level (Figure 4).

For plate-level analysis, the mean of the scramble values and the Median Absolute Deviation (MAD) value, that allow direct data comparison, were calculated for each plate. Subsequently, two cut-off threshold values corresponding to scramble mean+3MAD and scramble mean-3MAD were used to identify spacers and tethers respectively, for each plate. Since there are 4 or 5 Zscore values, based on the number of shRNA present in the library,

associated to each gene, we decided to select the genes that presented at least 3 Zscore values above the cut-off thresholds. At the end of this analysis we obtained the first lists of genes considered as tethers for basal and maximum MERC index in replicate 1 and replicate 2, and the same for spacers. Subsequently, the common genes between the two replicates for basal and maximum MERC index in both tethers and spacers, were identified. At the end, the genes in common between basal and maximum MERC index among the ones previously identified, provided us a list of tethers and spacers affecting both or only one of the MERC indexes (Figure 4B).

For experimental level normalization, after robust z score calculation, outliers were defined as (Turkey J.W., 1977), where Q1 represent the first quartile and Q3 the third quartile of the considered values (Figure 4A). The single outliers z score values were then removed. After outliers removal, the average of the z score per each gene was performed for Basal and Maximum MERC index in replicate 1 and 2. Then the average z score associated with each gene was averaged again between the two replicate for Basal and Maximum MERC index. A gene has been considered in the analysis even if present in only one replicate. After logarithmic transformation of the values, obtained as previously described, plotted from most negative to positive we obtained the z score distribution for Basal and Maximum MERC index (Figure 4C).

### **MAMs isolation and western blotting**

Biochemical fractionation of MAMs and western blots were performed as previously described (Wieckowski M.R. et al., 2009). Antibodies concentration is as follows: LRRK2 (1:1000, MJJF), FAACL4/ACSL4 (1:1000, Santa cruz), Mfn2 (1:1000, Abnova), Grp75 (1:1000, Santa cruz), BKDE1A (1:1000, Bethyl Laboratories).

### **Acquisition of FRET intensity for LRRK2 cells**

Immortalized MEF both WT and KO for LRRK2 were plated in a 384 well/plate at a density of 1000cells/well in a final volume of 90µl. upon harvesting with Trypsin 0.25% EGTA.

Primary MEF WT and KO for LRRK2 were plated at a density of 2000cells/well always in a final volume of 90 $\mu$ l.

24 hours post plating, the medium was changed and transfection complex was prepared in FBS free DMEM with a 1:3 ratio of FEMP cDNA (and other LRRK2 construct when cotransfected): Genjet lipid Transfection reagent (Signagen, #SL100488), according to the manufacturer instructions. The ratio between LRRK2 construct and FEMP was 3:1. The transfection mixture was dispensed at a concentration of 200ng/well.

Image acquisition was performed the day after transfection, as described above. For primary LRRK2 MEF, the selective inhibitor GSK2578215A or PF-06447475 (kindly provided by Prof. Elisa Greggio) were added at a concentration of 2 $\mu$ M or 150nM respectively for 90min (Reith A.D. et al., 2012; Henderson J.C. et al., 2014), and then the imaging of all the plate was performed normally. Note that the inhibitor-containing medium was removed only after Rapamycin incubation, because these are reversible LRRK2 inhibitors.

For both immortalized and primary cells, the image analysis was performed with the same parameters utilized in the HCS.

The subsequent image analysis has been performed with the same procedure described previously. Statistical analysis of the obtained data was performed with Origin8.

### **Confocal imaging and ER-mitochondria contacts analysis for LRRK2 primary MEF**

Primary MEF WT and KO for LRRK2 were plated at a density of 750000 cells/well in a 6-well plate. The day after plating, cells were transfected with two fluorescent probes: mitochondrial kate and ER GFP. Transfection mix was prepared in Optimem with a ratio of 1:4 DNA: polyethyleneimine (PEI), utilized as transfection reagent. The transfection mixture was dispensed at a concentration of 2 $\mu$ g/well. Images were acquired the day after by Andromeda Spinning disk confocal microscope with 60x objective and 30 planes were acquired in z-stack with a distance of 0.5 $\mu$ m between each plane for each cell. Images were analysed by ImaJ as described in (De Brito O. et al., 2008) and Mander's coefficient was used to quantify ER-mitochondria colocalization.

## **Acknowledgments**

LS is a Senior Scientist of the Dulbecco-Telethon institute supported by Telethon Italy (GGP12162 and GGP14187A), by the AIRC (the Italian Association for Research on Cancer), by the European Research Council (FP7-282280, FP7 CIG PCIG13-GA-2013-618697), and by the Italian Ministry of Research (FIRB RBAP11Z3YA\_005).

## References

- Area-Gomez, E., De Groof, A.J.C., Boldogh, I., Bird, T.D., Gibson, G.E., Koehler, C.M., Yu, W.H., Duff, K.E., Yaffe, M.P., Pon, L.A., and Schon, E.A. (2009). Presenilins are enriched in endoplasmic reticulum membranes associated with mitochondria. *Am. J. Pathol.* 175, 1810-1816.
- Betz, C., Stracka, D., Prescianotto-Baschong, C., Frieden, M., Demareux, N., and Hall, M.N. (2013). Feature Article: mTOR complex 2- Akt signaling at mitochondria-associated endoplasmic reticulum membranes (MAM) regulates mitochondrial physiology. *Proc. Natl. Acad. Sci. U. S. A.* 110, 12526-12534.
- Birmingham, A., Selfors, L.M., Forster, T., Wrobel, D., Kennedy, C.J., Shanks, E., Santoyo-Lopez, J., Dunican, D.J., Long, A., Kelleher, D., et al. (2009). Statistical methods for analysis of high-throughput RNA interference screens. *Nat Methods* 6, 569-575.
- Boutros, M., Bras, L.P., and Huber, W. (2006). Analysis of cell-based RNAi screens. *Genome Biol* 7, R66.
- Cosson, P., Marchetti, A., Ravazzola, M., and Orci, L. (2012). Mitofusin-2 Independent Juxtaposition of Endoplasmic Reticulum and Mitochondria: An Ultrastructural Study. *Plos One* 7(9).
- Csordás, G., Renken, C., Várnai, P., Walter, L., Weaver, D., Buttle, K.F., Balla, T., Mannella, C.A., and Hajnóczky, G. (2006). Structural and functional features and significance of the physical linkage between ER and mitochondria. *J. Cell Biol.* 174, 915-921.
- Csordas, G., Varnai, P., Golenar, T., Roy, S., Purkins, G., Schneider, T.G., Balla, T., and Hajnoczky, G. (2010). Imaging interorganelle contacts and local calcium dynamics at the ER-mitochondrial interface. *Mol Cell* 39, 121-132.
- Daniëls, V., Vancraenenbroeck, R., Law, B.M., Greggio, E., Lobbestael, E., Gao, F., De Maeyer, M., Cookson, M.R., Harvey, K., Baekelandt, V., Taymans, J.M. (2011). Insight into

the mode of action of the LRRK2 Y1699C pathogenic mutant. *J Neurochem.* 2011 116(2), 304-15.

de Brito, O.M., and Scorrano, L. (2008). Mitofusin 2 tethers endoplasmic-reticulum to mitochondria. *Nature* 456, 605-610.

Filadi, R., Greotti, E., Turacchio, G., Luini, A., Pozzan, T., and Pizzo, P. (2016). Presenilin 2 Modulates Endoplasmic Reticulum-Mitochondria Coupling by Tuning the Antagonistic Effect of Mitofusin 2. *Cell Rep.* 15, 2226-2238.

Giacomello, M., and Pellegrini, L. (2016). The coming of age of the mitochondria–ER contact: a matter of thickness. *Cell Death & Differentiation*, 1-11.

Henderson JL, Kormos BL, Hayward MM, Coffman KJ, Jasti J, Kurumbail RG, Wager TT, Verhoest PR, Noell GS, Chen Y, Needle E, Berger Z, Steyn SJ, Houle C, Hirst WD, Galatsis P. (2015). Discovery and preclinical profiling of 3-[4-(morpholin-4-yl)-7H-pyrrolo[2,3-d]pyrimidin-5-yl]benzotrile (PF-06447475), a highly potent, selective, brain penetrant, and in vivo active LRRK2 kinase inhibitor. *J Med Chem.* 58(1),419-32.

Malo, N., Hanley, J.A., Cerquozzi, S., Pelletier, J., and Nadon, R. (2006). Statistical practice in high-throughput screening data analysis. *Nat Biotechnol* 24, 167-175.

Naon D., Zaninello M., Giacomello M., Varanita T., Grespi F., Lakshminaranayan S., Serafini A., Semenzato M., Herkenne S., Hernández-Alvarez M.I., Zorzano A., De Stefani D., Dorn G.W. II and Scorrano L. (2016) Critical reappraisal confirms that Mitofusin 2 is an endoplasmic reticulum–mitochondria tether. *PNAS* 160678613.

Nichols, R.J., Dzamko, N., Morrice, N.A., Campbell, D.G., Deak, M., Ordureau, A., Macartney, T., Tong, Y., Shen, J., Prescott, A.R., and Alessi, D.R. (2010). 14-3-3 Binding to LRRK2 is disrupted by multiple Parkinson's disease-associated mutations and regulates cytoplasmic localization. *Biochem. J.* 430, 393-404.

Paillusson, S., Stoica, R., Gomez-Suaga, P., Lau, D.H.W., Mueller, S., Miller, T., and Miller, C.C.J. (2016). There's Something Wrong with my MAM; the ER-Mitochondria Axis and Neurodegenerative Diseases. *Trends Neurosci.* 39, 146-157.

- Reith, A.D., Bamborough, P., Jandu, K., Andreotti, D., Mensah, L., Dossang, P., Choi, H.G., Deng, X., Zhang, J., Alessi, D.R., Gray, N.S. (2012). GSK2578215A; a potent and highly selective 2-arylmethoxy-5-substituent-N-arylbenzamide LRRK2 kinase inhibitor. *Bioorg Med Chem Lett.* 22(17), 5625-9.
- Rizzuto, R., Pinton, P., Carrington, W., Fay, F.S., Fogarty, K.E., Lifshitz, L.M., Tuft, R.A., and Pozzan, T. (1998). Close contacts with the endoplasmic reticulum as determinants of mitochondrial Ca<sup>2+</sup> responses. *Science* 280, 1763- 1766.
- Simmen, T., Aslan, J.E., Blagoveshchenskaya, A.D., Thomas, L., Wan, L., Xiang, Y., Feliciangeli, S.F., Hung, C., Crump, C.M., and Thomas, G. (2005). PACS-2 controls endoplasmic reticulum-mitochondria communication and Bid-mediated apoptosis. *Embo j.* 24, 717-729.
- Smith, A.C., and Robinson, A.J. (2016). MitoMiner v3.1, an update on the mitochondrial proteomics database. *Nucleic Acids Res* 44, D1258-1261.
- Sood, A., Jeyaraju, D.V., Prudent, J., Caron, A., Lemieux, P., McBride, H.M., Laplante, M., Tóth, K., and Pellegrini, L. (2014). A Mitofusin-2-dependent inactivating cleavage of Opa1 links changes in mitochondria cristae and ER contacts in the postprandial liver. *Proc. Natl. Acad. Sci. U. S. A.* 111, 16017-16022.
- Tukey, J.W. (1977). *Exploratory Data Analysis*. Addison-Wesley.
- Vance, J.E. (1990). Phospholipid synthesis in a membrane fraction associated with mitochondria. *J. Biol. Chem.* 265, 7248-7256.
- Wallings, R., Manzoni, C., and Bandopadhyay, R. (2015). Cellular processes associated with LRRK2 function and dysfunction. *Febs j.* 282, 2806-2826.
- Wieckowski, M.R., Giorgi, C., Lebiedzinska, M., Duszynski, J., Pinton, P. (2009). Isolation of mitochondria-associated membranes and mitochondria from animal tissues and cells. *Nat Protoc.* 2009;4(11):1582-90.

## Figure Legends

### Figure 1. HCS workflow based on FEMP.

(A) Schematic representation of FEMP functioning: the two fluorescent proteins YFP and CFP are targeted respectively to mitochondria and ER membranes. The two functional domain FKBP and FRB are also associated with them. Upon rapamycin addition, the two functional domains closely interact, thus bringing the two organelles at the close possible distance. Given that FRET can occur between the two fluorophore, FRET intensity will mimick the distance between ER and mitochondria.

(B) Rationale for identification of genes involved in ER-mito contacts modulation. In resting state, cells expressing FEMP are characterized by a basal FRET intensity and addition of Rapamycin would allow measuring the maximum FRET intensity possible per each cell. Down regulation of a protein involved in the structural maintenance of ER-mito contacts would cause variations in FRET intensity. Accordingly, changes in FRET intensity could be used to classify the identified hits as a tether: if ablation of the candidate decreases the FRET intensity, due to an increased distance among the two organelles; or spacer in case of an increased FRET intensity, due to the reduced distance between the two organelles.

(C) Schematic of the workflow of the FEMP based HCS. A general workflow of the timeline that we have employed in performing HCS. See materials and methods for detailed description.

### Figure 2. A high-content screening assay to identify the molecular components of ER-mitochondria junctions.

(A) Representative images of mito-ER contacts assay. FRET intensity signal is shown before and after rapamycin addition/fixation (color scale: brgbcmyw).

(B) Kinetic of FEMP construct. WT MEFs transfected with FEMP were imaged for every 1 minute for 18 minutes. After the first 3 minutes, 100nM Rapamycin was added to the cells. Data represents average  $\pm$  S.E.M from 3 independent experiments.

(C) Basal and maximum FRET intensity measurements across a 384 well plate. Data represents average  $\pm$  S.E.M from 3 independent experiments.

**Figure 3. Automated image analysis procedure.**

(A) All the 384 wells present in each plate were analysed with 20x objective, each well is automatically divided in several field and we choose the same six fields to be analysed per well for every plate.

(B) Overview of the customized image analysis for the genome wide screen. Cells from the raw images were segmented using YFP channel and intensity measures of CFP, YFP and FRET along with corresponding background intensities were calculated. Mean FRET intensity was then calculated by subtracting the background and normalising to CFP intensity (detailed in Materials and methods).

**Figure 4. Statistical analysis performed on HCS data.**

(A) Workflow of the statistical analysis of HCS data. Raw data for basal and maximum MERC index for both the replicates were normalized for each plate (plate level normalization) or considering the whole experiment (experimental level normalization). Detailed in materials and methods.

(B) Schematic representation of the analysis of the data obtained from plate level normalization in order to identify the most prominent tethers and spacers. Detailed in Results and Materials and methods.

(C) Z score distribution obtained after experimental level normalization for basal and maximum MERC index. Representation of 205 common tethers (green) and 59 common spacers (red). Detailed in Materials and methods.

**Figure 5. Protein classes enrichment of the candidate lists.**

(A-C) Bioinformatics analysis using Panther database of the candidate hits. Genes were classified using Panther protein classes analysis for 205 common tethers and 59 spacers (A), 625 tethers and 696 spacers affecting only the basal MERC index (B) and 519 tethers and 67 spacers affecting only the maximum MERC index (C).

**Figure 6. LRRK2 is a novel tether between ER and mitochondria.**

(A) Representative images of masked FRET intensity (color scale: brgbcmw) for the respective cells cotransfected with FEMP and the indicated constructs.

(B-D) Quantification of the maximum MERC index for the indicated respective cells cotransfected with the indicated LRRK2 constructs. Comparison between WT, KO and reconstituted LRRK2<sup>-/-</sup> cells. Further comparison with LRRK2 pathological mutants. Data represents average  $\pm$  S.E.M from 5 independent experiments (p<0.05: \*; p<0.01: \*\*; p<0.001: \*\*\*).

**Figure 7. Effects of LRRK2 functional mutants on ER-mitochondria contacts.**

(A) Representative images of masked FRET intensity (color scale: brgbcmw) for the respective cells cotransfected with FEMP and the indicated constructs.

(B) Quantification of the maximum MERC index for the indicated respective cells cotransfected with the indicated LRRK2 functional mutant constructs. Data represents average  $\pm$  S.E.M from 5 independent experiments (p<0.05: \*).

**Figure 8. LRRK2 subcellular localization.**

Western blot of the subcellular fraction obtained after biochemical isolation. Mfn2 is a marker for MAMs, mitochondria and ER; Grp75 is a mitochondrial marker localized in OMM; branched-chain  $\alpha$ -keto acid dehydrogenase E1 (BCKDE1) is a component of the inner mitochondrial membrane; FAFL4 is the marker of election for MAMs.

**Figure 9. Confirmation of the role of LRRK2 also in primary MEF.**

(A) Three-dimensional reconstructions of ER and mitochondria in MEFs of indicated genotype. Mitochondria are represented in red while ER is represented in green. Yellow indicates that organelles are closer than 270nm.

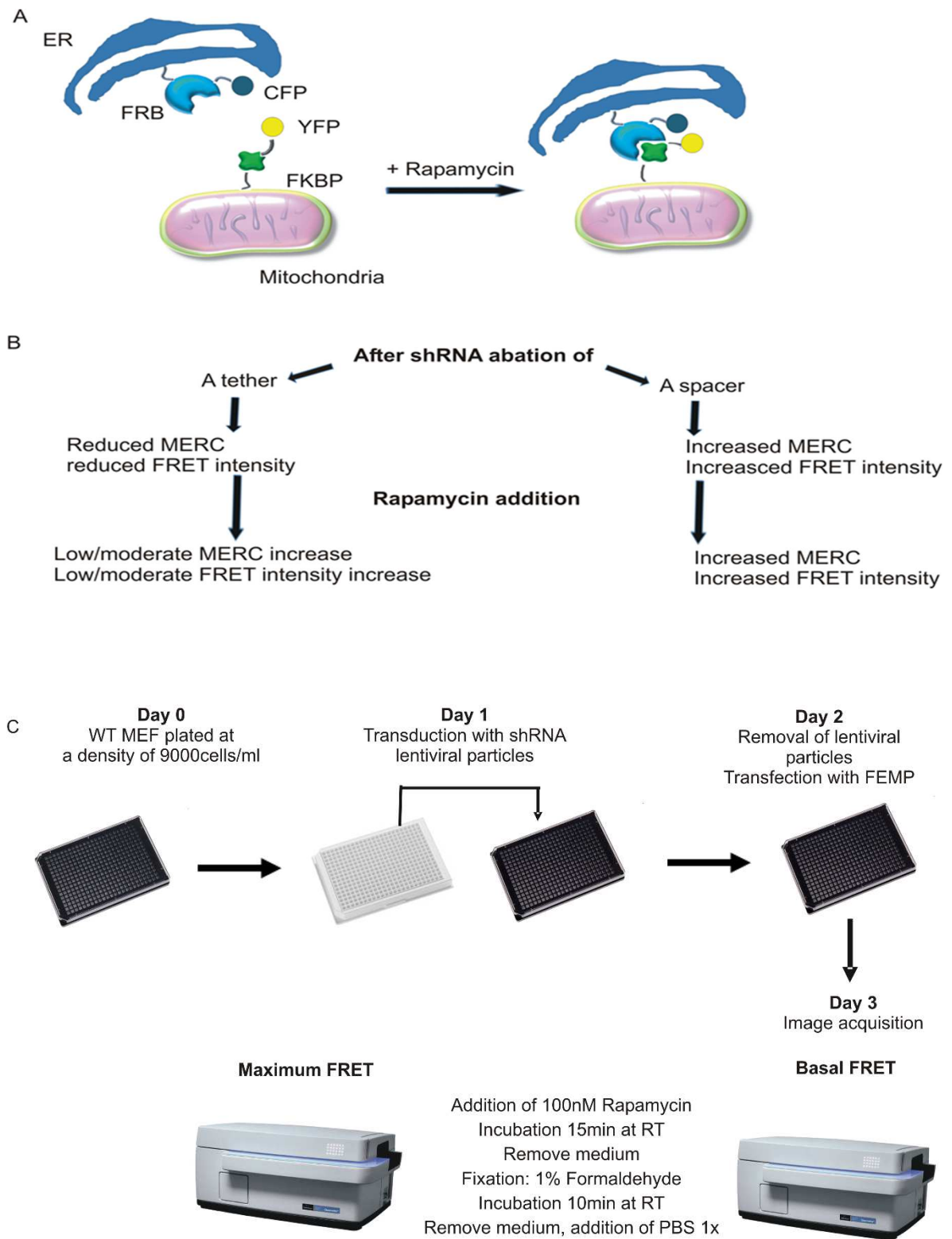
(B) Quantification of Mander's coefficient in MEFs of indicated genotype. Data represents average  $\pm$  S.E.M from 3 independent experiments (p<0.05: \*).

(C) Representative images of masked FRET intensity (color scale: brgbcmyw) for the respective cells transfected with FEMP, when reported reconstituted with WT protein or treated with the specified LRRK2 inhibitors, as detailed in Materials and method.

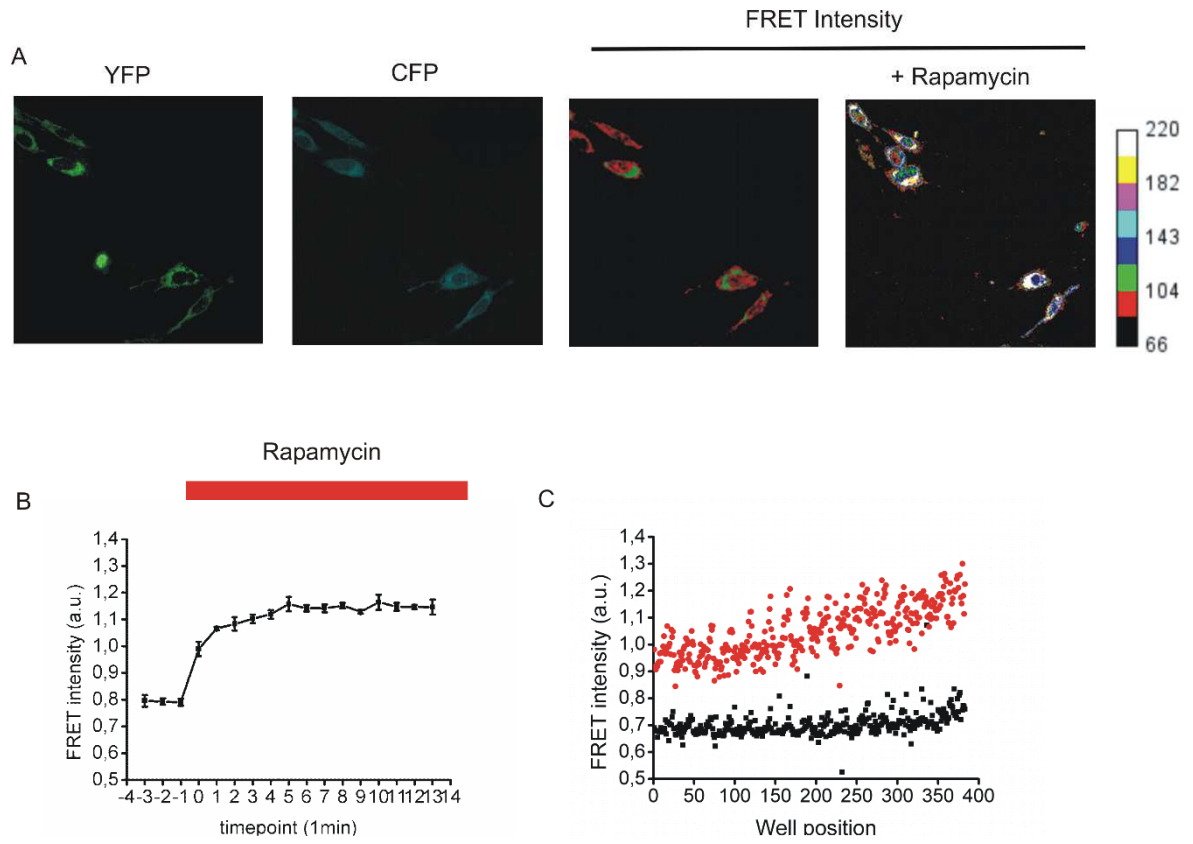
(D) Quantification of the maximum MERC index for the indicated genotype transfected with transfected with FEMP, when reported reconstituted with WT protein or treated with the specified LRRK2 inhibitors. Data represents average  $\pm$  S.E.M from 2 independent experiments.

**Table 1-3. List of proteins localised at both OMM and ER obtained after Mitominer analysis of the indicated list of genes.**

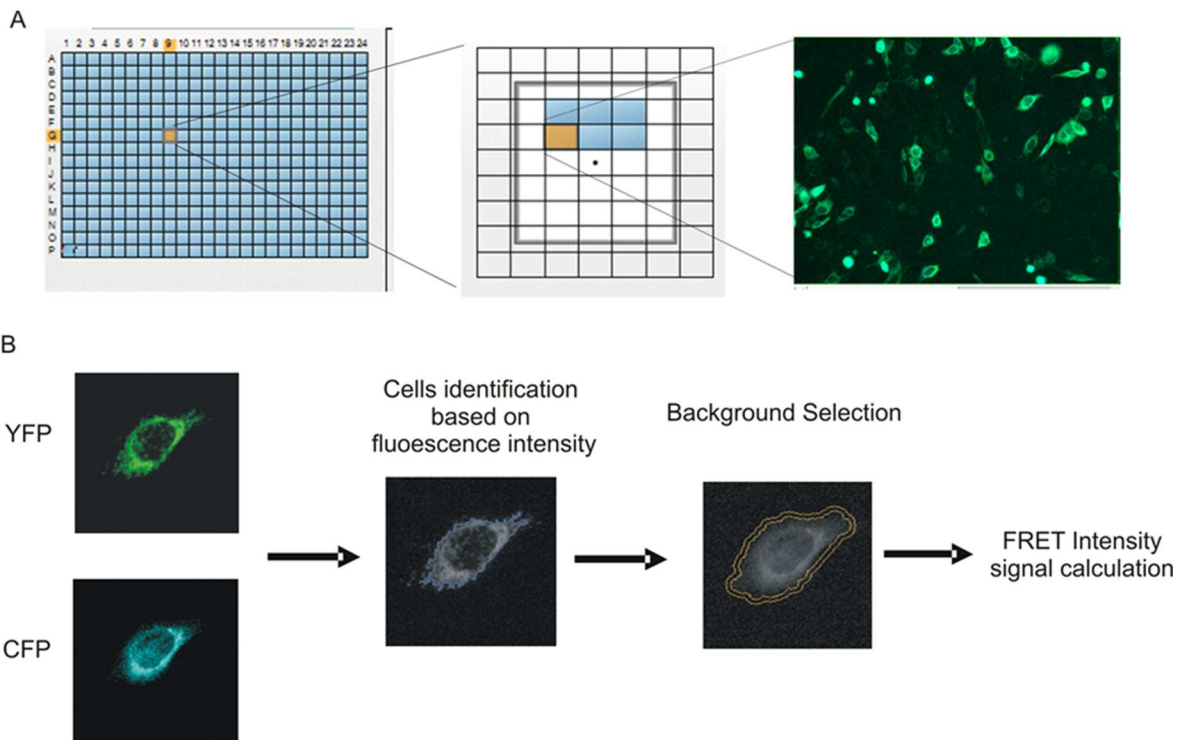
**Figure 1**



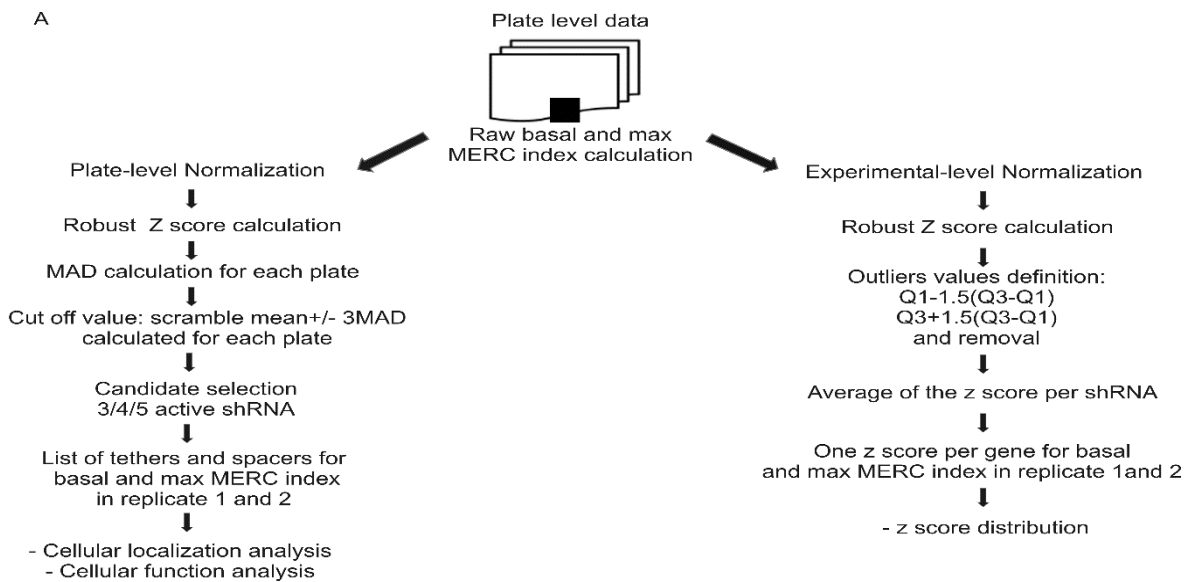
**Figure 2**



**Figure 3**



**Figure 4**



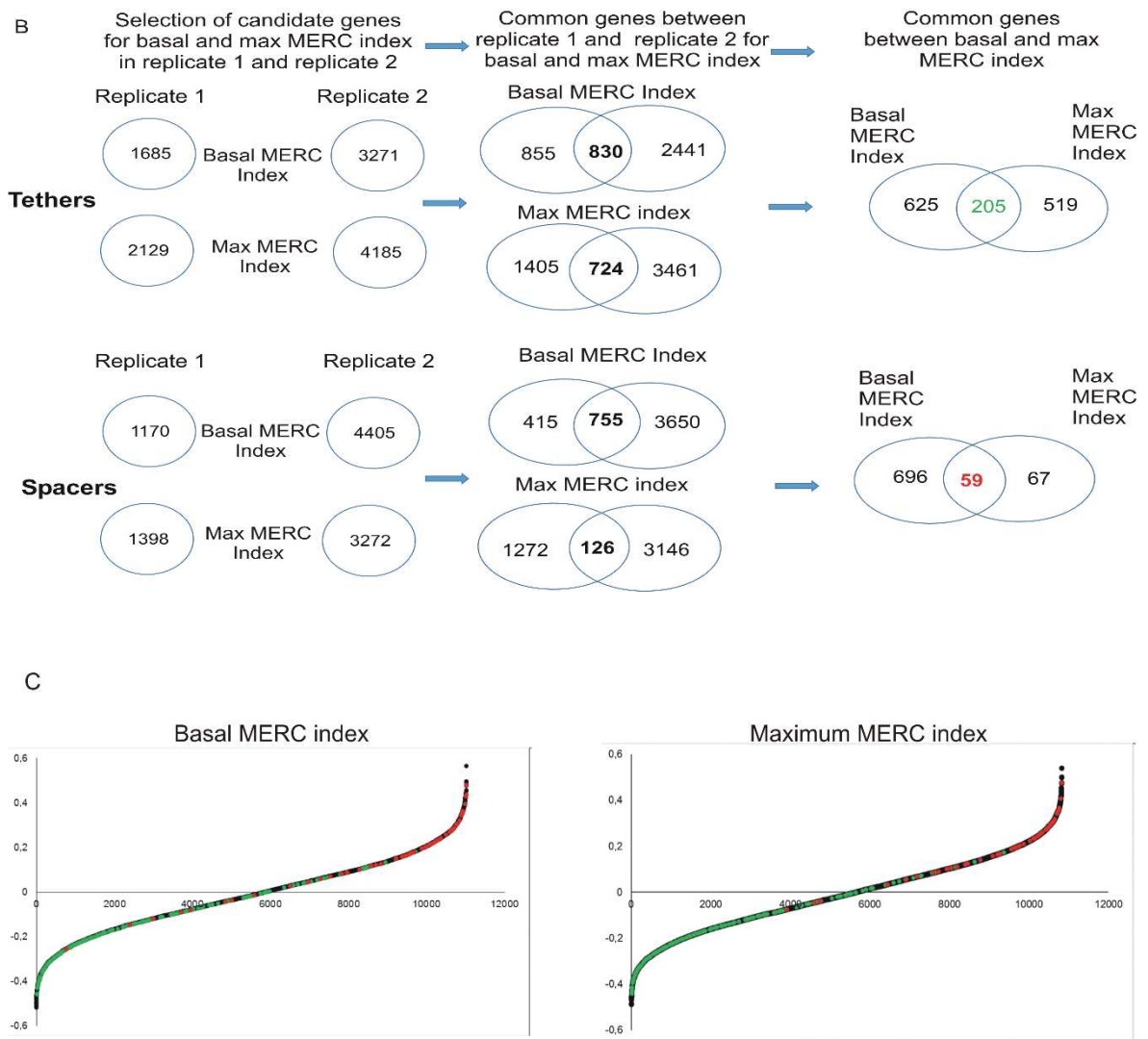
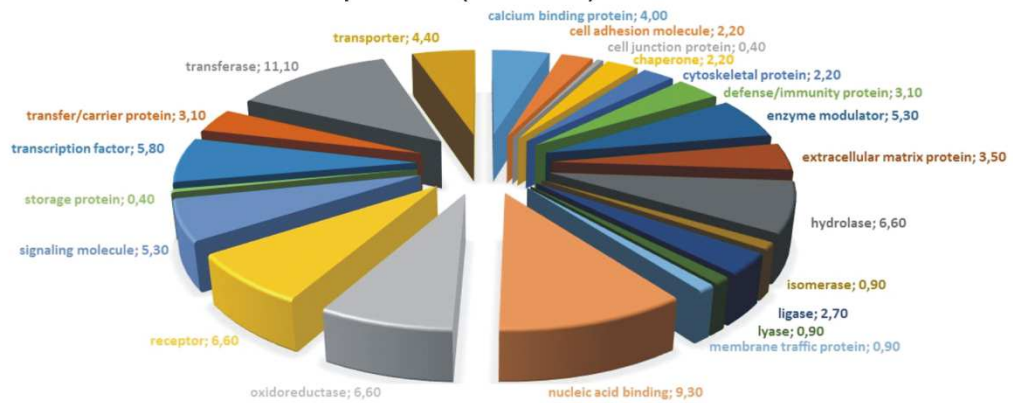
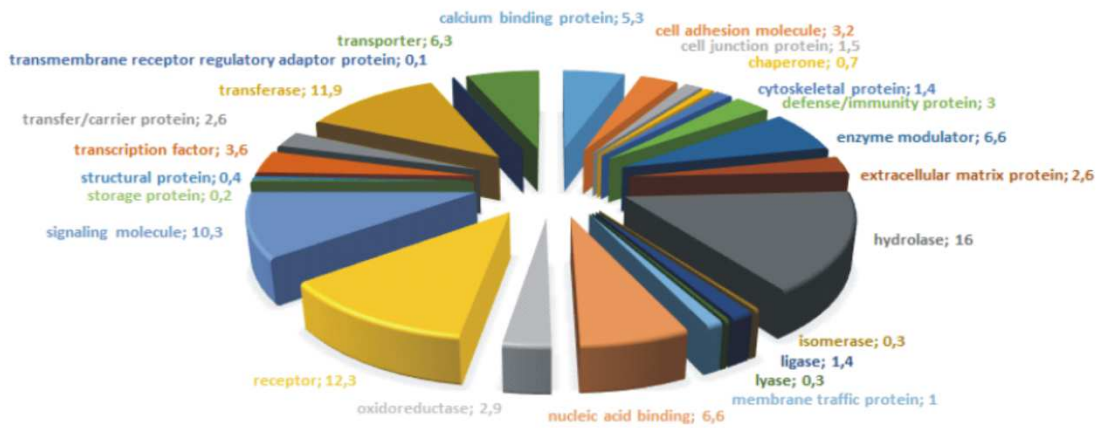


**Figure 5**

### A Common tethers and spacers (205+59)



### B Tethers and spacers affecting only basal MERC index (625+696)



### C Tethers and spacers affecting only maximum MERC index (519+67)

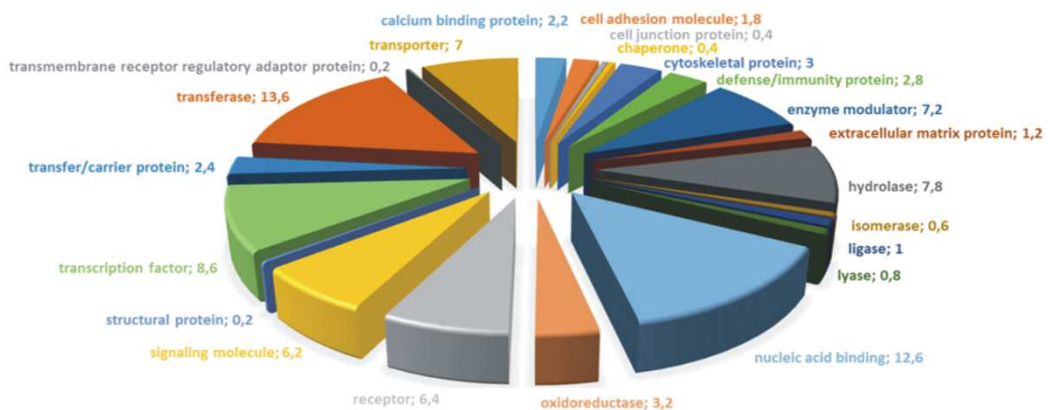


**Figure 6**

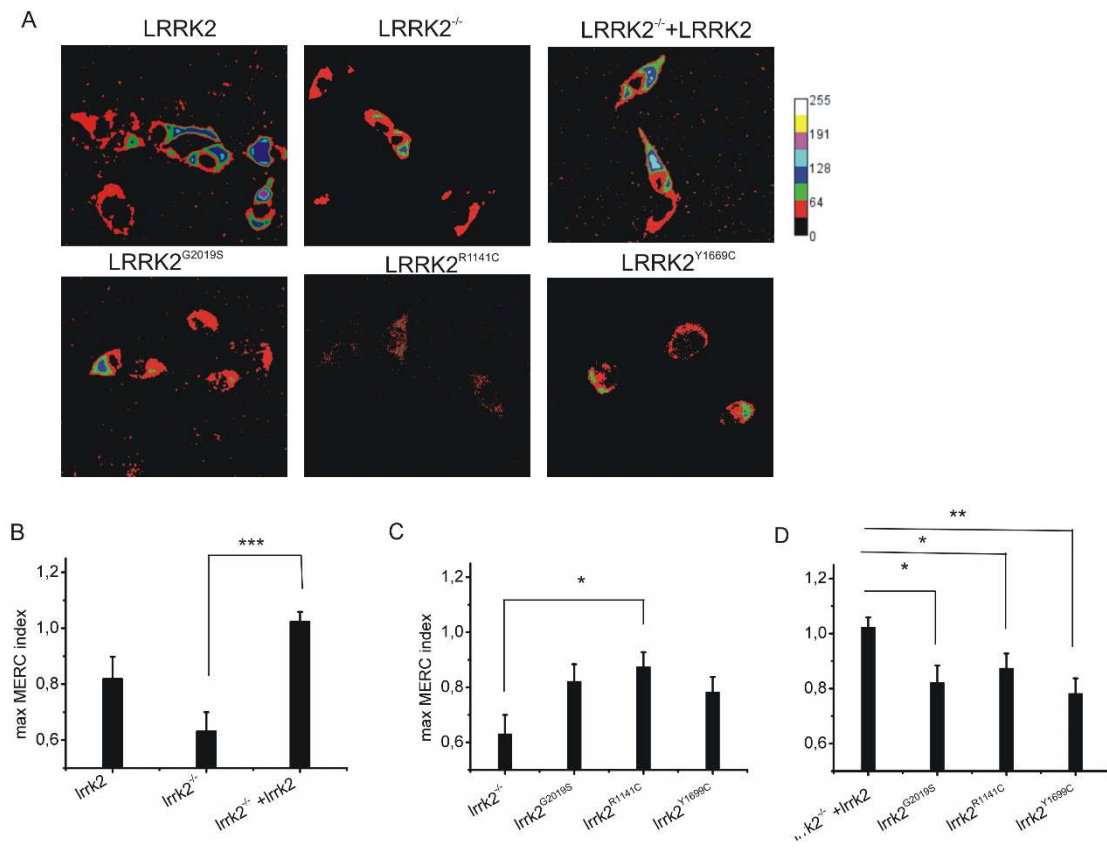
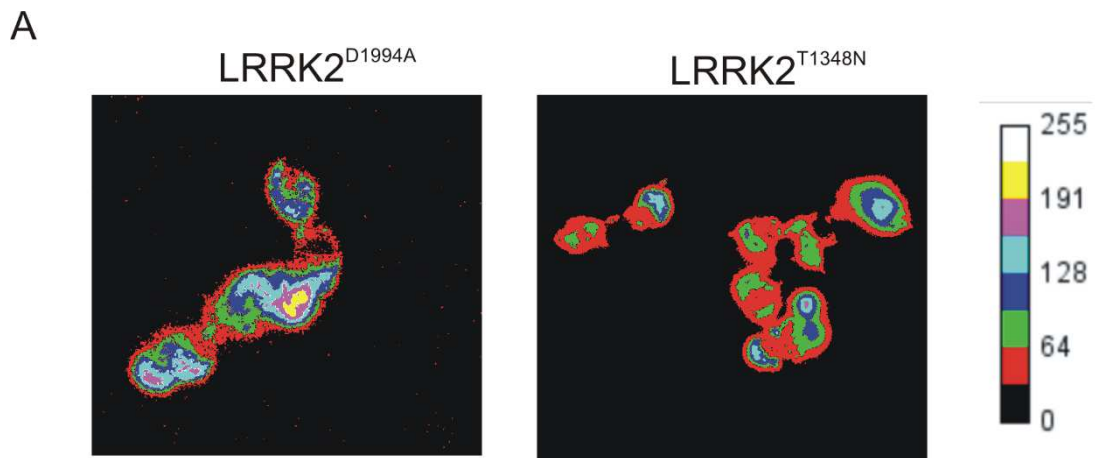


Figure 7



B

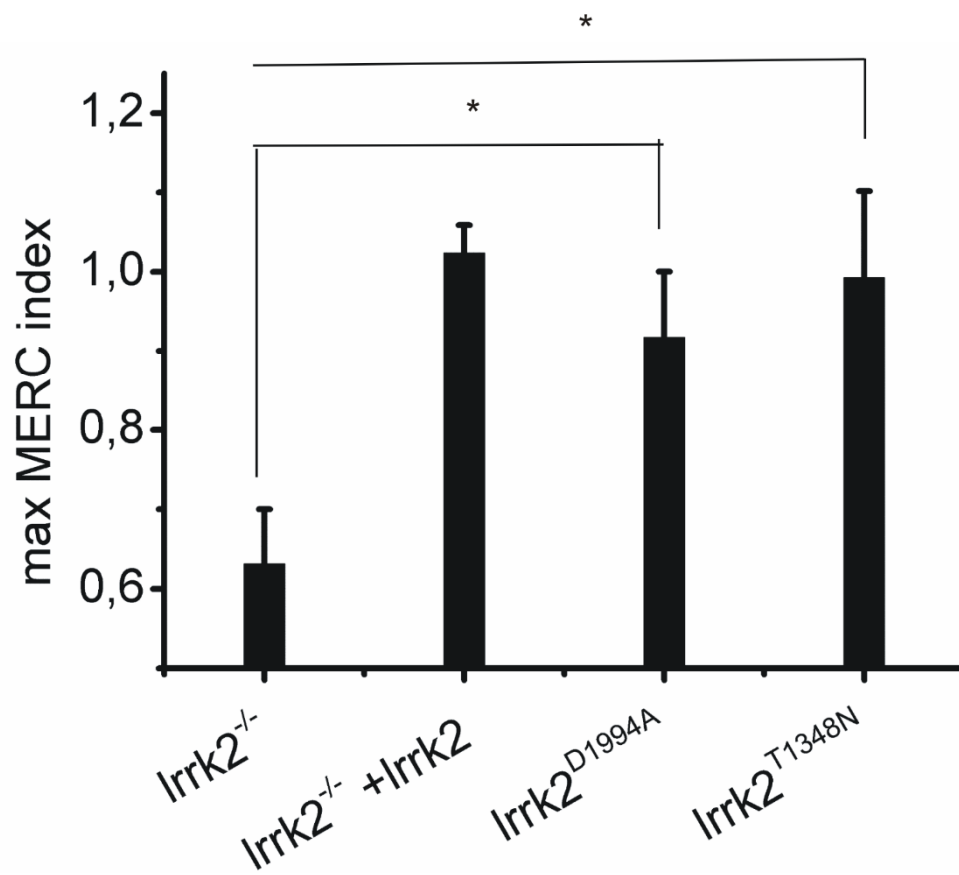
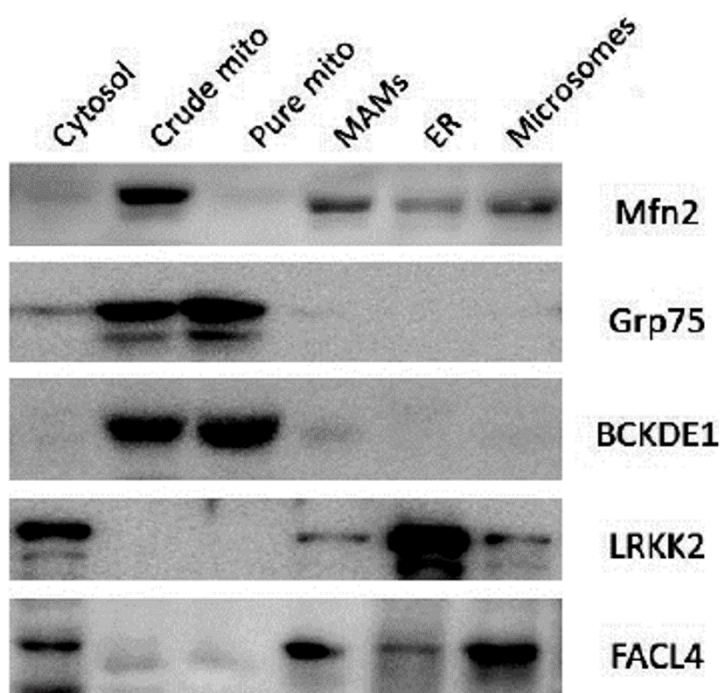
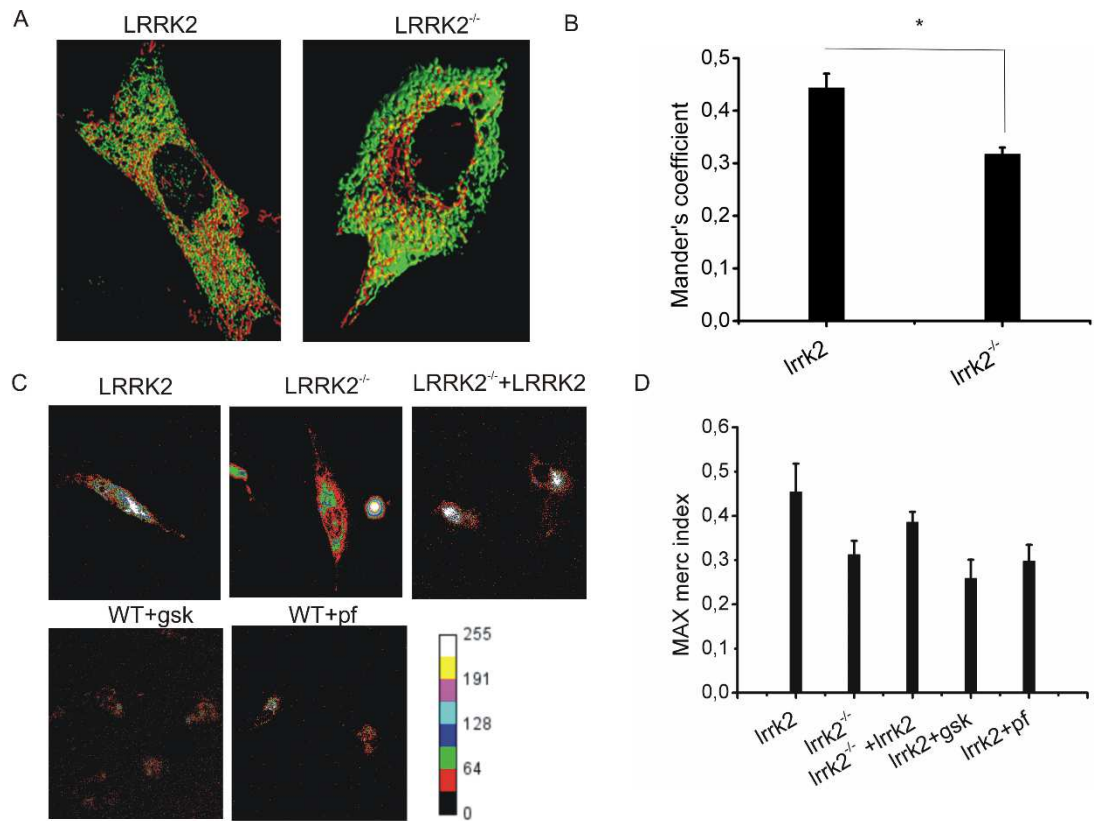


Figure 8



**Figure 9**



**Table 1**

**Common tethers and spacers (205+59)**

<b>Gene symbol</b>	<b>UniprotKB</b>	<b>Gene ID</b>	<b>Classification</b>
BNI3L	O60238	12176	spacer
BNIP3	Q12983	12177	spacer
CES5	Q8BK48	16402	tether
CYBB	P04839	13058	spacer
DHRS1	Q96LJ7	52585	spacer
DMPK	Q09013	243914	tether
IFRG15	Q9H496	67797	tether
ITGA5	P08648	194126	tether
KTN1	Q86UP2	16709	spacer
LMAN1	P49257	70361	spacer
PTGIS	Q16647	11920	tether
TOR1B	Q9ER41	80914	tether
UBE1X	P22314	12995	tether

**Table 2**

## Tethers and spacers affecting only maximum MERC index (519+67)

Gene symbol	UniprotKB	Gene ID	Classification
ASNA1	O54984	56495	tether
CD74	P04441	16149	tether
FRAP1	Q9JLN9	56717	tether
GOLT1B	Q9CR60	66964	tether
H6PD	Q8CFX1	100198	tether
ITGA5	P11688	16402	spacer
LRRK2	Q5S006	66725	tether
MGST1	Q91VS7	56615	tether
MYD116	P17564	17872	tether
PEBP1	P70296	23980	tether
PLD3	O35405	18807	tether
PRKCA	Q3TQ39	18750	tether
RHBL4	Q8BHC7	76867	tether
SLC39A7	Q31125	14977	tether
SERPINA1B	P22599	20701	tether
UBXD8	Q3TDN2	76577	tether

Table 3

**Tethers and spacers affecting only basal MERC index  
(625+696)**

Gene symbol	UniprotKB	Gene ID	Classification
AADAC	Q99PG0	67758	tether
ARTS1	Q9EQH2	80898	spacer
BDNF	P21237	12064	spacer
CALR	P14211	12317	spacer
CAMK2G	Q923T9	12325	tether
CTSZ	Q9WUU7	64138	spacer
CYP17A1	P27786	13074	tether
CYP1A2	P00186	13077	tether
DHRS7B	Q99J47	216820	spacer
DERL1	Q99J56	67819	spacer
FKBP2	P45878	14227	spacer
GLT25D1	Q8K297	234407	spacer
KCNA1	P16388	16485	spacer
ITGA8	A2ARA8	241226	tether
MYOC	O70624	17926	tether
NCSTN	D6RCJ2	59287	tether
PIK4CB	Q8BKC8	107650	spacer
PNPLA7	A2AJ88	241274	tether
PRKCD	P28867	18753	tether
PSEN2	Q3U4P5	19165	spacer
PTPLAD1	Q8K2C9	57874	spacer
PTPN1	P35821	19246	spacer
RAB18	P35293	19330	tether
RNF185	Q91YT2	193670	tether
S100A1	P56565	20193	spacer
SCN5A	Q9JJV9	20271	spacer
TAP1	P21958	21354	spacer
TAP2	P36371	21355	spacer
TMC3	F8VQI4	233424	spacer
TMC6	B1ATB5	217353	spacer

**A genome wide high content imaging screen identifies a novel function for the Parkinson's disease gene LRRK2 as endoplasmic reticulum-mitochondria tether**

Annalisa Serafini et al.

Supplementary online material

**Extended table 1.** List of 205 tethers common between basal and maximum MERC index found in both replicates

**Extended table 2.** List of 59 spacers common between basal and maximum MERC index found in both replicates

**Extended table 1.**

	<b>Gene symbol</b>	<b>Gene ID</b>
1	1300007F04Rik	51897
2	1700025E21Rik	13178
3	1700112C13Rik	67477
4	1810030N24Rik	13198
5	2310042G06Rik	13205
6	2310065K24Rik	75647
7	2600011C06Rik	110524
8	2700049P18Rik	27369
9	2810401C16Rik	54004
10	2810430M08Rik	74306
11	4930452B06Rik	13400
12	4930527D15Rik	69537
13	4930542C12Rik	319446
14	4931428L18Rik	73708
15	4933436I01Rik	13548
16	5830427D03Rik	106389
17	5830434P21Rik	68226
18	5830457H20Rik	27103
19	6030408C04Rik	30050
20	6530403A03Rik	30839
21	8430408G22Rik	66291
22	9430022F06Rik	66390
23	A830019P07Rik	14183
24	A930002I21Rik	14415
25	Aass	14464
26	Actr8	208188
27	Adam15	102122
28	Adamts1	75764
29	Adamts8	67039
30	Adcyap1r1	14626
31	Agxt2	269132
32	AI450540	108900
33	AI504432	271709
34	Angel2	14763
35	Arhgap23	52857
36	Arhgap5	107022
37	Arpp21	69146
38	Atm	66596
39	B230317C12Rik	72168
40	BC029169	56534
41	BC032265	15898

42	C530028O21Rik	64164
43	Ccar1	16172
44	Cd1d1	106347
45	Cdyl	16351
46	Ces5	16402
47	Chst12	67223
48	Cln3	69564
49	Coasy	16548
50	Csnk2a1	231855
51	D0H4S114	74430
52	D0HXS9928E	18048
53	D2Ertd391e	67736
54	Dck	93970
55	Ddit3	16636
56	Ddx3x	16643
57	Dgkq	16846
58	Dguok	107753
59	Diap2	246316
60	Dmpk	243914
61	Dnase1l1	242517
62	Dpep2	382243
63	Dppa3	67648
64	Dyrk1a	385049
65	Eaf2	72416
66	Efcab2	70988
67	Eif2ak4	76612
68	Fbxw2	66780
69	Fbxw5	76061
70	Fgfr2	192198
71	Gad1	74342
72	Gata5	216028
73	Ghsr	70082
74	Giyd2	56150
75	Gk2	17123
76	Glt25d2	227723
77	Gm642	66449
78	Gpr37	26398
79	Gramd1a	217708
80	Gramd3	225028
81	Gsdmdc1	17168
82	Gtf3a	17256
83	Hspb3	50932
84	Icam5	217558
85	Ifrg15	67797
86	Il17ra	381974

87	Ildr1	213393
88	Ipp	17686
89	Itga5	194126
90	Itgb1bp3	78388
91	Khk	214682
92	KIAA0415	27354
93	Klk1b4	68197
94	Klra18	66866
95	Klra5	18094
96	Klrd1	97961
97	Lep	225152
98	Lgals2	329056
99	Lgi2	109226
100	Lgi4	70078
101	LOC242517	70769
102	LOC382243	59015
103	LOC385049	100535
104	Lrpprc	258390
105	Lrrc27	30956
106	Lrrc4	258946
107	Lrrtm1	56249
108	Lrrtm3	258943
109	Lysmd2	258964
110	Mad2l1	259124
111	Madcam1	11490
112	Magmas	258663
113	Map2k4	258677
114	Map4k3	258232
115	Mare	18479
116	Mea1	18607
117	Mink1	170768
118	Mrgprg	11504
119	Msh3	225326
120	Mtmr11	83436
121	Mvp	233765
122	Myo3a	59047
123	Nbn	30806
124	Ndufc2	19134
125	Nhlrc2	11517
126	Nkx2-9	73677
127	Nol12	26445
128	Nol7	268782
129	Nolc1	66997
130	Nup160	22123
131	Oas1d	226252

132	Olfr1276	19223
133	Olfr348	103136
134	Olfr353	229694
135	Olfr541	19361
136	Olfr638	52477
137	Olfr739	71810
138	Olfr76	58996
139	Olfr774	11855
140	Pak1	72388
141	Pdpk1	57751
142	Pfkfb3	20111
143	Pik3c3	78785
144	Plekha2	170728
145	Plekha7	12399
146	Pnkp	74100
147	Prpf4b	56353
148	Psma8	219151
149	Psmb2	380713
150	Psmd12	399548
151	Psmd3	20768
152	Ptgis	11920
153	Pwp1	228071
154	Rad51	72193
155	Ranbp3	170755
156	Ripk4	56279
157	Rnf25	52551
158	Rps6ka1	21402
159	Rsnl2	208659
160	Rtn4ip1	238024
161	Runx3	224661
162	Rybp	108652
163	Scara3	20874
164	Scarf1	75788
165	Scn4b	20646
166	Sephs2	266781
167	Sestd1	320145
168	Sfrs2ip	319352
169	Sgk3	212518
170	Sgta	109267
171	Skp1a	269019
172	Slc26a8	67500
173	Slc35b3	232533
174	Slk	20944
175	Smurf1	118449
176	Snrpn	21405

177	Snx17	21808
178	Sp8	21846
179	Sprn	319880
180	Srcrb4d	30934
181	Stk32a	12479
182	Stk38l	58217
183	Svs5	12593
184	Synpo2	56771
185	Tcf1	22074
186	Tgfb2	234673
187	Tie1	80385
188	Tmcc3	22201
189	Tor1b	80914
190	Trem1	59031
191	Trfp	12752
192	Try4	71743
193	Tusc2	74112
194	Ube1x	12995
195	Uck2	30940
196	Usp16	100756
197	Usp25	75083
198	Usp30	171260
199	Usp50	22355
200	V1rj2	27528
201	Vipr2	66840
202	Wdr45l	72693
203	Zcchc12	66758
204	Zfp474	108160
205	Zfpn1a1	22778

## Extended Table 2

	<b>Gene symbol</b>	<b>Gene ID</b>
1	1700029I01Rik	70005
2	2410129H14Rik	76789
3	2610024A01Rik	72160
4	3110003A22Rik	68053
5	4921511I16Rik	70925
6	4930558O21Rik	68307
7	4930563M21Rik	75258
8	Adh7	11529
9	Akr1a4	58810
10	Akr1c13	27384
11	Blvra	109778
12	Bnip3	12176
13	Bnip3l	12177
14	C030048B08Rik	269623
15	C1qa	12259
16	Ccdc106	232821
17	Ceacam19	319930
18	Cxcl13	55985
19	Cyb5r4	266690
20	Cybb	13058
21	Dclre1b	140917
22	Ddit4	74747
23	Defb4	56519
24	Dhrs1	52585
25	Dus3l	224907
26	Eif4g2	13690
27	Ep400	75560
28	Evc2	68525
29	Ftmt	14177
30	Gdpd4	233537
31	Gnb2	14693
32	Gss	14854
33	Hand2	15111
34	Hivep1	110521
35	Kcnh2	16511
36	Kcnt1	227632
37	Kctd1	106931
38	Klra17	170733
39	Ktn1	16709
40	Lactb2	212442

41	Lman1	70361
42	LOC268650	268650
43	Neurod4	11923
44	Olfcr801	258282
45	Olfcr993	258427
46	Pecr	111175
47	Pycr2	69051
48	Rhoa	11848
49	Slc12a7	20499
50	Slc36a2	246049
51	Slc43a1	72401
52	Slc8a1	20541
53	Slmap	83997
54	Sp4	20688
55	Taf10	24075
56	Tmc5	74424
57	Tnfrsf1a	21937
58	Txnrd2	26462
59	Uqcrb	67530

## 6 Conclusions and future perspectives

In this thesis, we had set a high content screen to unravel the molecular components of mitochondria-ER contact sites (MERCs). We have developed and utilized a modified FRET based biosensor whose FRET intensity mirror the proximity between ER and mitochondria. FRET based biosensor (FEMP) provided us with a distinct advantage of measuring both basal MERC index, defined as the proximity of ER-mitochondria contacts at any time point, but also maximum MERC index, that corresponded to the maximum possible contacts. Statistical and bioinformatic analysis of our high-throughput data suggested new previously unknown role as regulator of ER-mitochondria juxtaposition for many proteins. High content screening of ~10,000 genes in two replicates and rigorous statistical analysis yielded 205 tethers and 59 spacers to be most significant, and also 625 tethers and 696 spacers affecting only the basal MERC index, and 519 tethers and 67 spacers modulating only the Maximum MERC index. Bioinformatics analysis by Mitominer yielded 13 proteins affecting both the indexes, 30 proteins affecting only the Basal MERC index and 16 proteins affecting only the Maximum MERC index reported to be localized in both ER and mitochondria membranes. Panther database classification also provided high confidence protein classes to which the “hits” belong to.

LRRK2 was identified as a tether of ER and mitochondria in the high-throughput screen. Of note, mutations of LRRK2 are the main cause of familial forms of PD. Biochemical fractionation data also confirmed the localisation of LRRK2 to MAMs, thus supporting the high content screen analysis. LRRK2 ablation decreases the contacts between mitochondria and ER, that can be rescued by reintroduction of LRRK2 WT protein, but not of LRRK2 pathological mutants. Since recently alterations observed in several neurodegenerative disease have been related to dysregulation of MERC structure (Paillusson S. et al., 2016), this newly identified role for LRRK2 will add a fundamental piece in this intriguing puzzle.

Our study on ER-mitochondria contacts modulator will be of crucial importance in several future research directions considering that the genes which we have identified belong to cellular pathways that are already known to be involved in ER-mitochondria communications and to others that were never related to it before.

## 7 References

Ahn, T.B., Kim, S.Y., Kim, J.Y., Park, S.S., Lee, D.S., Min, H.J., Kim, Y.K., Kim, S.E., Kim, J.M., Kim, H.J., Cho, J., and Jeon, B.S. (2008). alpha-Synuclein gene duplication is present in sporadic Parkinson disease. *Neurology* 70, 43-49.

Alegre-Abarategui, J., Christian, H., Lufino, M.M.P., Mutihac, R., Venda, L.L., Ansorge, O., and Wade-Martins, R. (2009). LRRK2 regulates autophagic activity and localizes to specific membrane microdomains in a novel human genomic reporter cellular model. *Hum. Mol. Genet.* 18, 4022-4034.

Alexander, C., Votruba, M., Pesch, U.E.A., Thiselton, D.L., Mayer, S., Moore, A., Rodriguez, M., Kellner, U., Leo- Kottler, B., Auburger, G., Bhattacharya, S.S., and Wissinger, B. (2000). OPA1, encoding a dynamin-related GTPase, is mutated in autosomal dominant optic atrophy linked to chromosome 3q28. *Nat. Genet.* 26, 211-215.

Alexander, G.E. (2004). Biology of Parkinson's disease: Pathogenesis and pathophysiology of a multisystem neurodegenerative disorder. *Dialogues Clin. Neurosci.* 6, 259-280.

Alford, S.C., Ding, Y., Simmen, T., and Campbell, R.E. (2012). Dimerization-dependent green and yellow fluorescent proteins. *ACS Synth. Biol.* 1, 569-575.

Al-Saif, A., Al-Mohanna, F., and Bohlega, S. (2011). A mutation in sigma-1 receptor causes juvenile amyotrophic lateral sclerosis. *Ann. Neurol.* 70, 913-919.

Anand, R., Wai, T., Baker, M.J., Kladt, N., Schauss, A.C., Rugarli, E., and Langer, T. (2014). The i-AAA protease YME1L and OMA1 cleave OPA1 to balance mitochondrial fusion and fission. *J. Cell Biol.* 204, 919-929.

Appel-Cresswell, S., Vilarino-Guell, C., Encarnacion, M., Sherman, H., Yu, I., Shah, B., Weir, D., Thompson, C., Szu-Tu, C., Trinh, J., Aasly, J.O., Rajput, A., Rajput, A.H., Jon Stoessl, A., and Farrer., M.J. (2013). Alpha-synuclein p.H50Q, a novel pathogenic mutation for Parkinson's disease. *Movement Disorders* 28, 811-813.

Area-Gomez, E., De Groof, A.J.C., Boldogh, I., Bird, T.D., Gibson, G.E., Koehler, C.M., Yu, W.H., Duff, K.E., Yaffe, M.P., Pon, L.A., and Schon, E.A. (2009). Presenilins are enriched in endoplasmic reticulum membranes associated with mitochondria. *Am. J. Pathol.* 175, 1810-1816.

Area-Gomez, E., Del Carmen Lara Castillo, M., Tambini, M.D., Guardia-Laguarta, C., De Groof, A.J.C., Madra, M., Ikenouchi, J., Umeda, M., Bird, T.D., Sturley, S.L., and Schon, E.A. (2012). Upregulated function of mitochondria- associated ER membranes in Alzheimer disease. *Embo J.* 31, 4106-4123.

Axe, E.L., Walker, S.A., Manifava, M., Chandra, P., Roderick, H.L., Habermann, A., Griffiths, G., and Ktistakis, N.T. (2008). Autophagosome formation from membrane compartments enriched in phosphatidylinositol 3-phosphate and dynamically connected to the endoplasmic reticulum. *J. Cell Biol.* 182, 685-701.

Axelrod, D. (1977). Cell surface heating during fluorescence photobleaching recovery experiments. *Biophys. J.* 18, 129-131.

Bae, J.R., and Lee, B.D. (2015). Function and dysfunction of leucine-rich repeat kinase 2 (LRRK2): Parkinson's disease and beyond. *BMB Rep.* 48, 243-248.

Banaszynski, L.A., Liu, C.W., and Wandless, T.J. (2005). Characterization of the FKBP-rapamycin-FRB ternary complex. *J. Am. Chem. Soc.* 127, 4715-4721.

Banchs, I., Casasnovas, C., Albertí, A., De Jorge, L., Povedano, M., Montero, J., Martínez-Matos, J.A., and Volpini, V. (2009). Diagnosis of Charcot-Marie-Tooth disease. *J. Biomed. Biotechnol.* 2009.

Baumann, N.A., Sullivan, D.P., Ohvo-Rekilä, H., Simonot, C., Pottekat, A., Klaassen, Z., Beh, C.T., and Menon, A.K. (2005). Transport of newly synthesized sterol to the sterol-enriched plasma membrane occurs via nonvesicular equilibration. *Biochemistry* 44, 5816-5826.

Becker M., Kleinsmith L.J., Hardin J. (2008). *Il Mondo della Cellula*, Pearson.

Beilina, A., Rudenko, I.N., Kaganovich, A., Civiero, L., Chau, H., Kalia, S.K., Kalia, L.V., Lobbstaël, E., Chia, R., Ndukwe, K., Ding J, Nalls, M.A., Olszewski, M., Hauser, D.N., Kumaran, R., Lozano, A.M., Baekelandt, V., Greene, L.E., Taymans, J.M., Greggio, E., and Cookson, M.R. (2014). Unbiased screen for interactors of leucine-rich repeat kinase 2 supports a common pathway for sporadic and familial Parkinson disease. *Proc. Natl. Acad. Sci. U. S. A.* 111, 2626-2631.

Bereiter-Hahn, J., and Voth, M. (1994). Dynamics of mitochondria in living cells: Shape changes, dislocations, fusion, and fission of mitochondria. *Microsc. Res. Tech.* 27, 198-219.

Berger, Z., Smith, K.A., and Lavoie, M.J. (2010). Membrane localization of LRRK2 is associated with increased formation of the highly active lrrk2 dimer and changes in its phosphorylation. *Biochemistry* 49, 5511-5523.

Bernardi P. (1999). Mitochondrial transport of cations: channels, exchangers, and permeability transition. *Physiol Rev.* 79(4), 1127-1155.

Bertoncini, C.W., Fernandez, C.O., Griesinger, C., Jovin, T.M., and Zweckstetter, M. (2005). Familial mutants of  $\alpha$ -synuclein with increased neurotoxicity have a destabilized conformation. *J. Biol. Chem.* 280, 30649-30652.

Berwick, D.C., and Harvey, K. (2012). LRRK2 functions as a wnt signaling scaffold, bridging cytosolic proteins and membrane-localized LRP6. *Hum. Mol. Genet.* 21, 4966-4979.

Betz, C., Stracka, D., Prescianotto-Baschong, C., Frieden, M., Demaurex, N., and Hall, M.N. (2013). Feature Article: mTOR complex 2- Akt signaling at mitochondria-associated endoplasmic reticulum membranes (MAM) regulates mitochondrial physiology. *Proc. Natl. Acad. Sci. U. S. A.* 110, 12526-12534.

Biosa, A., Trancikova, A., Civiero, L., Glauser, L., Bubacco, L., Greggio, E., and Moore, D.J. (2013). GTPase activity regulates kinase activity and cellular phenotypes of parkinson's disease-associated LRRK2. *Hum. Mol. Genet.* 22, 1140-1156.

Birmingham, A., Selfors, L.M., Forster, T., Wrobel, D., Kennedy, C.J., Shanks, E., Santoyo-Lopez, J., Dunican, D.J., Long, A., Kelleher, D., Beijersbergen, R.L., Ghazal, P.,

and Shamu, C.E. (2009). Statistical methods for analysis of high-throughput RNA interference screens. *Nat. Methods* 6, 569-575.

Biskup, S., Moore, D.J., Celsi, F., Higashi, S., West, A.B., Andrabi, S.A., Kurkinen, K., Yu, S., Savitt, J.M., and Waldvogel, H.J. (2006). Localization of LRRK2 to membranous and vesicular structures in mammalian brain. *Ann. Neurol.* 60, 557-569.

Biskup, S., Moore, D.J., Rea, A., Lorenz-Deperieux, B., Coombes, C.E., Dawson, V.L., Dawson, T.M., and West, A.B. (2007). Dynamic and redundant regulation of LRRK2 and LRRK1 expression. *BMC Neuroscience* 8, 1.

Blesa, J., and Przedborski, S. (2014). Parkinson's disease: Animal models and dopaminergic cell vulnerability. *Front. Neuroanat.* 8,

Blum, D., Torch, S., Lambeng, N., Nissou, M., Benabid, A., Sadoul, R., and Verna, J. (2001). Molecular pathways involved in the neurotoxicity of 6-OHDA, dopamine and MPTP: Contribution to the apoptotic theory in Parkinson's disease. *Prog. Neurobiol.* 65, 135-172.

Bonifati, V., Rohé, C.F., Breedveld, G.J., Fabrizio, E., De Mari, M., Tassorelli, C., Tavella, A., Marconi, R., Nicholl, D.J., Chien, H.F., Fincati, E., Abbruzzese, G., Marini, P., De Gaetano, A., Horstink, M.W., Maat-Kievit, J.A., Sampaio, C., Antonini, A., Stocchi, F., Montagna, P., Toni, V., Guidi, M., Dalla Libera, A., Tinazzi, M., De Pandis, F., Fabbrini, G., Goldwurm, S., de Klein, A., Barbosa, E., Lopiano, L., Martignoni, E., Lamberti, P., Vanacore, N., Meco, G., and Oostra, B.A. (2005). Early-onset parkinsonism associated with PINK1 mutations: Frequency, genotypes, and phenotypes. *Neurology* 65, 87-95.

Bourne, H.R., Sanders, D.A., and McCormick, F. (1991). The GTPase superfamily: conserved structure and molecular mechanism. *Nature* 349, 117-127.

Boutros, M., Brás, L.P., and Huber, W. (2006). Analysis of cell-based RNAi screens. *Genome Biol.* 7.

Boyer, O., Nevo, F., Plaisier, E., Funalot, B., Gribouval, O., Benoit, G., Cong, E.H., Arrondel, C., Tete, M., Montjean, R., Richard, L., Karras, A., Pouteil-Noble, C., Balafrej, L., Bonnardeaux, A., Canaud, G., Charasse, C., Dantal, J., Deschenes, G., Deteix, P., Dubourg, O., Petiot, P., Pouthier, D., Leguern, E., Guiochon-Mantel, A., Broutin, I., Gubler, M.C., Saunier, S., Ronco, P., Vallat, J.M., Alonso, M.A., Antignac, C., and Mollet, G. (2011). INF2 mutations in Charcot-Marie-Tooth disease with glomerulopathy. *New Engl. J. Med.* 365, 2377-2388.

Bravo, R., Vicencio, J.M., Parra, V., Troncoso, R., Munoz, J.P., Bui, M., Quiroga, C., Rodriguez, A.E., Verdejo, H.E., Ferreira, J., Iglewski, M., Chiong, M., Simmen, T., Zorzano, A., Hill, J.A., Rothermel, B.A., Szabadkai, G., and Lavandero, S. (2011). Increased ER-mitochondrial coupling promotes mitochondrial respiration and bioenergetics during early phases of ER stress. *J. Cell. Sci.* 124, 2143-2152.

Brown, E.B., Wu, E.S., Zipfel, W., and Webb, W.W. (1999). Measurement of molecular diffusion in solution by multiphoton fluorescence photobleaching recovery. *Biophys. J.* 77, 2837-2849.

Bui, M., Gilady, S.Y., Fitzsimmons, R.E., Benson, M.D., Lynes, E.M., Gesson, K., Alto, N.M., Strack, S., Scott, J.D., and Simmen, T. (2010). Rab32 modulates apoptosis onset and mitochondria-associated membrane (MAM) properties. *J. Biol. Chem.* 285, 31590-31602.

Byrnes, L.J., Singh, A., Szeto, K., Benveniste, N.M., O'Donnell, J.P., Zipfel, W.R., and Sonderegger, H. (2013). Structural basis for conformational switching and GTP loading of the large G protein atlastin. *Embo J.* 32, 369-384.

Caesar, M., Felk, S., Aasly, J.O., and Gillardon, F. (2015). Changes in actin dynamics and F-actin structure both in synaptoneurosomes of LRRK2(R1441G) mutant mice and in primary human fibroblasts of LRRK2(G2019S) mutation carriers. *Neuroscience* 284, 311-324.

Calì, T., Ottolini, D., Negro, A., and Brini, M. (2013). Enhanced parkin levels favor ER-mitochondria crosstalk and guarantee  $\text{Ca}^{2+}$  transfer to sustain cell bioenergetics. *Biochim. Biophys. Acta Mol. Basis Dis.* 1832, 495-508.

Calì, T., Ottolini, D., Negro, A., and Brini, M. (2012).  $\alpha$ -synuclein controls mitochondrial calcium homeostasis by enhancing endoplasmic reticulum-mitochondria interactions. *J. Biol. Chem.* 287, 17914-17929.

Canet-Avilés, R.M., Wilson, M.A., Miller, D.W., Ahmad, R., McLendon, C., Bandyopadhyay, S., Baptista, M.J., Ringe, D., Petsko, G.A., and Cookson, M.R. (2004). The Parkinson's disease DJ-1 is neuroprotective due to cysteine- sulfenic acid-driven mitochondrial localization. *Proc. Natl. Acad. Sci. U. S. A.* 101, 9103-9108.

Cárdenas, C., Miller, R.A., Smith, I., Bui, T., Molgó, J., Müller, M., Vais, H., Cheung, K.-., Yang, J., Parker, I., Thompson, C.B., Birnbaum, M.J., Hallows, K.R., and Foskett, J.K. (2010). Essential Regulation of Cell Bioenergetics by Constitutive InsP3 Receptor  $\text{Ca}^{2+}$  Transfer to Mitochondria. *Cell* 142, 270-283.

Cardullo, R.A. (2013). Theoretical principles and practical considerations for fluorescence resonance energy transfer microscopy. *Methods Cell Biol.* 114, 441-456.

Carisey, A., Stroud, M., Tsang, R., and Ballestrom, C. (2011). Fluorescence recovery after photobleaching. *Methods Mol. Biol.* 769, 387-402.

Chan, D., Citro, A., Cordy, J.M., Shen, G.C., and Wolozin, B. (2011). Rac1 protein rescues neurite retraction caused by G2019s leucine-rich repeat kinase 2 (LRRK2). *J. Biol. Chem.* 286, 16140-16149.

Chan, D.C. (2006). Mitochondrial fusion and fission in mammals. *Annu. Rev. Cell Dev. Biol.* 22, 79-99.

Chen, H., Detmer, S.A., Ewald, A.J., Griffin, E.E., Fraser, S.E., and Chan, D.C. (2003). Mitofusins Mfn1 and Mfn2 coordinately regulate mitochondrial fusion and are essential for embryonic development. *J. Cell Biol.* 160, 189-200.

Chen, H., Vermulst, M., Wang, Y.E., Chomyn, A., Prolla, T.A., McCaffery, J.M., and Chan, D.C. (2010). Mitochondrial fusion is required for mtDNA stability in skeletal muscle and tolerance of mtDNA mutations. *Cell* 141, 280-289.

Chen, L., Lloyd, W.R., Chang, C., Sud, D., and Mycek, M. (2013). Fluorescence lifetime imaging microscopy for quantitative biological imaging. *Methods Cell Biol.* 114, 457-488.

Cherra III, S.J., Steer, E., Gusdon, A.M., Kiselyov, K., and Chu, C.T. (2013). Mutant LRRK2 elicits calcium imbalance and depletion of dendritic mitochondria in neurons. *Am. J. Pathol.* 182, 474-484.

Cheung, K., Mei, L., Mak, D.D., Hayashi, I., Iwatsubo, T., Kang, D.E., and Foskett, J.K. (2010). Gain-of-function enhancement of IP3 receptor modal gating by familial Alzheimer's disease-linked presenilin mutants in human cells and mouse neurons. *Sci. Signal.* 3(114).

Cheung, K., Shineman, D., Müller, M., Cárdenas, C., Mei, L., Yang, J., Tomita, T., Iwatsubo, T., Lee, V.M., and Foskett, J.K. (2008). Mechanism of Ca<sup>2+</sup> Disruption in Alzheimer's Disease by Presenilin Regulation of InsP3 Receptor Channel Gating. *Neuron* 58, 871-883.

Cipolat, S., De Brito, O.M., Dal Zilio, B., and Scorrano, L. (2004). OPA1 requires mitofusin 1 to promote mitochondrial fusion. *Proc. Natl. Acad. Sci. U. S. A.* 101, 15927-15932.

Civiero, L., Dihanich, S., Lewis, P.A., and Greggio, E. (2014). Genetic, structural, and molecular insights into the function of RAS of complex proteins domains. *Chem. Biol.* 21, 809-818.

Civiero, L., Vancraenenbroeck, R., Belluzzi, E., Beilina, A., Lobbstaël, E., Reyniers, L., Gao, F., Micetic, I., de Maeyer, M., Bubacco, L., Baekelandt, V., Cookson, M.R., Greggio, E., and Taymans, J.M. (2012). Biochemical Characterization of Highly Purified Leucine-Rich Repeat Kinases 1 and 2 Demonstrates Formation of Homodimers. *Plos One* 7(8).

Clapham, D.E. (2007). Calcium signaling. *Cell* 131, 1047-1058.

Cogliati, S., Frezza, C., Soriano, M.E., Varanita. T., Quintana-Cabrera. R., Corrado, M., Cipolat, S., Costa, V., Casarin, A., Gomes, L.C., Perales-Clemente, E., Salviati. L., Fernandez-Silva, P., Enriquez, J.A., Scorrano, L. (2013). Mitochondrial cristae shape determines respiratory chain supercomplexes assembly and respiratory efficiency *Cell*. 155(1), 160-71

Cohen, G. (1984). Oxy-radical toxicity in catecholamine neurons. *Neurotoxicology* 5, 77-82.

Colombi, M., Molle, K.D., Benjamin, D., Rattenbacher-Kiser, K., Schaefer, C., Betz, C., Thiemeyer, A., Regenass, U., Hall, M.N., and Moroni, C. (2011). Genome-wide shRNA screen reveals increased mitochondrial dependence upon mTORC2 addiction. *Oncogene* 30, 1551-1565.

Cookson, M.R. (2015). LRRK2 Pathways Leading to Neurodegeneration. *Curr. Neurol. Neurosci. Rep.* 15(7), 42.

Copeland, D.E., and Dalton, A.J. (1959). An association between mitochondria and the endoplasmic reticulum in cells of the pseudobranch gland of a teleost. *J. Biophys. Biochem. Cytol.* 5, 393-396.

Cosson, P., Marchetti, A., Ravazzola, M., and Orci, L. (2012). Mitofusin-2 Independent Juxtaposition of Endoplasmic Reticulum and Mitochondria: An Ultrastructural Study. *Plos One* 7(9).

Crompton, M. (1999). The mitochondrial permeability transition pore and its role in cell death. *Biochem. J.* 341 (Pt 2), 233-249.

Csordás, G., Renken, C., Várnai, P., Walter, L., Weaver, D., Buttle, K.F., Balla, T., Mannella, C.A., and Hajnóczky, G. (2006). Structural and functional features and significance of the physical linkage between ER and mitochondria. *J. Cell Biol.* 174, 915-921.

Csordás, G., Várnai, P., Golenár, T., Roy, S., Purkins, G., Schneider, T.G., Balla, T., and Hajnóczky, G. (2010). Imaging Interorganelle Contacts and Local Calcium Dynamics at the ER-Mitochondrial Interface. *Mol. Cell* 39, 121- 132.

D'Angelo, G., Polishchuk, E., Tullio, G.D., Santoro, M., Campli, A.D., Godi, A., West, G., Bielawski, J., Chuang, C., Van Der Spoel, A.C., Platt, F.M., Hannun, Y.A., Polishchuk, R., Mattjus, P., and De Matteis, M.A. (2007). Glycosphingolipid synthesis requires FAPP2 transfer of glucosylceramide. *Nature* 449, 62-67.

Daniele, T., and Schiaffino, M.V. (2014). Organelle biogenesis and interorganellar connections: Better in contact than in isolation. *Communicative & Integrative Biology* 7, e29587.

Daniëls, V., Vancraenenbroeck, R., Law, B.M.H., Greggio, E., Lobbstaël, E., Gao, F., De Maeyer, M., Cookson, M.R., Harvey, K., Baekelandt, V., and Taymans, J. (2011). Insight into the mode of action of the LRRK2 Y1699C pathogenic mutant. *J. Neurochem.* 116, 304-315.

Davison, E.J., Pennington, K., Hung, C., Peng, J., Rafiq, R., Ostareck-Lederer, A., Ostareck, D.H., Ardley, H.C., Banks, R.E., and Robinson, P.A. (2009). Proteomic analysis of increased

Parkin expression and its interactants provides evidence for a role in modulation of mitochondrial function. *Proteomics* 9, 4284-4297.

Day, R.N., and Davidson, M.W. (2012). Fluorescent proteins for FRET microscopy: Monitoring protein interactions in living cells. *Bioessays* 34, 341-350.

Dayel, M.J., Horn, E.F.Y., and Verkman, A.S. (1999). Diffusion of green fluorescent protein in the aqueous-phase lumen of endoplasmic reticulum. *Biophys. J.* 76, 2843-2851.

De Brito, O.M., and Scorrano, L. (2008). Mitofusin 2 tethers endoplasmic reticulum to mitochondria. *Nature* 456, 605-610.

De Los Santos, C., Chang, C., Mycek, M., and Cardullo, R.A. (2015). FRAP, FLIM, and FRET: Detection and analysis of cellular dynamics on a molecular scale using fluorescence microscopy. *Mol. Reprod. Dev.* 82, 587-604.

De Strooper, B. (2007). Loss-of-function presenilin mutations in Alzheimer disease. Talking Point on the role of presenilin mutations in Alzheimer disease. *EMBO Rep.* 8, 141-146.

De Strooper, B. (2003). Aph-1, Pen-2, and Nicastrin with Presenilin generate an active  $\gamma$ -Secretase complex. *Neuron* 38, 9-12.

De vos, K.J., Mórotz, G.M., Stoica, R., Tudor, E.L., Lau, K., Ackerley, S., Warley, A., Shaw, C.E., and Miller, C.C. (2012). VAPB interacts with the mitochondrial protein PTPIP51 to regulate calcium homeostasis. *Hum. Mol. Genet.* 21, 1299-1311.

Decuypere, J., Monaco, G., Bultynck, G., Missiaen, L., De Smedt, H., and Parys, J.B. (2011). The IP 3 receptor– mitochondria connection in apoptosis and autophagy. *Biochimica Et Biophysica Acta (BBA)-Molecular Cell Research* 1813, 1003-1013.

Deng, J., Lewis, P.A., Greggio, E., Sluch, E., Beilina, A., and Cookson, M.R. (2008). Structure of the ROC domain from the Parkinson's disease-associated leucine-rich repeat kinase 2 reveals a dimeric GTPase. *Proc. Natl. Acad. Sci. U. S. A.* 105, 1499-1504.

Deng, X., Dzamko, N., Prescott, A., Davies, P., Liu, Q., Yang, Q., Lee, J.-., Patricelli, M.P., Nomanbhoy, T.K., Alessi, D.R., and Gray, N.S. (2011). Characterization of a selective inhibitor of the Parkinson's disease kinase LRRK2. *Nat. Chem. Biol.* 7, 203-205.

Diéterlen, F., and Lucotte, G. (2010) Original Synthetic Report: Origin of the G2019S mutation associated to Parkinson's disease in Europeans and in North Africans. *International Journal of Modern Anthropology* 1, 81-96.

Dykxhoorn, D.M., Novina, C.D., and Sharp, P.A. (2003). Killing the messenger: Short RNAs that silence gene expression. *Nat. Rev. Mol. Cell Biol.* 4, 457-467.

Echarri, A., and Del Pozo, M.A. (2015). Caveolae-mechanosensitive membrane invaginations linked to actin filaments. *J. Cell. Sci.* 128, 2747-2758.

Echeverri, C.J., Beachy, P.A., Baum, B., Boutros, M., Buchholz, F., Chanda, S.K., Downward, J., Ellenberg, J., Fraser, A.G., Hacohen, N., Hahn, W.C., Jackson, A.L., Kiger, A., Linsley, P.S., Lum, L., Ma, Y., Mathey-Prévôt, B., Root, D.E., Sabatini, D.M., Taipale, J., Perrimon, N., and Bernards, R. (2006). Minimizing the risk of reporting false positives in large-scale RNAi screens. *Nat. Methods* 3, 777-779.

Echeverri, C.J., and Perrimon, N. (2006). High-throughput RNAi screening in cultured cells: A user's guide. *Nat. Rev. Gen.* 7, 373-384.

Elbashir, S.M., Harborth, J., Lendeckel, W., Yalcin, A., Weber, K., and Tuschl, T. (2001). Duplexes of 21-nucleotide RNAs mediate RNA interference in cultured mammalian cells. *Nature* 411, 494-498.

Elbaz, Y., and Schuldiner, M. (2011). Staying in touch: The molecular era of organelle contact sites. *Trends Biochem. Sci.* 36, 616-623.

Ercius, P., Alaidi, O., Rames, M.J., and Ren, G. (2015). Electron Tomography: A Three-Dimensional Analytic Tool for Hard and Soft Materials Research. *Adv Mater* 27, 5638-5663.

Estrada, A.A., and Sweeney, Z.K. (2015). Chemical Biology of Leucine-Rich Repeat Kinase 2 (LRRK2) Inhibitors. *J. Med. Chem.* 58, 6733-6746.

Eura, Y., Ishihara, N., Yokota, S., and Mihara, K. (2003). Two Mitofusin Proteins, Mammalian Homologues of FZO, with Distinct Functions Are Both Required for Mitochondrial Fusion. *J. Biochem.* 134, 333-344.

Falschlehner, C., Steinbrink, S., Erdmann, G., and Boutros, M. (2010). High-throughput RNAi screening to dissect cellular pathways: A how-to guide. *Biotechnol. J.* 5, 368-376.

Ferreira, M., and Massano, J. (2016). An updated review of Parkinson's disease genetics and clinicopathological correlations. *Acta Neurol. Scand.*

Feske, S., Gwack, Y., Prakriya, M., Srikanth, S., Puppel, S.-., Tanasa, B., Hogan, P.G., Lewis, R.S., Daly, M., and Rao, A. (2006). A mutation in *Orai1* causes immune deficiency by abrogating CRAC channel function. *Nature* 441, 179- 185.

Filadi, R., Greotti, E., Turacchio, G., Luini, A., Pozzan, T., and Pizzo, P. (2016). Presenilin 2 Modulates Endoplasmic Reticulum-Mitochondria Coupling by Tuning the Antagonistic Effect of Mitofusin 2. *Cell Rep.* 15, 2226-2238.

Fire, A., Xu, S., Montgomery, M.K., Kostas, S.A., Driver, S.E., and Mello, C.C. (1998). Potent and specific genetic interference by double-stranded RNA in *caenorhabditis elegans*. *Nature* 391, 806-811.

Fornasiero, E.F., and Opazo, F. (2015). Super-resolution imaging for cell biologists: Concepts, applications, current challenges and developments *Prospects & Overviews E. F. Fornasiero and F. Opazo. Bioessays* 37, 436-451.

Fortin, D.L., Troyer, M.D., Nakamura, K., Kubo, S., Anthony, M.D., and Edwards, R.H. (2004). Lipid rafts mediate the synaptic localization of  $\alpha$ -synuclein. *J. Neurosci.* 24, 6715-6723.

Fowler, S.L., Akins, M., Zhou, H., Figeys, D., and Bennett, S.A.L. (2013). The liver connexin32 interactome is a novel plasma membrane-mitochondrial signaling nexus. *J. Proteome Res.* 12, 2597-2610.

Franco-Iborra, S., Vila, M., and Perier, C. (2015). The Parkinson Disease Mitochondrial Hypothesis: Where Are We at? *Neuroscientist* 22, 266-277.

Fransson, Å., Ruusala, A., and Aspenström, P. (2003). Atypical Rho GTPases have roles in mitochondrial homeostasis and apoptosis. *J. Biol. Chem.* 278, 6495-6502.

Frieden, M., Arnaudeau, S., Castelbou, C., and Demaurex, N. (2005). Subplasmalemmal mitochondria modulate the activity of plasma membrane  $\text{Ca}^{2+}$ -ATPases. *J. Biol. Chem.* 280, 43198-43208.

Friedman, J.R., Lackner, L.L., West, M., DiBenedetto, J.R., Nunnari, J., and Voeltz, G.K. (2011). ER tubules mark sites of mitochondrial division. *Science* 334, 358-362.

Friedman, J.R., and Voeltz, G.K. (2011). The ER in 3D: A multifunctional dynamic membrane network. *Trends Cell Biol.* 21, 709-717.

Frigault, M.M., Lacoste, J., Swift, J.L., and Brown, C.M. (2009). Live-cell microscopy - Tips and tools. *J. Cell. Sci.* 122, 753-767.

Fuchs, J., Nilsson, C., Kachergus, J., Munz, M., Larsson, E.-., Schüle, B., Langston, J.W., Middleton, F.A., Ross, O.A., Hulihan, M., Gasser, T., and Farrer, M.J. (2007). Phenotypic variation in a large Swedish pedigree due to SNCA duplication and triplication. *Neurology* 68, 916-922.

Funayama, M., Hasegawa, K., Kowa, H., Saito, M., Tsuji, S., and Obata, F. (2002). A new locus for Parkinson's disease (PARK8) maps to chromosome 12p11. 2–q13. 1. *Ann. Neurol.* 51, 296-301.

Gandhi, P.N., Chen, S.G., and Wilson-Delfosse, A.L. (2009). Leucine-rich repeat kinase 2 (LRRK2): A key player in the pathogenesis of Parkinson's disease. *J. Neurosci. Res.* 87, 1283-1295.

Gasser, T. (2009). Molecular pathogenesis of Parkinson disease: Insights from genetic studies. *Expert Rev. Mol. Med.* 11.

Gautier, C.A., Erpapazoglou, Z., Mouton-Liger, F., Muriel, M.P., Cormier, F., Bigou, S., Duffaure, S., Girard, M., Foret, B., Iannielli, A., Broccoli, V., Dalle, C., Bohl, D., Michel, P.P., Corvol, J.C., Brice, A., and Corti, O. (2016). The endoplasmic reticulum-mitochondria interface is perturbed in PARK2 knockout mice and patients with PARK2 mutations. *Hum. Mol. Genet.*

Gegg, M.E., Cooper, J.M., Chau, K., Rojo, M., Schapira, A.H.V., and Taanman, J. (2010). Mitofusin 1 and mitofusin 2 are ubiquitinated in a PINK1/parkin-dependent manner upon induction of mitophagy. *Hum. Mol. Genet.* 19, 4861-4870.

George, J.L., Mok, S., Moses, D., Wilkins, S., Bush, A.I., Cherny, R.A., and Finkelstein, D.I. (2009). Targeting the progression of Parkinson's disease. *Curr. Neuropharmacol.* 7, 9-36.

Giacomello, M., Drago, I., Pizzo, P., and Pozzan, T. (2007). Mitochondrial Ca<sup>2+</sup>; as a key regulator of cell life and death. *Cell Death & Differentiation* 14, 1267-1274.

Giacomello, M., and Pellegrini, L. (2016). The coming of age of the mitochondria–ER contact: a matter of thickness. *Cell Death & Differentiation*, 1-11.

Giasson, B.I., Murray, I.V.J., Trojanowski, J.Q., and Lee, V.M. (2001). A Hydrophobic Stretch of 12 Amino Acid Residues in the Middle of  $\alpha$ -Synuclein Is Essential for Filament Assembly. *J. Biol. Chem.* 276, 2380-2386.

Gilkerson, R.W., Selker, J.M.L., and Capaldi, R.A. (2003). The cristal membrane of mitochondria is the principal site of oxidative phosphorylation. *FEBS Lett.* 546, 355-358.

Gillardot, F. (2009). Interaction of elongation factor 1-alpha with leucine-rich repeat kinase 2 impairs kinase activity and microtubule bundling in vitro. *Neuroscience* 163, 533-539.

Giorgi, C., Bonora, M., Sorrentino, G., Missiroli, S., Poletti, F., Suski, J.M., Ramirez, F.G., Rizzuto, R., Virgilio, F.D., Zito, E., Pandolfi, P.P., Wieckowski, M.R., Mammano, F., Del Sal, G., and Pinton, P. (2015). P53 at the endoplasmic reticulum regulates apoptosis in a  $Ca^{2+}$  dependent manner. *Proc. Natl. Acad. Sci. U. S. A.* 112, 1779-1784.

Giorgi, C., Ito, K., Lin, H.-., Santangelo, C., Wieckowski, M.R., Lebiedzinska, M., Bononi, A., Bonora, M., Duszynski, J., Bernardi, R., Rizzuto, R., Tacchetti, C., Pinton, P., and Pandolfi, P.P. (2010). PML regulates apoptosis at endoplasmic reticulum by modulating calcium release. *Science* 330, 1247-1251.

Giot, L., Bader, J.S., Brouwer, C., Chaudhuri, A., Kuang, B., Li, Y., Hao, Y.L., Ooi, C.E., Godwin, B., Vitols, E., Vijayadamodar, G., Pochart, P., Machineni, H., Welsh, M., Kong, Y., Zerhusen, B., Malcolm, R., Varrone, Z., Collis, A., Minto, M., Burgess, S., McDaniel,

L., Stimpson, E., Spriggs, F., Williams, J., Neurath, K., Ioime, N., Agee, M., Voss, E., Furtak, K., Renzulli, R., Aanensen, N., Carrola, S., Bickelhaupt, E., Lazovatsky, Y., DaSilva, A., Zhong, J., Stanyon, C.A., , R.L. Jr, White, K.P., Braverman, M., Jarvie, T., Gold, S., Leach, M., Knight, J., Shimkets, R.A., McKenna, M.P., Chant, J, and Rothberg, J.M. (2003). A Protein Interaction Map of *Drosophila melanogaster*. *Science* 302, 1727-1736.

Giuliano, K.A., DeBiasio, R.L., Terry Dunlay, R., Gough, A., Volosky, J.M., Zock, J., Pavlakis, G.N., and Lansing Taylor, D. (1997). High-content screening: A new approach to easing key bottlenecks in the drug discovery process. *J. Biomol. Screen.* 2, 249-259.

Glick, B.S., and Nakano, A. (2009). Membrane traffic within the Golgi apparatus. *Annu. Rev. Cell Dev. Biol.* 25, 113- 132.

Gloeckner, C.J., Kinkl, N., Schumacher, A., Braun, R.J., O'Neill, E., Meitinger, T., Kolch, W., Prokisch, H., and Ueffing, M. (2006). The Parkinson disease causing LRRK2 mutation I2020T is associated with increased kinase activity. *Hum. Mol. Genet.* 15, 223-232.

Gloeckner, C.J., Schumacher, A., Boldt, K., and Ueffing, M. (2009). The Parkinson disease-associated protein kinase LRRK2 exhibits MAPKKK activity and phosphorylates MKK3/6 and MKK4/7, in vitro. *J. Neurochem.* 109, 959-968.

Goedert, M., and Spillantini, M.G. (2006). A century of Alzheimer's disease. *Science* 314, 777-781.

Goldman, J.G., and Postuma, R. (2014). Premotor and nonmotor features of Parkinson's disease. *Curr. Opin. Neurol.* 27, 434-441.

Gómez-Suaga, P., Luzón-Toro, B., Churamani, D., Zhang, L., Bloor-Young, D., Patel, S., Woodman, P.G., Churchill, G.C., and Hilfiker, S. (2012). Leucine-rich repeat kinase 2 regulates autophagy through a calcium-dependent pathway involving NAADP. *Hum. Mol. Genet.* 21, 511-525.

Gorostidi, A., Ruiz-Martínez, J., Lopez De Munain, A., Alzualde, A., and Martí Massó, J.F. (2009). LRRK2 G2019S and R1441G mutations associated with Parkinson's disease are common in the Basque Country, but relative prevalence is determined by ethnicity. *Neurogenetics* 10, 157-159.

Greggio, E., Jain, S., Kingsbury, A., Bandopadhyay, R., Lewis, P., Kaganovich, A., van der Brug, M.P., Beilina, A., Blackinton, J., Thomas, K.J., Ahmad, R., Miller, D.W., Kesavapany, S., Singleton, A., Lees, A., Harvey, R.J., Harvey, K., and Cookson, M.R. (2006). Kinase activity is required for the toxic effects of mutant LRRK2/dardarin. *Neurobiol. Dis.* 23, 329-341.

Guardia-Laguarta, C., Area-Gomez, E., Rüb, C., Liu, Y., Magrané, J., Becker, D., Voos, W., Schon, E.A., and Przedborski, S. (2014).  $\alpha$ -synuclein is localized to mitochondria-associated ER membranes. *J. Neurosci.* 34, 249- 259.

Guo, L., Gandhi, P.N., Wang, W., Petersen, R.B., Wilson-Delfosse, A.L., and Chen, S.G. (2007). The Parkinson's disease-associated protein, leucine-rich repeat kinase 2 (LRRK2), is an authentic GTPase that stimulates kinase activity. *Exp. Cell Res.* 313, 3658-3670.

Hailey, D.W., Rambold, A.S., Satpute-Krishnan, P., Mitra, K., Sougrat, R., Kim, P.K., and Lippincott-Schwartz, J. (2010). Mitochondria Supply Membranes for Autophagosome Biogenesis during Starvation. *Cell* 141, 656-667.

Hales, K.G., and Fuller, M.T. (1997). Developmentally regulated mitochondrial fusion mediated by a conserved, novel, predicted GTPase. *Cell* 90, 121-129.

Hamasaki, M., Furuta, N., Matsuda, A., Nezu, A., Yamamoto, A., Fujita, N., Oomori, H., Noda, T., Haraguchi, T., Hiraoka, Y., Amano, A., and Yoshimori, T. (2013). Autophagosomes form at ER-mitochondria contact sites. *Nature* 495, 389-393.

Harner, M., Körner, C., Walther, D., Mokranjac, D., Kaesmacher, J., Welsch, U., Griffith, J., Mann, M., Reggiori, F., and Neupert, W. (2011). The mitochondrial contact site complex, a determinant of mitochondrial architecture. *Embo J.* 30, 4356-4370.

Hatano, T., Kubo, S., Imai, S., Maeda, M., Ishikawa, K., Mizuno, Y., and Hattori, N. (2007). Leucine-rich repeat kinase 2 associates with lipid rafts. *Hum. Mol. Genet.* 16, 678-690.

Hayashi, T., and Su, T. (2007). Sigma-1 Receptor Chaperones at the ER- Mitochondrion Interface Regulate Ca<sup>2+</sup> Signaling and Cell Survival. *Cell* 131, 596-610.

He, C., and Klionsky, D.J. (2009). Regulation mechanisms and signaling pathways of autophagy. *Annu. Rev. Genet.* 43, 67-93.

Healy, D.G., Abou-Sleiman, P.M., Casas, J.P., Ahmadi, K.R., Lynch, T., Gandhi, S., Muqit, M.M., Foltynie, T., Barker, R., and Bhatia, K.P. (2006). UCHL-1 is not a Parkinson's disease susceptibility gene. *Ann. Neurol.* 59, 627-633.

Healy, D.G., Falchi, M., O'Sullivan, S.S., Bonifati, V., Durr, A., Bressman, S., Brice, A., Aasly, J., Zabetian, C.P., Goldwurm, S., Ferreira, J.J., Tolosa, E., Kay, D.M., Klein, C., Williams, D.R., Marras, C., Lang, A.E., Wszolek, Z.K., Berciano, J., Schapira, A.H., Lynch, T., Bhatia, K.P., Gasser, T., Lees, A.J., and Wood, N.W. (2008). Phenotype, genotype, and worldwide genetic penetrance of LRRK2-associated Parkinson's disease: a case-control study. *Lancet Neurol.* 7, 583-590.

Hedskog, L., Pinho, C.M., Filadi, R., Rönnbäck, A., Hertwig, L., Wiehager, B., Larssen, P., Gellhaar, S., Sandebring, A., Westerlund, M., Graff, C., Winblad, B., Galter, D., Behbahani, H., Pizzo, P., Glaser, E., and Ankarcrona, M. (2013). Modulation of the endoplasmic reticulum-mitochondria interface in Alzheimer's disease and related models. *Proc. Natl. Acad. Sci. U. S. A.* 110, 7916-7921.

Helle, S.C.J., Kanfer, G., Kolar, K., Lang, A., Michel, A.H., and Kornmann, B. (2013). Organization and function of membrane contact sites. *Biochim. Biophys. Acta Mol. Cell Res.* 1833, 2526-2541.

Hetzer, M.W., Walther, T.C., and Mattaj, I.W. (2005). Pushing the envelope: Structure, function, and dynamics of the nuclear periphery. *Annu. Rev. Cell Dev. Biol.* 21, 347-380.

Higashi, S., Biskup, S., West, A.B., Trinkaus, D., Dawson, V.L., Faull, R.L.M., Waldvogel, H.J., Arai, H., Dawson, T.M., Moore, D.J., and Emson, P.C. (2007). Localization of Parkinson's disease-associated LRRK2 in normal and pathological human brain. *Brain Res.* 1155, 208-219.

Hirano, Y., Matsuda, A., and Hiraoka, Y. (2015). Recent advancements in structured-illumination microscopy toward live-cell imaging. *Microsc.* 64, 237-249.

Hirota, Y., and Tanaka, Y. (2009). A small GTPase, human Rab32, is required for the formation of autophagic vacuoles under basal conditions. *Cell Mol. Life Sci.* 66, 2913-2932.

Hong, Y.B., Kang, J., Kim, J.H., Lee, J., Kwak, G., Hyun, Y.S., Nam, S.H., Hong, H.D., Choi, Y., Jung, S., Koo, H., Lee, J.E., Choi, B.O., and Chung, K.W. (2016). DGAT2 Mutation in a Family with Autosomal-Dominant Early-Onset Axonal Charcot-Marie-Tooth Disease. *Hum. Mutat.* 37, 473-480.

Horner, S.M., Wilkins, C., Badil, S., Iskarpatyoti, J., and Gale Jr, M. (2015). Proteomic analysis of mitochondrial-associated ER membranes (MAM) during RNA virus infection reveals dynamic changes in protein and organelle trafficking. *PLoS One* 10, e0117963.

Hu, J., Shibata, Y., Voss, C., Shemesh, T., Li, Z., Coughlin, M., Kozlov, M.M., Rapoport, T.A., and Prinz, W.A. (2008). Membrane proteins of the endoplasmic reticulum induce high-curvature tubules. *Science* 319, 1247-1250.

Hu, J., Shibata, Y., Zhu, P., Voss, C., Rismanchi, N., Prinz, W.A., Rapoport, T.A., and Blackstone, C. (2009). A Class of Dynamin-like GTPases Involved in the Generation of the Tubular ER Network. *Cell* 138, 549-561.

Huang, F., Khvorova, A., Marshall, W., and Sorkin, A. (2004). Analysis of Clathrin-mediated Endocytosis of Epidermal Growth Factor Receptor by RNA Interference. *J. Biol. Chem.* 279, 16657-16661.

Huber, N., Guimaraes, S., Schrader, M., Suter, U., and Niemann, A. (2013). Charcot-Marie-Tooth disease-associated mutants of GDAP1 dissociate its roles in peroxisomal and mitochondrial fission. *EMBO Rep.* 14, 545-552.

Hübner, C.A., and Kurth, I. (2014). Membrane-shaping disorders: A common pathway in axon degeneration. *Brain* 137, 3109-3121.

Imai, Y., Gehrke, S., Wang, H., Takahashi, R., Hasegawa, K., Oota, E., and Lu, B. (2008). Phosphorylation of 4E- BP by LRRK2 affects the maintenance of dopaminergic neurons in *Drosophila*. *Embo j.* 27, 2432-2443.

Imai, Y., Soda, M., and Takahashi, R. (2000). Parkin suppresses unfolded protein stress-induced cell death through its E3 ubiquitin-protein ligase activity. *J. Biol. Chem.* 275, 35661-35664.

Ishihara, N., Eura, Y., and Mihara, K. (2004). Mitofusin 1 and 2 play distinct roles in mitochondrial fusion reactions via GTPase activity. *J. Cell. Sci.* 117, 6535-6546.

Ishihara, N., Fujita, Y., Oka, T., and Mihara, K. (2006). Regulation of mitochondrial morphology through proteolytic cleavage of OPA1. *Embo J.* 25, 2966-2977.

Ito, G., Okai, T., Fujino, G., Takeda, K., Ichijo, H., Katada, T., and Iwatsubo, T. (2007). GTP binding is essential to the protein kinase activity of LRRK2, a causative gene product for familial Parkinson's disease. *Biochemistry* 46, 1380-1388.

Iwasawa, R., Mahul-Mellier, A., Datler, C., Pazarentzos, E., and Grimm, S. (2011). Fis1 and Bap31 bridge the mitochondria-ER interface to establish a platform for apoptosis induction. *Embo J.* 30, 556-568.

Jaleel, M., Nichols, R.J., Deak, M., Campbell, D.G., Gillardon, F., Knebel, A., and Alessi, D.R. (2007). LRRK2 phosphorylates moesin at threonine-558: Characterization of how Parkinson's disease mutants affect kinase activity. *Biochem. J.* 405, 307-317.

Jorgensen, N.D., Peng, Y., Ho, C.C., Rideout, H.J., Petrey, D., Liu, P., and Dauer, W.T. (2009). The WD40 domain is required for LRRK2 neurotoxicity. *PLoS One* 4, e8463.

Kalia, L.V., Lang, A.E., Hazrati, L., Fujioka, S., Wszolek, Z.K., Dickson, D.W., Ross, O.A., Van Deerlin, V.M., Trojanowski, J.Q., Hurtig, H.I., Alcalay, R.N., Marder, K.S., Clark, L.N., Gaig, C., Tolosa, E., Ruiz-Martínez, J., Martí-Masso, J.F., Ferrer, I., López de Munain, A., Goldman, S.M., Schüle, B., Langston, J.W., Aasly, J.O., Giordana, M.T., Bonifati, V., Puschmann, A., Canesi, M., Pezzoli, G., Maues De Paula, A., Hasegawa, K., Duyckaerts, C., Brice, A., Stoessl, A.J., and Marras, C. (2015). Clinical correlations with lewy body pathology in LRRK2-related Parkinson disease. *JAMA Neurol.* 72, 100-105.

Karp, G. (2008). *Cell and Molecular Biology*, 5th Ed. Wiley.

Kawakami, F., Yabata, T., Ohta, E., Maekawa, T., Shimada, N., Suzuki, M., Maruyama, H., Ichikawa, T., and Obata, F. (2012). LRRK2 phosphorylates tubulin-associated tau but not the free molecule: LRRK2-mediated regulation of the tau-tubulin association and neurite outgrowth. *Plos One* 7.

Kett, L.R., Boassa, D., Ho, C.C., Rideout, H.J., Hu, J., Terada, M., Ellisman, M., and Dauer, W.T. (2012). LRRK2 Parkinson disease mutations enhance its microtubule association. *Hum. Mol. Genet.* 21, 890-899.

Kitada, T., Asakawa, S., Hattori, N., Matsumine, H., Yamamura, Y., Minoshima, S., Yokochi, M., Mizuno, Y., and Shimizu, N. (1998). Mutations in the parkin gene cause autosomal recessive juvenile parkinsonism. *Nature* 392, 605-608.

Klecker, T., Böckler, S., and Westermann, B. (2014). Making connections: Interorganelle contacts orchestrate mitochondrial behavior. *Trends Cell Biol.* 24, 537-545.

Klein, C., and Westenberger, A. (2012). Genetics of Parkinson's disease. *Cold Spring Harbor Perspect. Med.* 2.

Kobayashi, S., Tanaka, A., and Fujiki, Y. (2007). Fis1, DLP1, and Pex11p coordinately regulate peroxisome morphogenesis. *Exp. Cell Res.* 313, 1675-1686.

Koch, A., Thiemann, M., Grabenbauer, M., Yoon, Y., McNiven, M.A., and Schrader, M. (2003). Dynamin-like protein 1 is involved in peroxisomal fission. *J. Biol. Chem.* 278, 8597-8605.

Kopec, K.O., Alva, V., and Lupas, A.N. (2010). Homology of SMP domains to the TULIP superfamily of lipid-binding proteins provides a structural basis for lipid exchange between ER and mitochondria. *Bioinformatics* 26, 1927-1931.

Korobova, F., Ramabhadran, V., and Higgs, H.N. (2013). An actin-dependent step in mitochondrial fission mediated by the ER-associated formin INF2. *Science* 339, 464-467.

Koshiba, T., Detmer, S.A., Kaiser, J.T., Chen, H., McCaffery, J.M., and Chan, D.C. (2004). Structural basis of mitochondrial tethering by mitofusin complexes. *Science* 305, 858-862.

Kramer, R., and Cohen, D. (2004). Functional genomics to new drug targets. *Nat. Rev. Drug Discov.* 3, 965-972. Krausz, E. (2007). High-content siRNA screening. *Mol. Biosyst.* 3, 232-240.

Krols, M., van Isterdael, G., Asselbergh, B., Kremer, A., Lippens, S., Timmerman, V., and Janssens, S. (2016). Mitochondria-associated membranes as hubs for neurodegeneration. *Acta Neuropathol.* 131, 505-523.

Kühlbrandt, W. (2015). Structure and function of mitochondrial membrane protein complexes. *BMC Biol.* 13.

Kumar, A., Greggio, E., Beilina, A., Kaganovich, A., Chan, D., Taymans, J., Wolozin, B., and Cookson, M.R. (2010). The Parkinson's disease associated LRRK2 exhibits weaker in vitro phosphorylation of 4E-BP compared to autophosphorylation. *Plos One* 5.

Kumazawa, R., Tomiyama, H., Li, Y., Imamichi, Y., Funayama, M., Yoshino, H., Yokochi, F., Fukusako, T., Takehisa, Y., Kashihara, K., Kondo, T., Elibol, B., Bostantjopoulou, S., Toda, T., Takahashi, H., Yoshii, F., Mizuno, Y., and Hattori, N. (2008). Mutation analysis of the PINK1 gene in 391 patients with Parkinson disease. *Arch. Neurol.* 65, 802-808.

Kuss, M., Adamopoulou, E., and Kahle, P.J. (2014). Interferon- $\gamma$  induces leucine-rich repeat kinase LRRK2 via extracellular signal-regulated kinase ERK5 in macrophages. *J. Neurochem.* 129, 980-987.

Ladinsky, M.S., Mastronarde, D.N., McIntosh, J.R., Howell, K.E., and Staehelin, L.A. (1999). Golgi structure in three dimensions: Functional insights from the normal rat kidney cell. *J. Cell Biol.* 144, 1135-1149.

Lai, B.C.L., Marion, S.A., Teschke, K., and Tsui, J.K.C. (2002). Occupational and environmental risk factors for Parkinson's disease. *Parkinsonism Relat. Disord.* 8, 297-309.

Lattante, S., Rouleau, G.A., and Kabashi, E. (2013). TARDBP and FUS Mutations Associated with Amyotrophic Lateral Sclerosis: Summary and Update. *Hum. Mutat.* 34, 812-826.

Law, B.M.H., Spain, V.A., Leinster, V.H.L., Chia, R., Beilina, A., Cho, H.J., Taymans, J., Urban, M.K., Sancho, R.M., Ramírez, M.B., Biskup, S., Baekelandt, V., Cai, H., Cookson, M.R., Berwick, D.C., and Harvey, K. (2014). A direct interaction between leucine-rich repeat kinase 2 and specific  $\beta$ -Tubulin isoforms regulates tubulin acetylation. *J. Biol. Chem.* 289, 895-908.

Leal, N.S., Schreiner, B., Pinho, C.M., Filadi, R., Wiehager, B., Karlstrom, H., Pizzo, P., and Ankarcrona, M. (2016). Mitofusin-2 knockdown increases ER-mitochondria contact and decreases amyloid beta-peptide production. *J. Cell. Mol. Med.*

Lee, B.D., Dawson, V.L., and Dawson, T.M. (2012). Leucine-rich repeat kinase 2 (LRRK2) as a potential therapeutic target in Parkinson's disease. *Trends Pharmacol. Sci.* 33, 365-373.

Leroy, E., Boyer, R., Auburger, G., Leube, B., Ulm, G., Mezey, E., Harta, G., Brownstein, M.J., Jonnalagada, S., Chernova, T., Dehejia, A., Lavedan, C., Gasser, T., Steinbach, P.J., Wilkinson, K.D., and Polymeropoulos, M.H. (1998). The ubiquitin pathway in Parkinson's disease. *Nature* 395, 451-452.

Lesage, S., Anheim, M., Letournel, F., Bousset, L., Honoré, A., Rozas, N., Pieri, L., Madiona, K., Dürr, A., Melki, R., Verny, C., and Brice, A. (2013). G51D a-synuclein mutation causes a novel Parkinsonian-pyramidal syndrome. *Ann. Neurol.* 73, 459-471.

Lewis, P.A., Greggio, E., Beilina, A., Jain, S., Baker, A., and Cookson, M.R. (2007). The R1441C mutation of LRRK2 disrupts GTP hydrolysis. *Biochem. Biophys. Res. Commun.* 357, 668-671.

Li, T., Yang, D., Zhong, S., Thomas, J.M., Xue, F., Liu, J., Kong, L., Voulalas, P., Hassan, H.E., Park, J.-., MacKerell, A.D., and Smith, W.W. (2014). Novel LRRK2 GTP-binding inhibitors reduced degeneration in Parkinson's disease cell and mouse models. *Hum. Mol. Genet.* 23, 6212-6222.

Li, Y., Tomiyama, H., Sato, K., Hatano, Y., Yoshino, H., Atsumi, M., Kitaguchi, M., Sasaki, S., Kawaguchi, S., Miyajima, H., Toda, T., Mizuno, Y., and Hattori, N. (2005). Clinicogenetic study of PINK1 mutations in autosomal recessive early-onset parkinsonism. *Neurology* 64, 1955-1957.

Liao, J., Wu, C., Burlak, C., Zhang, S., Sahm, H., Wang, M., Zhang, Z., Vogel, K.W., Federici, M., Riddle, S.M., Nichols, R.J., Liu, D., Cookson, M.R., Stone, T.A., and Hoang,

Q.Q. (2014). Parkinson disease-associated mutation R1441H in LRRK2 prolongs the "active state" of its GTPase domain. *Proc. Natl. Acad. Sci. U. S. A.* 111, 4055-4060.

Lidke, D.S., and Lidke, K.A. (2012). Advances in high-resolution imaging - techniques for three-dimensional imaging of cellular structures. *J. Cell. Sci.* 125, 2571-2580.

Lim, Y., Cho, I., Schoel, L.J., Cho, G., and Golden, J.A. (2015). Hereditary spastic paraplegia-linked REEP1 modulates endoplasmic reticulum/mitochondria contacts. *Ann. Neurol.* 78, 679-696.

Ling, S.-., Polymenidou, M., and Cleveland, D.W. (2013). Converging mechanisms in als and FTD: Disrupted RNA and protein homeostasis. *Neuron* 79, 416-438.

Liou, J., Kim, M.L., Won, D.H., Jones, J.T., Myers, J.W., Ferrell Jr., J.E., and Meyer, T. (2005). STIM is a Ca<sup>2+</sup> sensor essential for Ca<sup>2+</sup>-store- depletion-triggered Ca<sup>2+</sup> influx. *Curr. Biol.* 15, 1235-1241.

Litvak, V., Dahan, N., Ramachandran, S., Sabanay, H., and Lev, S. (2005). Maintenance of the diacylglycerol level in the Golgi apparatus by the Nir2 protein is critical for Golgi secretory function. *Nature Cell Biol.* 7, 225-234.

Liu, S., Sawada, T., Lee, S., Yu, W., Silverio, G., Alapatt, P., Millan, I., Shen, A., Saxton, W., Kanao, T., Takahashi, R., Hattori, N., Imai, Y., and Lu, B. (2012). Parkinson's disease-associated kinase PINK1 regulates miro protein level and axonal transport of mitochondria. *PLoS Genet.* 8.

Liu, Z., Hamamichi, S., Lee, B.D., Yang, D., Ray, A., Caldwell, G.A., Caldwell, K.A., Dawson, T.M., Smith, W.W., and Dawson, V.L. (2011). Inhibitors of LRRK2 kinase attenuate neurodegeneration and Parkinson-like phenotypes in *Caenorhabditis elegans* and *Drosophila* Parkinson's disease models. *Hum. Mol. Genet.* 20, 3933-3942.

Loewen, C.J.R., Roy, A., and Levine, T.P. (2003). A conserved ER targeting motif in three families of lipid binding proteins and in Opi1p binds VAP. *Embo j.* 22, 2025-2035.

Lohmann, E., Periquet, M., Bonifati, V., Wood, N.W., De Michele, G., Bonnet, A., Fraix, V., Broussolle, E., Horstink, M.W.I.M., Vidailhet, M., Verpillat, P., Gasser, T., Nicholl, D., Teive, H., Raskin, S., Rascol, O., Destée, A., Ruberg, M., Gasparini, F., Meco, G., Agid, Y., Durr, A., and Brice, A. (2003). How much phenotypic variation can be attributed to parkin genotype? *Ann. Neurol.* 54, 176-185.

Losón, O.C., Song, Z., Chen, H., and Chan, D.C. (2013). Fis1, Mff, MiD49, and MiD51 mediate Drp1 recruitment in mitochondrial fission. *Mol. Biol. Cell* 24, 659-667.

Luty, A.A., Kwok, J.B., Dobson-Stone, C., Loy, C.T., Coupland, K.G., Karlstrom, H., Sobow, T., Tchorzewska, J., Maruszak, A., Barcikowska, M., Panegyres, P.K., Zekanowski, C., Brooks, W.S., Williams, K.L., Blair, I.P., Mather, K.A., Sachdev, P.S., Halliday, G.M., and Schofield, P.R. (2010). Sigma nonopioid intracellular receptor 1 mutations cause frontotemporal lobar degeneration-motor neuron disease. *Ann. Neurol.* 68, 639-649.

Lynes, E.M., Bui, M., Yap, M.C., Benson, M.D., Schneider, B., Ellgaard, L., Berthiaume, L.G., and Simmen, T. (2012). Palmitoylated TMX and calnexin target to the mitochondria-associated membrane. *Embo j.* 31, 457-470.

Lynes, E.M., Raturi, A., Shenkman, M., Sandoval, C.O., Yap, M.C., Wu, J., Janowicz, A., Myhill, N., Benson, M.D., Campbell, R.E., Berthiaume, L.G., Lederkremer, G.Z., and Simmen, T. (2013). Palmitoylation is the switch that assigns calnexin to quality control or ER Ca<sup>2+</sup> signaling. *J. Cell. Sci.* 126, 3893-3903.

MacAskill, A.F., Brickley, K., Stephenson, F.A., and Kittler, J.T. (2009). GTPase dependent recruitment of Grif-1 by Miro1 regulates mitochondrial trafficking in hippocampal neurons. *Mol. Cell. Neurosci.* 40, 301-312.

Macedo, M.G., Anar, B., Bronner, I.F., Cannella, M., Squitieri, F., Bonifati, V., Hoogeveen, A., Heutink, P., and Rizzu, P. (2003). The DJ-1 L166P mutant protein associated with early onset Parkinson's disease is unstable and forms higher-order protein complexes. *Hum. Mol. Genet.* 12, 2807-2816.

MacLeod, D.A., Dowman, J., Hammond, R., Leete, T., Inoue, K., and Abeliovich, A. (2006). The Familial Parkinsonism Gene LRRK2 Regulates Neurite Process Morphology. *Neuron* 52, 587-593.

MacLeod, D.A., Rhinn, H., Kuwahara, T., Zolin, A., Di Paolo, G., MacCabe, B.D., Marder, K.S., Honig, L.S., Clark, L.N., Small, S.A., and Abeliovich, A. (2013). RAB7L1 Interacts with LRRK2 to Modify Intraneuronal Protein Sorting and Parkinson's Disease Risk. *Neuron* 77, 425-439.

Maddox, C.B., Rasmussen, L., and White, E.L. (2008). Adapting Cell-Based Assays to the High-Throughput Screening Platform: Problems Encountered and Lessons Learned. *JALA J. Assoc. Lab. Autom.* 13, 168-173.

Malgieri, G., and Eliezer, D. (2008). Structural effects of Parkinson's disease linked DJ-1 mutations. *Protein Sci.* 17, 855-868.

Manders, E., Verbeek, F., and Aten, J. (1993). Measurement of co-localization of objects in dual-colour confocal images. *J. Microsc.* 169, 375-382.

Manor, U., Bartholomew, S., Golani, G., Christenson, E., Kozlov, M., Higgs, H., Spudich, J., and Lippincott-Schwartz, J. (2015). A mitochondria-anchored isoform of the actin-nucleating spire protein regulates mitochondrial division. *Elife* 4.

Marchi, S., Patergnani, S., and Pinton, P. (2014). The endoplasmic reticulum-mitochondria connection: One touch, multiple functions. *Biochim. Biophys. Acta Bioenerg.* 1837, 461-469.

Marchi, S., Rimessi, A., Giorgi, C., Baldini, C., Ferroni, L., Rizzuto, R., and Pinton, P. (2008). Akt kinase reducing endoplasmic reticulum  $Ca^{2+}$  release protects cells from  $Ca^{2+}$ -dependent apoptotic stimuli. *Biochem. Biophys. Res. Commun.* 375, 501-505.

Marín, I. (2006). The Parkinson disease gene LRRK2: Evolutionary and structural insights. *Mol. Biol. Evol.* 23, 2423-2433.

Marín, I., Van Egmond, W.N., and Van Haastert, P.J.M. (2008). The Roco protein family: A functional perspective. *Faseb j.* 22, 3103-3110.

Matsuda, N. (2016). Phospho-ubiquitin: Upending the PINK-Parkin-ubiquitin cascade. *J. Biochem.* 159, 379-385.

Matta, S., Van Kolen, K., da Cunha, R., van den Bogaart, G., Mandemakers, W., Miskiewicz, K., De Bock, P., Morais, V.A., Vilain, S., Haddad, D., Delbroek, L., Swerts, J., Chávez-Gutiérrez, L., Esposito, G., Daneels, G., Karran, E., Holt, M., Gevaert, K., Moechars, D.W., De Strooper, B., and Verstreken, P. (2012). LRRK2 Controls an EndoA Phosphorylation Cycle in Synaptic Endocytosis. *Neuron* 75, 1008-1021.

McBride, H.M., Neuspiel, M., and Wasiak, S. (2006). Mitochondria: More Than Just a Powerhouse. *Curr. Biol.* 16.

McLelland, G.L., Soubannier, V., Chen, C.X., McBride, H.M., and Fon, E.A. (2014). Parkin and PINK1 function in a vesicular trafficking pathway regulating mitochondrial quality control. *Embo J.* 33, 282-295.

Meixner, A., Boldt, K., Van Troys, M., Askenazi, M., Gloeckner, C.J., Bauer, M., Marto, J.A., Ampe, C., Kinkl, N., and Ueffing, M. (2011). A QUICK screen for Lrrk2 interaction partners - Leucine-rich repeat kinase 2 is involved in actin cytoskeleton dynamics. *Mol. Cell. Proteomics* 10.

Melrose, H. (2008). Update on the functional biology of Lrrk2. *Future Neurol.* 3, 669-681.

Mesmin, B., Bigay, J., von Filseck, J.M., Lacas-Gervais, S., Drin, G., and Antonny, B. (2013). A four-step cycle driven by PI (4) P hydrolysis directs sterol/PI (4) P exchange by the ER-Golgi tether OSBP. *Cell* 155, 830-843.

Migheli, R., Del Giudice, M.G., Spissu, Y., Sanna, G., Xiong, Y., Dawson, T.M., Dawson, V.L., Galioto, M., Rocchitta, G., Biosa, A., Serra, P.A., Carri, M.T., Crosio, C., and

Iaccarino, C. (2013). LRRK2 Affects Vesicle Trafficking, Neurotransmitter Extracellular Level and Membrane Receptor Localization. *Plos One* 8.

Miklossy, J., Arai, T., Guo, J.-., Klegeris, A., Yu, S., McGeer, E.G., and McGeer, P.L. (2006). LRRK2 expression in normal and pathologic human brain and in human cell lines. *J. Neuropathol. Exp. Neurol.* 65, 953-963.

Milosevic, I., Giovedi, S., Lou, X., Raimondi, A., Collesi, C., Shen, H., Paradise, S., O'Toole, E., Ferguson, S., Cremona, O., and De Camilli, P. (2011). Recruitment of endophilin to clathrin-coated pit necks is required for efficient vesicle uncoating after fission. *Neuron* 72, 587-601.

Mishra, P., Carelli, V., Manfredi, G., and Chan, D.C. (2014). Proteolytic cleavage of Opa1 stimulates mitochondrial inner membrane fusion and couples fusion to oxidative phosphorylation. *Cell Metab.* 19, 630-641.

Misko, A., Jiang, S., Wegorzewska, I., Milbrandt, J., and Baloh, R.H. (2010). Mitofusin 2 is necessary for transport of axonal mitochondria and interacts with the Miro/Milton complex. *J. Neurosci.* 30, 4232-4240.

Misko, A.L., Sasaki, Y., Tuck, E., Milbrandt, J., and Baloh, R.H. (2012). Mitofusin2 mutations disrupt axonal mitochondrial positioning and promote axon degeneration. *J. Neurosci.* 32, 4145-4155.

Moehle, M.S., Webber, P.J., Tse, T., Sukar, N., Standaert, D.G., Desilva, T.M., Cowell, R.M., and West, A.B. (2012). LRRK2 inhibition attenuates microglial inflammatory responses. *J. Neurosci.* 32, 1602-1611.

Montisano, D.F., Cascarano, J., Pickett, C.B., and James, T.W. (1982). Association between mitochondria and rough endoplasmic reticulum in rat liver. *Anat. Rec.* 203, 441-450.

Moore, C.B., Guthrie, E.H., Huang, M.T., and Taxman, D.J. (2010). Short hairpin RNA (shRNA): design, delivery, and assessment of gene knockdown. *Methods Mol. Biol.* 629, 141-158.

Mórotz, G.M., De Vos, K.J., Vagnoni, A., Ackerley, S., Shaw, C.E., and Miller, C.C.J. (2012). Amyotrophic lateral sclerosis-associated mutant VAPBP56s perturbs calcium homeostasis to disrupt axonal transport of mitochondria. *Hum. Mol. Genet.* 21, 1979-1988.

Mortiboys, H., Johansen, K.K., Aasly, J.O., and Bandmann, O. (2010). Mitochondrial impairment in patients with Parkinson disease with the G2019S mutation in LRRK2. *Neurology* 75, 2017-2020.

Myhill, N., Lynes, E.M., Nanji, J.A., Blagoveshchenskaya, A.D., Fei, H., Simmen, K.C., Cooper, T.J., Thomas, G., and Simmen, T. (2008). The subcellular distribution of calnexin is mediated by PACS-2. *Mol. Biol. Cell* 19, 2777-2788.

Nalls, M.A., Pankratz, N., Lill, C.M., Do, C.B., Hernandez, D.G., Saad, M., Destefano, A.L., Kara, E., Bras, J., Sharma, M., Schulte, C., Keller, M.F., Arepalli, S., Letson, C., Edsall, C., Stefansson, H., Liu, X., Pliner, H., Lee, J.H., Cheng, R., Ikram, M.A., Ioannidis, J.P., Hadjigeorgiou, G.M., Bis, J.C., Martinez, M., Perlmutter, J.S., Goate, A., Marder, K., Fiske, B., Sutherland, M., Xiromerisiou, G., Myers, R.H., Clark, L.N., Stefansson, K., Hardy, J.A., Heutink, P., Chen, H., Wood, N.W., Houlden, H., Payami, H., Brice, A., Scott, W.K., Gasser, T., Bertram, L., Eriksson, N., Foroud, T., and Singleton, A.B. (2014). Large-scale

meta-analysis of genome-wide association data identifies six new risk loci for Parkinson's disease. *Nat. Genet.* 46, 989-993.

Naon, D., and Scorrano, L. (2014). At the right distance: ER-mitochondria juxtaposition in cell life and death. *Biochim. Biophys. Acta Mol. Cell Res.* 1843, 2184-2194.

Narendra, D., Tanaka, A., Suen, D., and Youle, R.J. (2008). Parkin is recruited selectively to impaired mitochondria and promotes their autophagy. *J. Cell Biol.* 183, 795-803.

Ng, A.S.L., Rademakers, R., and Miller, B.L. (2015). Frontotemporal dementia: A bridge between dementia and neuromuscular disease. *Ann. New York Acad. Sci.* 1338, 71-93.

Nichols, R.J., Dzamko, N., Morrice, N.A., Campbell, D.G., Deak, M., Ordureau, A., Macartney, T., Tong, Y., Shen, J., Prescott, A.R., and Alessi, D.R. (2010). 14-3-3 Binding to LRRK2 is disrupted by multiple Parkinson's disease-associated mutations and regulates cytoplasmic localization. *Biochem. J.* 430, 393-404.

Nishimura, A.L., Mitne-Neto, M., Silva, H.C.A., Richieri-Costa, A., Middleton, S., Cascio, D., Kok, F., Oliveira, J.R.M., Gillingwater, T., Webb, J., Skehel, P., and Zatz, M. (2004). A mutation in the vesicle-trafficking protein VAPB causes late-onset spinal muscular atrophy and amyotrophic lateral sclerosis. *Am. J. Hum. Genet.* 75, 822-831.

Niu, J., Yu, M., Wang, C., and Xu, Z. (2012). Leucine-rich repeat kinase 2 disturbs mitochondrial dynamics via dynamin-like protein. *J. Neurochem.* 122, 650-658.

Obbard, D.J., Gordon, K.H.J., Buck, A.H., and Jiggins, F.M. (2009). The evolution of RNAi as a defence against viruses and transposable elements. *Philos. Trans. R. Soc. B Biol. Sci.* 364, 99-115.

Oertle, T., Klinger, M., Stuermer, C.A.O., and Schwab, M.E. (2003). A reticular rhapsody: Phylogenic evolution and nomenclature of the RTN/Nogo gene family. *Faseb j.* 17, 1238-1247.

Ohr, T., Merkle, D., Birkenfeld, K., Echeverri, C.J., and Schwille, P. (2006). In situ fluorescence analysis demonstrates active siRNA exclusion from the nucleus by Exportin 5. *Nucleic Acids Res.* 34, 1369-1380.

Okatsu, K., Kimura, M., Oka, T., Tanaka, K., and Matsuda, N. (2015). Unconventional PINK1 localization to the outer membrane of depolarized mitochondria drives Parkin recruitment. *J. Cell. Sci.* 128, 964-978.

Olszewska, D. (2015). Recognising the phenotype of genetic forms of Parkinson's disease in clinical practice. *ACNR*

Orso, G., Pendin, D., Liu, S., Tassetto, J., Moss, T.J., Faust, J.E., Micaroni, M., Egorova, A., Martinuzzi, A., McNew, J.A., and Daga, A. (2009). Homotypic fusion of ER membranes requires the dynamin-like GTPase Atlastin. *Nature* 460, 978-983.

Paillusson, S., Stoica, R., Gomez-Suaga, P., Lau, D.H.W., Mueller, S., Miller, T., and Miller, C.C.J. (2016). There's Something Wrong with my MAM; the ER-Mitochondria Axis and Neurodegenerative Diseases. *Trends Neurosci.* 39, 146-157.

Paisán-Ruíz, C., Jain, S., Evans, E.W., Gilks, W.P., Simón, J., Van Der Brug, M., De Munain, A.L., Aparicio, S., Gil, A.M., Khan, N., Johnson, J., Martinez, J.R., Nicholl, D., Carrera, I.M., Pena, A.S., de Silva, R., Lees, A., Martí-Massó, J.F., Pérez-Tur, J., Wood, N.W., and Singleton, A.B. (2004). Cloning of the gene containing mutations that cause PARK8-linked Parkinson's disease. *Neuron* 44, 595-600.

Paisán-Ruiz, C., Lewis, P.A., and Singleton, A.B. (2013). LRRK2: Cause, risk, and mechanism. *J. Parkinson's Dis.* 3, 85-103.

Palty, R., Silverman, W.F., Hershfinkel, M., Caporale, T., Sensi, S.L., Parnis, J., Nolte, C., Fishman, D., Shoshan- Barmatz, V., Herrmann, S., Khananshvoli, D., and Sekler, I. (2010). NCLX is an essential component of mitochondrial Na<sup>+</sup>/Ca<sup>2+</sup> exchange. *Proc. Natl. Acad. Sci. U. S. A.* 107, 436-441.

Palumbo, A., Napolitano, A., Barone, P., and D'Ischia, M. (1999). Nitrite- and peroxide-dependent oxidation pathways of dopamine: 6-nitrodopamine and 6-hydroxydopamine formation as potential contributory mechanisms of oxidative stress- and nitric oxide-induced neurotoxicity in neuronal degeneration. *Chem. Res. Toxicol.* 12, 1213-1222.

Pankratz, N., and Foroud, T. (2007). Genetics of Parkinson disease. *Gen. Med.* 9, 801-811.

Pankratz, N., Pauciulo, M.W., Elsaesser, V.E., Marek, D.K., Halter, C.A., Wojcieszek, J., Rudolph, A., Shults, C.W., Foroud, T., and Nichols, W.C. (2006). Mutations in DJ-1 are rare in familial Parkinson disease. *Neurosci. Lett.* 408, 209-213.

Parisiadou, L., Xie, C., Hyun, J.C., Lin, X., Gu, X., Long, C., Lobbestael, E., Baekelandt, V., Taymans, J., Sun, L., and Cai, H. (2009). Phosphorylation of ezrin/radixin/moesin proteins by LRRK2 promotes the rearrangement of actin cytoskeleton in neuronal morphogenesis. *J. Neurosci.* 29, 13971-13980.

Perkins, G., Renken, C., Martone, M.E., Young, S.J., Ellisman, M., and Frey, T. (1997). Electron tomography of neuronal mitochondria: Three-dimensional structure and organization of cristae and membrane contacts. *J. Struct. Biol.* 119, 260-272.

Pernas, L., and Scorrano, L. (2016). Mito-Morphosis: Mitochondrial Fusion, Fission, and Cristae Remodeling as Key Mediators of Cellular Function. *Annu. Rev. Physiol.* 78, 505-531.

Phillips, M.J., and Voeltz, G.K. (2016). Structure and function of ER membrane contact sites with other organelles. *Nat. Rev. Mol. Cell Biol.* 17, 69-82.

Piccoli, G., Condliffe, S.B., Bauer, M., Giesert, F., Boldt, K., De Astis, S., Meixner, A., Sarioglu, H., Vogt-Weisenhorn, D.M., Wurst, W., Gloeckner, C.J., Matteoli, M., Sala, C., and Ueffing, M. (2011). LRRK2 controls synaptic vesicle storage and mobilization within the recycling pool. *J. Neurosci.* 31, 2225-2237.

Pla-Martín, D., Rueda, C.B., Estela, A., Sánchez-Piris, M., González-Sánchez, P., Traba, J., de la Fuente, S., Scorrano, L., Renau-Piqueras, J., and Alvarez, J. (2013). Silencing of the Charcot–Marie–Tooth disease-associated gene *GDAP1* induces abnormal mitochondrial distribution and affects Ca<sup>2+</sup> homeostasis by reducing store-operated Ca<sup>2+</sup> entry. *Neurobiol. Dis.* 55, 140-151.

Plowey, E.D., Cherra III, S.J., Liu, Y., and Chu, C.T. (2008). Role of autophagy in G2019S-LRRK2-associated neurite shortening in differentiated SH-SY5Y cells. *J. Neurochem.* 105, 1048-1056.

Polymeropoulos, M.H., Higgins, J.J., Golbe, L.I., Johnson, W.G., Ide, S.E., Di Iorio, G., Sanges, G., Stenroos, E.S., Pho, L.T., Schaffer, A.A., Lazzarini, A.M., Nussbaum, R.L., and Duvoisin, R.C. (1996). Mapping of a gene for Parkinson's disease to chromosome 4q21-q23. *Science* 274, 1197-1199.

Polymeropoulos, M.H., Lavedan, C., Leroy, E., Ide, S.E., Dehejia, A., Dutra, A., Pike, B., Root, H., Rubenstein, J., Boyer, R., Stenroos, E.S., Chandrasekharappa, S., Athanassiadou, A., Papapetropoulos, T., Johnson, W.G., Lazzarini, A.M., Duvoisin, R.C., Di Iorio, G., Golbe, L.I., and Nussbaum, R.L. (1997). Mutation in the  $\alpha$ -synuclein gene identified in families with Parkinson's disease. *Science* 276, 2045-2047.

Poston, C.N., Krishnan, S.C., and Bazemore-Walker, C.R. (2013). In-depth proteomic analysis of mammalian mitochondria-associated membranes (MAM). *Journal of Proteomics* 79, 219-230.

Prause, J., Goswami, A., Katona, I., Roos, A., Schnizler, M., Bushuven, E., Dreier, A., Buchkremer, S., Johann, S., Beyer, C., Deschauer, M., Troost, D., and Weis, J. (2013). Altered localization, abnormal modification and loss of function of sigma receptor-1 in amyotrophic lateral sclerosis. *Hum. Mol. Genet.* 22, 1581-1600.

Prince, M., Wimo, A., Guerchet, M., Ali, G., Wu, Y., and Prina, M. (2015). *The Global Impact of Dementia: An analysis of prevalence, incidence, cost and trends.* Adi London

Prinz, W.A. (2014). Bridging the gap: Membrane contact sites in signaling, metabolism, and organelle dynamics. *J. Cell Biol.* 205, 759-769.

Pungaliya, P.P., Bai, Y., Lipinski, K., Anand, V.S., Sen, S., Brown, E.L., Bates, B., Reinhart, P.H., West, A.B., Hirst, W.D., and Braithwaite, S.P. (2010). Identification and characterization of a leucine-rich repeat kinase 2 (LRRK2) consensus phosphorylation motif. *Plos One* 5.

Rangel-Barajas, C., Coronel, I., and Florán, B. (2015). Dopamine receptors and neurodegeneration. *Aging Dis.* 6, 349-368.

Ravikumar, B., Imarisio, S., Sarkar, S., O'Kane, C.J., and Rubinsztein, D.C. (2008). Rab5 modulates aggregation and toxicity of mutant huntingtin through macroautophagy in cell and fly models of Huntington disease. *J. Cell. Sci.* 121, 1649-1660.

Reichert, A.S., and Neupert, W. (2002). Contact sites between the outer and inner membrane of mitochondria - Role in protein transport. *Biochim. Biophys. Acta Mol. Cell Res.* 1592, 41-49.

Reyniers, L., Del Giudice, M.G., Civiero, L., Belluzzi, E., Lobbestael, E., Beilina, A., Arrigoni, G., Derua, R., Waelkens, E., Li, Y., Crosio, C., Iaccarino, C., Cookson, M.R., Baekelandt, V., Greggio, E., and Taymans, J.M. (2014). Differential protein protein interactions of LRRK1 and LRRK2 indicate roles in distinct cellular signaling pathways. *J. Neurochem.* 131, 239-250.

Reynolds, A., Leake, D., Boese, Q., Scaringe, S., Marshall, W.S., and Khvorova, A. (2004). Rational siRNA design for RNA interference. *Nat. Biotechnol.* 22, 326-330.

Rizzuto, R., Pinton, P., Carrington, W., Fay, F.S., Fogarty, K.E., Lifshitz, L.M., Tuft, R.A., and Pozzan, T. (1998). Close contacts with the endoplasmic reticulum as determinants of mitochondrial  $Ca^{2+}$  responses. *Science* 280, 1763- 1766.

Rodriguez-Oroz, M.C., Jahanshahi, M., Krack, P., Litvan, I., Macias, R., Bezard, E., and Obeso, J.A. (2009). Initial clinical manifestations of Parkinson's disease: features and pathophysiological mechanisms. *Lancet Neurol.* 8, 1128-1139.

Rosenbusch, K.E., and Kortholt, A. (2016). Activation Mechanism of LRRK2 and Its Cellular Functions in Parkinson's Disease. *Parkinson's Disease*.

Ross, O.A., Braithwaite, A.T., Skipper, L.M., Kachergus, J., Hulihan, M.M., Middleton, F.A., Nishioka, K., Fuchs, J., Gasser, T., Maraganore, D.M., Adler, C.H., Larvor, L., Chartier-Harlin, M.C., Nilsson, C., Langston, J.W., Gwinn, K., Hattori, N., and Farrer, M.J. (2008). Genomic investigation of  $\alpha$ -synuclein multiplication and parkinsonism. *Ann. Neurol.* 63, 743-750.

Rowland, A.A., and Voeltz, G.K. (2012). Endoplasmic reticulum-mitochondria contacts: Function of the junction. *Nat. Rev. Mol. Cell Biol.* 13, 607-615.

Rudenko, I.N., Chia, R., and Cookson, M.R. (2012). Is inhibition of kinase activity the only therapeutic strategy for LRRK2-associated Parkinson's disease? *BMC Med.* 10.

Rudenko, I.N., and Cookson, M.R. (2014). Heterogeneity of Leucine-Rich Repeat Kinase 2 Mutations: Genetics, Mechanisms and Therapeutic Implications. *Neurotherapeutics* 11.

Rudenko, I.N., Kaganovich, A., Hauser, D.N., Beylina, A., Chia, R., Ding, J., Maric, D., Jaffe, H., and Cookson, M.R. (2012). The G2385R variant of leucine-rich repeat kinase 2 associated with Parkinson's disease is a partial loss-of- function mutation. *Biochem. J.* 446, 99-111.

Ruiz-Martínez, J., Gorostidi, A., Ibañez, B., Alzualde, A., Otaegui, D., Moreno, F., De Munain, A.L., Bergareche, A., Gómez-Esteban, J.C., and Massó, J.F.M. (2010). Penetrance in Parkinson's disease related to the LRRK2 R1441G mutation in the Basque country (Spain). *Mov. Disord.* 25, 2340-2345.

Russo, I., Bubacco, L., and Greggio, E. (2014). LRRK2 and neuroinflammation: Partners in crime in Parkinson's disease? *J. Neuroinflamm.* 11.

Ryan, B.J., Hoek, S., Fon, E.A., and Wade-Martins, R. (2015). Mitochondrial dysfunction and mitophagy in Parkinson's: From familial to sporadic disease. *Trends Biochem. Sci.* 40, 200-210.

Sancho, R.M., Law, B.M.H., and Harvey, K. (2009). Mutations in the LRRK2 Roc-COR tandem domain link Parkinson's disease to Wnt signalling pathways. *Hum. Mol. Genet.* 18, 3955-3968.

Santetl, A., Frank, S., Gaume, B., Herrler, M., Youle, R.J., and Fuller, M.T. (2003). Mitofusin-1 protein is a generally expressed mediator of mitochondrial fusion in mammalian cells. *J. Cell. Sci.* 116, 2763-2774.

Satoh, M., Hamamoto, T., Seo, N., Kagawa, Y., and Endo, H. (2003). Differential sublocalization of the dynamin- related protein OPA1 isoforms in mitochondria. *Biochem. Biophys. Res. Commun.* 300, 482-493.

Savitt, J.M., Dawson, V.L., and Dawson, T.M. (2006). Diagnosis and treatment of Parkinson disease: Molecules to medicine. *J. Clin. Invest.* 116, 1744-1754.

Schapira, A.H.V., Cooper, J.M., Dexter, D., Jenner, P., Clark, J.B., and Marsden, C.D. (1989). Mitochondrial Complex I Deficiency in Parkinson's Disease. *Lancet* 333, 1269.

Schober, A. (2004). Classic toxin-induced animal models of Parkinson's disease: 6-OHDA and MPTP. *Cell Tissue Res.* 318, 215-224.

Schrader, M., Godinho, L.F., Costello, J.L., and Islinger, M. (2015). The different facets of organelle interplay-an overview of organelle interactions. *Frontiers in Cell and Developmental Biology* 3.

Schrader, M., Costello, J.L., Godinho, L.F., Azadi, A.S., and Islinger, M. (2016). Proliferation and fission of peroxisomes - An update. *Biochim. Biophys. Acta Mol. Cell Res.* 1863, 971-983.

Schrader, M., Grille, S., Fahimi, H.D., and Islinger, M. (2013). Peroxisome interactions and cross-talk with other subcellular compartments in animal cells. *Subcell. Biochem.* 69, 1-22.

Schreiner, B., Hedskog, L., Wiehager, B., and Ankarcrona, M. (2015). Amyloid- $\beta$  peptides are generated in mitochondria-associated endoplasmic reticulum membranes. *J. Alzheimer's Dis.* 43, 369-374.

Schulte, E.C., Ellwanger, D.C., Dihanich, S., Manzoni, C., Stangl, K., Schormair, B., Graf, E., Eck, S., Mollenhauer, B., Haubenberger, D., Pirker, W., Zimprich, A., Brücke, T., Lichtner, P., Peters, A., Gieger, C., Trenkwalder, C., Mewes, H.W., Meitinger, T., Lewis, P.A., Klünemann, H.H., and Winkelmann, J. (2014). Rare variants in LRRK1 and Parkinson's disease. *Neurogenetics* 15, 49-57.

Scorrano, L. (2013). Keeping mitochondria in shape: A matter of life and death. *Eur. J. Clin. Invest.* 43, 886-893.

Scorrano, L., Ashiya, M., Buttle, K., Weiler, S., Oakes, S.A., Mannella, C.A., and Korsmeyer, S.J. (2002). A distinct pathway remodels mitochondrial cristae and mobilizes cytochrome c during apoptosis. *Dev. Cell* 2, 55-67.

Sen, S., Webber, P.J., and West, A.B. (2009). Dependence of leucine-rich repeat kinase 2 (LRRK2) kinase activity on dimerization. *J. Biol. Chem.* 284, 36346-36356.

Sengupta, P., Garai, K., Sahoo, B., Shi, Y., Callaway, D.J.E., and Maiti, S. (2003). The amyloid  $\beta$  peptide (A $\beta$  1-40) is thermodynamically soluble at physiological concentrations. *Biochemistry* 42, 10506-10513.

Sepulveda-Falla, D., Barrera-Ocampo, A., Hagel, C., Korwitz, A., Vinueza-Veloz, M.F., Zhou, K., Schonewille, M., Zhou, H., Velazquez-Perez, L., Rodriguez-Labrada, R., Villegas, A., Ferrer, I., Lopera, F., Langer, T., De Zeeuw, C.I., and Glatzel, M. (2014). Familial

Alzheimer's disease-associated presenilin-1 alters cerebellar activity and calcium homeostasis. *J. Clin. Invest.* 124, 1552-1567.

Shendelman, S., Jonason, A., Martinat, C., Leete, T., and Abeliovich, A. (2004). DJ-1 Is a redox-dependent molecular chaperone that inhibits a-synuclein aggregate formation. *PLoS Biol.* 2.

Sheng, Z., Zhang, S., Bustos, D., Kleinheinz, T., Le Pichon, C.E., Dominguez, S.L., Solanoy, H.O., Drummond, J., Zhang, X., Ding, X., Cai, F., Song, Q., Li, X., Yue, Z., van der Brug, M.P., Burdick, D.J., Gunzner-Toste, J., Chen, H., Liu, X., Estrada, A.A., Sweeney, Z.K., Scarce-Levie, K., Moffat, J.G., Kirkpatrick, D.S., and Zhu, H. (2012). Ser1292 autophosphorylation is an indicator of LRRK2 kinase activity and contributes to the cellular effects of PD mutations. *Sci Transl Med* 4.

Sheng, Z. (2014). Mitochondrial trafficking and anchoring in neurons: New insight and implications. *J. Cell Biol.* 204, 1087-1098.

Shibata, Y., Shemesh, T., Prinz, W.A., Palazzo, A.F., Kozlov, M.M., and Rapoport, T.A. (2010). Mechanisms determining the morphology of the peripheral ER. *Cell* 143, 774-788.

Shibata, Y., Voeltz, G.K., and Rapoport, T.A. (2006). Rough Sheets and Smooth Tubules. *Cell* 126, 435-439.

Shibata, Y., Voss, C., Rist, J.M., Hu, J., Rapoport, T.A., Prinz, W.A., and Voeltz, G.K. (2008). The reticulon and Dp1/Yop1p proteins form immobile oligomers in the tubular endoplasmic reticulum. *J. Biol. Chem.* 283, 18892- 18904.

Shim, S., Xia, C., Zhong, G., Babcock, H.P., Vaughan, J.C., Huang, B., Wang, X., Xu, C., Bi, G., and Zhuang, X. (2012). Super-resolution fluorescence imaging of organelles in live cells with photoswitchable membrane probes. *Proc. Natl. Acad. Sci. U. S. A.* 109, 13978-13983.

Shin, N., Jeong, H., Kwon, J., Heo, H.Y., Kwon, J.J., Yun, H.J., Kim, C., Han, B.S., Tong, Y., Shen, J., Hatano, T., Hattori, N., Kim, K.S., Chang, S., and Seol, W. (2008). LRRK2 regulates synaptic vesicle endocytosis. *Exp. Cell Res.* 314, 2055-2065.

Simmen, T., Aslan, J.E., Blagoveshchenskaya, A.D., Thomas, L., Wan, L., Xiang, Y., Feliciangeli, S.F., Hung, C., Crump, C.M., and Thomas, G. (2005). PACS-2 controls endoplasmic reticulum-mitochondria communication and Bid-mediated apoptosis. *Embo j.* 24, 717-729.

Simola, N., Morelli, M., and Carta, A.R. (2007). The 6-hydroxydopamine model of Parkinson's disease. *Neurotoxic. Res.* 11, 151-167.

Singleton, A.B., and Vaux, K.K. (2016). Parkinson Disease and LRRK2. *Medscape*

Singleton, A.B., Farrer, M.J., and Bonifati, V. (2013). The genetics of Parkinson's disease: Progress and therapeutic implications. *Mov. Disord.* 28, 14-23.

Smith, W.W., Pei, Z., Jiang, H., Moore, D.J., Liang, Y., West, A.B., Dawson, V.L., Dawson, T.M., and Ross, C.A. (2005). Leucine-rich repeat kinase 2 (LRRK2) interacts with parkin, and mutant LRRK2 induces neuronal degeneration. *Proc. Natl. Acad. Sci. U. S. A.* 102, 18676-18681.

Söderberg, O., Gullberg, M., Jarvius, M., Ridderstråle, K., Leuchowius, K., Jarvius, J., Wester, K., Hydbring, P., Bahram, F., Larsson, L., and Landegren, U. (2006). Direct observation of individual endogenous protein complexes in situ by proximity ligation. *Nat. Methods* 3, 995-1000.

Song, Z., Chen, H., Fiket, M., Alexander, C., and Chan, D.C. (2007). OPA1 processing controls mitochondrial fusion and is regulated by mRNA splicing, membrane potential, and Yme1L. *J. Cell Biol.* 178, 749-755.

Sood, A., Jeyaraju, D.V., Prudent, J., Caron, A., Lemieux, P., McBride, H.M., Laplante, M., Tóth, K., and Pellegrini, L. (2014). A Mitofusin-2-dependent inactivating cleavage of Opa1 links changes in mitochondria cristae and ER contacts in the postprandial liver. *Proc. Natl. Acad. Sci. U. S. A.* 111, 16017-16022.

Spillantini, M.G., Schmidt, M.L., Lee, V.M., Trojanowski, J.Q., Jakes, R., and Goedert, M. (1997).  $\alpha$ -synuclein in Lewy bodies. *Nature* 388, 839-840.

Stafa, K., Tsika, E., Moser, R., Musso, A., Glauser, L., Jones, A., Biskup, S., Xiong, Y., Bandopadhyay, R., Dawson, V.L., Dawson, T.M., and Moore, D.J. (2014). Functional interaction of Parkinson's disease-associated LRRK2 with members of the dynamin GTPase superfamily. *Hum. Mol. Genet.* 23, 2055-2077.

Stefan, C.J., Manford, A.G., and Emr, S.D. (2013). ER-PM connections: Sites of information transfer and inter- organelle communication. *Curr. Opin. Cell Biol.* 25, 434-442.

Stefanis, L. (2012).  $\alpha$ -Synuclein in Parkinson's disease. *Cold Spring Harbor Perspect. Med.* 2.

Steger, M., Tonelli, F., Ito, G., Davies, P., Trost, M., Vetter, M., Wachter, S., Lorentzen, E., Duddy, G., Wilson, S., Baptista, M.A., Fiske, B.K., Fell, M.J., Morrow, J.A., Reith, A.D., Alessi, D.R., and Mann, M. (2016). Phosphoproteomics reveals that Parkinson's disease kinase LRRK2 regulates a subset of Rab GTPases. *Elife* 5.

Stoica, R., De Vos, K.J., Paillusson, S., Mueller, S., Sancho, R.M., Lau, K., Vizcay-Barrena, G., Lin, W., Xu, Y., Lewis, J., Dickson, D.W., Petrucelli, L., Mitchell, J.C., Shaw, C.E., and Miller, C.C. (2014). ER-mitochondria associations are regulated by the VAPB-PTPIP51 interaction and are disrupted by ALS/FTD-associated TDP-43. *Nat. Commun.* 5.

Subramaniam, S.R., and Chesselet, M. (2013). Mitochondrial dysfunction and oxidative stress in Parkinson's disease. *Prog. Neurobiol.* 106-107, 17-32.

Sugiura, A., Nagashima, S., Tokuyama, T., Amo, T., Matsuki, Y., Ishido, S., Kudo, Y., McBride, H.M., Fukuda, T., Matsushita, N., Inatome, R., and Yanagi, S. (2013). MITOL regulates endoplasmic reticulum-mitochondria contacts via Mitofusin2. *Mol. Cell* 51, 20-34.

Szabadkai, G., Bianchi, K., Várnai, P., De Stefani, D., Wieckowski, M.R., Cavagna, D., Nagy, A.I., Balla, T., and Rizzuto, R. (2006). Chaperone-mediated coupling of endoplasmic reticulum and mitochondrial Ca<sup>2+</sup> channels. *J. Cell Biol.* 175, 901-911.

Taira, T., Saito, Y., Niki, T., Iguchi-Arigo, S.M.M., Takahashi, K., and Arigo, H. (2004). DJ-1 has a role in antioxidative stress to prevent cell death. *EMBO Rep.* 5, 213-218.

Takahashi-Niki, K., Niki, T., Taira, T., Iguchi-Ariga, S.M.M., and Ariga, H. (2004). Reduced anti-oxidative stress activities of DJ-1 mutants found in Parkinson's disease patients. *Biochem. Biophys. Res. Commun.* 320, 389-397.

Tambini, M.D., Pera, M., Kanter, E., Yang, H., Guardia-Laguarta, C., Holtzman, D., Sulzer, D., Area-Gomez, E., and Schon, E.A. (2016). ApoE4 upregulates the activity of mitochondria-associated ER membranes. *EMBO Rep.* 17, 27- 36.

Tan, E.K., Tan, L.C., Lim, H.Q., Li, R., Tang, M., Yih, Y., Pavanni, R., Prakash, K.M., Fook-Chong, S., and Zhao, Y. (2008). LRRK2 R1628P increases risk of Parkinson's disease: Replication evidence. *Hum. Genet.* 124, 287-288.

Tanaka, A., Cleland, M.M., Xu, S., Narendra, D.P., Suen, D., Karbowski, M., and Youle, R.J. (2010). Proteasome and p97 mediate mitophagy and degradation of mitofusins induced by Parkin. *J. Cell Biol.* 191, 1367-1380.

Terasaki, M., Shemesh, T., Kasthuri, N., Klemm, R.W., Schalek, R., Hayworth, K.J., Hand, A.R., Yankova, M., Huber, G., and Lichtman, J.W. (2013). Stacked endoplasmic reticulum sheets are connected by helicoidal membrane motifs. *Cell* 154, 285-296.

Thomas, B., and Flint Beal, M. (2007). Parkinson's disease. *Hum. Mol. Genet.* 16.

Timmerman, V., Clowes, V.E., and Reid, E. (2013). Overlapping molecular pathological themes link Charcot-Marie-Tooth neuropathies and hereditary spastic paraplegias. *Exp. Neurol.* 246, 14-25.

Tubbs, E., Theurey, P., Vial, G., Bendridi, N., Bravard, A., Chauvin, M.A., Ji-Cao, J., Zoulim, F., Bartosch, B., Ovize, M., Vidal, H., and Rieusset, J. (2014). Mitochondria-associated endoplasmic reticulum membrane (MAM) integrity is required for insulin signaling and is implicated in hepatic insulin resistance. *Diabetes* 63, 3279-3294.

Uemura, K., Lill, C.M., Li, X., Peters, J.A., Ivanov, A., Fan, Z., DeStrooper, B., Bacskai, B.J., Hyman, B.T., and Berezovska, O. (2009). Allosteric modulation of PS1/ $\gamma$ -secretase conformation correlates with amyloid  $\beta$  42/40 ratio. *PLoS One* 4, e7893.

Ungerstedt, U., and Arbuthnott, G.W. (1970). Quantitative recording of rotational behavior in rats after 6-hydroxy- dopamine lesions of the nigrostriatal dopamine system. *Brain Res.* 24, 485-493.

Urano, Y., Hayashi, I., Isoo, N., Reid, P.C., Shibasaki, Y., Noguchi, N., Tomita, T., Iwatsubo, T., Hamakubo, T., and Kodama, T. (2005). Association of active  $\gamma$ -secretase complex with lipid rafts. *J. Lipid Res.* 46, 904-912.

Valero, T. (2014). Mitochondrial biogenesis: Pharmacological approaches. *Curr. Pharm. Des.* 20, 5507.

Van Den Eeden, S.K., Tanner, C.M., Bernstein, A.L., Fross, R.D., Leimpeter, A., Bloch, D.A., and Nelson, L.M. (2003). Incidence of Parkinson's disease: Variation by age, gender, and race/ethnicity. *Am. J. Epidemiol.* 157, 1015-1022.

van Egmond, W.N., and van Haastert, P.J.M. (2010). Characterization of the Roco protein family in *Dictyostelium discoideum*. *Eukaryotic Cell* 9, 751-761.

Van Laar, V.S., Roy, N., Liu, A., Rajprohat, S., Arnold, B., Dukes, A.A., Holbein, C.D., and Berman, S.B. (2015). Glutamate excitotoxicity in neurons triggers mitochondrial and endoplasmic reticulum accumulation of Parkin, and, in the presence of N-acetyl cysteine, mitophagy. *Neurobiol. Dis.* 74, 180-193.

Vance, J.E. (2014). MAM (mitochondria-associated membranes) in mammalian cells: lipids and beyond. *Biochimica Et Biophysica Acta (BBA)-Molecular and Cell Biology of Lipids* 1841, 595-609.

Vance, J.E. (1990). Phospholipid synthesis in a membrane fraction associated with mitochondria. *J. Biol. Chem.* 265, 7248-7256.

Veratti, E. (1961). Investigations on the fine structure of striated muscle fiber read before the Reale Istituto Lombardo, 13 March 1902. *J Biophys Biochem Cytol* 10.

Vetter, I.R., and Wittinghofer, A. (2001). The guanine nucleotide-binding switch in three dimensions. *Science* 294, 1299-1304.

Vitte, J., Traver, S., Maues De Paula, A., Lesage, S., Rovelli, G., Corti, O., Duyckaerts, C., and Brice, A. (2010). Leucine-rich repeat kinase 2 is associated with the endoplasmic reticulum in dopaminergic neurons and accumulates in the core of Lewy bodies in Parkinson disease. *J. Neuropathol. Exp. Neurol.* 69, 959-972.

Voeltz, G.K., Prinz, W.A., Shibata, Y., Rist, J.M., and Rapoport, T.A. (2006). A class of membrane proteins shaping the tubular endoplasmic reticulum. *Cell* 124, 573-586.

Voeltz, G.K., Rolls, M.M., and Rapoport, T.A. (2002). Structural organization of the endoplasmic reticulum. *EMBO Rep.* 3, 944-950.

Vogel, F., Bornhövd, C., Neupert, W., and Reichert, A.S. (2006). Dynamic subcompartmentalization of the mitochondrial inner membrane. *J. Cell Biol.* 175, 237-247.

Wallings, R., Manzoni, C., and Bandopadhyay, R. (2015). Cellular processes associated with LRRK2 function and dysfunction. *Febs j.* 282, 2806-2826.

Wang, L.H., Besirli, C.G., and Johnson Jr, E.M. (2004). Mixed-lineage kinases: a target for the prevention of neurodegeneration. *Annu. Rev. Pharmacol. Toxicol.* 44, 451-474.

Wang, P.T., Garcin, P.O., Fu, M., Masoudi, M., St-Pierre, P., Panté, N., and Nabi, I.R. (2015). Distinct mechanisms controlling rough and smooth endoplasmic reticulum contacts with mitochondria. *J. Cell. Sci.* 128, 2759-2765.

Wang, X., Winter, D., Ashrafi, G., Schlehe, J., Wong, Y.L., Selkoe, D., Rice, S., Steen, J., Lavoie, M.J., and Schwarz, T.L. (2011). PINK1 and Parkin target miro for phosphorylation and degradation to arrest mitochondrial motility. *Cell* 147, 893-906.

Wang, X., Yan, M.H., Fujioka, H., Liu, J., Wilson-delfosse, A., Chen, S.G., Perry, G., Casadesus, G., and Zhu, X. (2012). LRRK2 regulates mitochondrial dynamics and function through direct interaction with DLP1. *Hum. Mol. Genet.* 21, 1931-1944.

Wasti, A.Z., Khan, R., Jehan, F., Anees, Z., and Karim, H. (2015). Computational Analysis of Parkinson's disease Associated Pink1 Gene: A Neuroinformatics Approach. *International Journal* 3, 645-652.

Webber, P.J., Smith, A.D., Sen, S., Renfrow, M.B., Mobley, J.A., and West, A.B. (2011). Autophosphorylation in the leucine-rich repeat kinase 2 (LRRK2) GTPase domain modifies kinase and GTP-binding activities. *J. Mol. Biol.* 412, 94-110.

Weggen, S., and Beher, D. (2012). Molecular consequences of amyloid precursor protein and presenilin mutations causing autosomal-dominant Alzheimer's disease. *Alzheimers Res. Ther.* 4.

West, M., Zurek, N., Hoenger, A., and Voeltz, G.K. (2011). A 3D analysis of yeast ER structure reveals how ER domains are organized by membrane curvature. *J. Cell Biol.* 193, 333-346.

Westermann, B. (2010). Mitochondrial fusion and fission in cell life and death. *Nat. Rev. Mol. Cell Biol.* 11, 872-884.

Wilson, R.C., and Doudna, J.A. (2013). Molecular mechanisms of RNA interference. *Annu. Rev. Biophys.* 42, 217- 239.

Yang, Y.S., and Strittmatter, S.M. (2007). The reticulons: A family of proteins with diverse functions. *Genome Biol.* 8.

Ylä-Anttila, P., Vihinen, H., Jokitalo, E., and Eskelinen, E. (2009). 3D tomography reveals connections between the phagophore and endoplasmic reticulum. *Autophagy* 5, 1180-1185.

Zampese, E., Fasolato, C., Kipanyula, M.J., Bortolozzi, M., Pozzan, T., and Pizzo, P. (2011). Presenilin 2 modulates endoplasmic reticulum (ER)-mitochondria interactions and Ca<sup>2+</sup> cross-talk. *Proc. Natl. Acad. Sci. U. S. A.* 108, 2777-2782.

Zhang, J.H., Wu, X., and Sills, M.A. (2005). Probing the primary screening efficiency by multiple replicate testing: a quantitative analysis of hit confirmation and false screening results of a biochemical assay. *J. Biomol. Screen.* 10, 695-704.

Zhu, P.P., Denton, K.R., Pierson, T.M., Li, X., and Blackstone, C. (2014). Pharmacologic rescue of axon growth defects in a human iPSC model of hereditary spastic paraplegia SPG3A. *Hum. Mol. Genet.* 23, 5638-5648.

Zhu, P.P., Patterson, A., Lavoie, B., Stadler, J., Shoeb, M., Patel, R., and Blackstone, C. (2003). Cellular localization, oligomerization, and membrane association of the hereditary spastic paraplegia 3A (SPG3A) protein atlastin. *J. Biol. Chem.* 278, 49063-49071.

Zorzano, A., Liesa, M., Sebastián, D., Segalés, J., and Palacín, M. (2010). Mitochondrial fusion proteins: Dual regulators of morphology and metabolism. *Semin. Cell Dev. Biol.* 21, 566-574.